2015-01-01

Computational Search For Novel Magnetic Clusters With Large Magnetic Anisotropy Energy

Nabil Md Rakinul Hoque
University of Texas at El Paso, nhoque@miners.utep.edu

COMPUTATIONAL SEARCH FOR NOVEL MAGNETIC CLUSTERS WITH LARGE MAGNETIC ANISOTROPY ENERGY

NABIL MD RAKINUL HOQUE

Department of Physics

APPROVED:

Rajendra Zope, Ph.D., Chair

Tunna Baruah, Ph.D., Co-Chair

Michael Paul Eastman, Ph.D.

Efrain Ferrer, Ph.D.

Charles Ambler, Ph.D.
Dean of the Graduate School

COMPUTATIONAL SEARCH FOR NOVEL MAGNETIC CLUSTERS WITH LARGE MAGNETIC ANISOTROPY ENERGY

by

NABIL MD RAKINUL HOQUE

THESIS

Presented to the Faculty of the Graduate School of

The University of Texas at El Paso

in Partial Fulfillment

of the Requirements

for the Degree of

MASTER OF SCIENCE

Department of Physics

THE UNIVERSITY OF TEXAS AT EL PASO

August 2015

ACKNOWLEDGEMENTS

I express my heartiest gratitude to the Almighty Allah and heartfelt thanks for the blessing, guidance, protection and help in all aspects of my life.

It is my great pleasure to express my utmost gratitude to my teacher, and supervisor of this thesis work **Prof Dr. Rajendra Zope**, Department of Physics, University of Texas at El Paso. It was an extraordinary experience for me to work under his supervision in such a well-equipped lab. I am truly indebted to him for allowing me to work in this laboratory. His constant guidance, valuable suggestions, encouragement, innovative ideas and new innovative techniques was the driving force behind the success of the research work. I thank him for everything he did and for helping me for completion of this work.

I would also like to express my deepest thanks to my venerable teacher and Co-supervisor **Prof Dr Tunna Baruah**, Dept. of Physics, University of Texas at El Paso, for her guidance, thoughtful suggestions, continuous encouragement and assistance have been a great source of inspiration throughout the progress of my research work. I would like to offer her my utmost gratitude.

Special thanks to **Dr Luis Basurto**, and **Dr Yoh Yamamoto** for their utmost help, encouragements, critical comments and cordial dealings throughout the research. I am really thankful to my friend and lab mates **Shusil Bhusal**, **Mahmudul Hassan** and **Nakul Karle** for their co-operation and supportive company throughout the research work.

No words are sufficient to express my gratitude to my father **Prof Dr Md Mazharul Hoque**, my mother **Mrs Nasima Akther Hoque**, my brother **Radin** and my sister **Nafisha** for their endless love, exemplary patience, understanding and co-operation during the preparation of this thesis work.

ABSTRACT

The clusters of transition metal atoms often show high spin moments but generally are reactive with the environment. Passivation of the surface atoms can lead to more stable clusters. We have explored one such avenue for passivation in this work. We picked the $As@Ni_{12}@As_{20}$ cluster which in the neutral state has a magnetic moment of 3 μ_B. We doped this cluster with various numbers of Mn atoms by substituting Ni atoms. The substitutional doping leads to spin moments located on the Mn atoms. The doping leads to symmetry breaking and as a consequence the number of structural isomers and spin ordered states for each isomer becomes very large. We have investigated all possible ferromagnetic Mn doped clusters for a given number of dopants. Subsequently all the possible anti-ferromagnetic states for the lowest energy structure were examined. The results show that the encapsulation within the As_{20} cage stabilizes the clusters and the atomization energy of the clusters increases as the number of dopant increases. These clusters have small energy barrier for reversal of magnetization and also have rich configuration space with many low-lying spin states.

TABLE OF CONTENTS

LIST OF TABLES

LIST OF FIGURES

CHAPTER 1: INTRODUCTION

1.1: MAGNETISM AND MOLECULAR MAGNET

Magnetic materials play critical roles in our daily lives. Magnetism was first discovered by ancient Greeks and used by the Chinese to create a "south pointing" compass (Mattis, 1981). Since the invention of the compass, the number of devices that use magnetic components has skyrocketed. A small number of applications of magnetic materials include frictionless bearings, medical devices, magnetic separators, loudspeakers, microphones, switches, sensors, data storage devices, motors, and generators (Miller and Epstein, 1994). The extensive commercial viability of magnetic materials has driven research in this area.

Traditional magnetic materials are two- and three-dimensional arrays of inorganic atoms, composed of transition metal or lanthanide metal containing spin units. These materials are typically produced at very high temperatures using metallurgical methodologies. In contrast to traditional magnetic materials, molecular magnets are organic or inorganic/organic hybrid materials, comprised of either metal containing spin units or organic radical containing spin units. It has been postulated that these materials will allow for the low temperature synthesis of magnetic materials and also with better optical properties. The combination of magnetic properties with mechanical, electrical, and/or optical properties gives better control over a material's magnetic characteristics, and materials that can be easily processed (Miller and Epstein, 1994).

The transition metals are the elements of periodic table which have a d orbital partially occupied by electrons. There are five d orbitals (characterized by the quantum number $l = 2$), which makes it possible to obtain spins of $S=0$ to $S=5/2$: the manganese (II) ion, or Mn (II), and the ferric ion, or Fe (III) have a $S=5/2$ spin (Figure 1.1).

Other elements, like lanthanides, have seven f orbitals ($l = 3$) which can be partially filled, giving a possible spin of $S=7/2$ for the gadolinium(III) ion, or Gd (III). If an isolated transition metal ion has

orbitals with the same energy, it is said that they are degenerate.

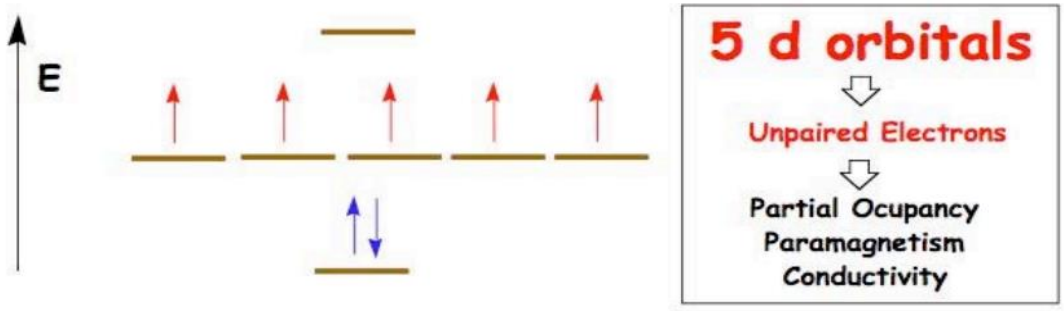

Figure 1.1: The d orbitals of transition elements are at the origin of the magnetic, conducting and optical properties of those elements.

1.2: DIAMAGNETISM AND PARAMAGNETISM

On the atomic level there exist two fundamental types of magnetism: diamagnetism and paramagnetism. All of the more complex magnetic behaviors which are observed evolve from these basic magnetic phenomena.

Diamagnetic behavior is characterized by repulsion of a substance out of an applied magnetic field. This behavior arises from the interaction of the applied magnetic field with molecular or atomic orbitals containing paired electrons. With the exception of the hydrogen radical, all atomic or molecular materials exhibit some diamagnetic behavior. This magnetic behavior is temperature independent, and the strength of the interaction is roughly proportional to the molecular weight of the material.

Paramagnetism is characterized by the attraction of a substance into an applied magnetic field. This behavior arises as a result of an interaction between the applied magnetic field and unpaired electrons in atomic or molecular orbitals.

Classically, the term magnetism refers to substances that at the atomic level exhibit temperature dependent paramagnetic behavior and will thus be used in this context. The non-zero spin angular moment

associated with an unpaired electron gives rise to a magnetic moment. Upon pairing, electrons within an orbital exhibit opposing magnetic moments resulting in no net magnetic moment. In general, bulk magnetic properties arise as a result of long-range interactions between unpaired electrons.

Bulk magnetic behavior arises from interactions between paramagnetic atoms or molecules. These interactions can create materials that are either magnetic or nonmagnetic, depending on how adjacent magnetic spins align with each other. Over 14 different possible magnetic interactions have been described in the literature (Hurd, 1982). Several of the important types of magnetic interactions are presented below.

1.3: PARAMAGNETISM, ANTIFERROMAGNETISM, FERROMAGNETISM, AND FERRIMAGNETISM

Generally, the bulk magnetic behavior of a material can be described by one of the four major classes of magnetism. The major classes of magnetism are paramagnetism, ferromagnetism, antiferromagnetism, and ferrimangetism. These classes of magnetic behavior describe how adjacent magnetic moments would interact with each other at absolute zero. The interactions are shown in Figure 1.2 and described below

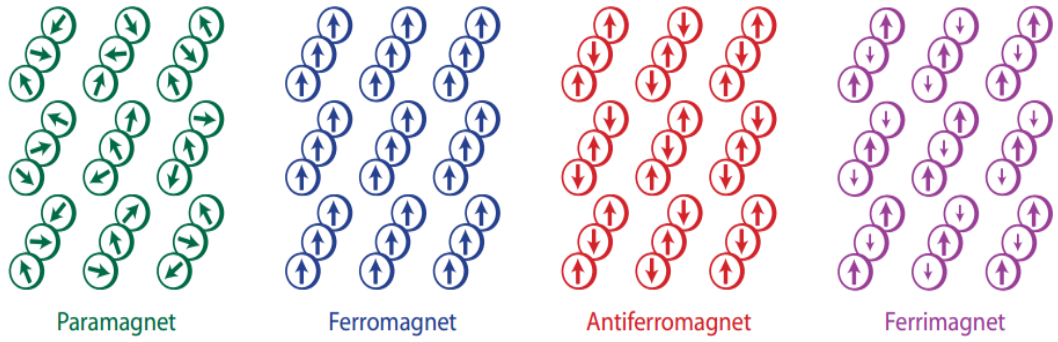

Figure 1.2: The alignment of magnetic moments at absolute zero for the four principle classes of magnetism.

No alignment of adjacent magnetic moments is observed for paramagnets. Ferromagnets exhibit parallel alignment of adjacent magnetic moments. Antiferromagnets exhibit antiparallel of adjacent

magnetic moments. Ferrimagnets are composed of two magnetic spins of different strength and exhibit antiparallel alignment.

1.3.1: Paramagnetism

In a paramagnetic material each individual electron spin is unaffected by its neighbors. The spins of a paramagnetic material can easily be aligned by an applied magnetic field. However the alignment is weak, and upon removal of the magnetic field the system relaxes back to a random distribution of magnetic moments. True paramagnetic materials are extremely rare, since most materials exhibit one of the other three principle classes of magnetism at very low temperatures.

1.3.2: Ferromagnetism

Ferromagnetism is characterized by parallel alignment of adjacent magnetic spins that results in a large net magnetic moment. Ferromagnetic alignment of adjacent magnetic spins is rare since it can only be achieved if there is zero quantum mechanical overlap between the spin-containing orbitals. In this case alignment of the spins, which correlates their motions and minimizes electron-electron repulsions, is the most stable state. Unlike paramagnets, ferromagnets exhibit a net magnetic moment in the absence of an applied magnetic field.

1.3.3: Antiferromagnetism

In an antiferromagnet, magnetic spins are aligned antiparallel, which results in a material with no net magnetic moment. At absolute zero, antiferromagnets exhibit a diamagnetic response to an applied magnetic field. The alignment of spins antiferromagnetically is analogous to the process of bonding and is thus favorable. Antiferromagnetism is the most commonly observed bulk magnetic behavior, and long-range antiferromagnetism is even exhibited by materials that order locally ferromagnetically.

1.3.4: Ferrimagnetism

Ferrimagnetism is a special case of antiferromagnetism, where the material consists of a lattice of rigidly alternating spins of different magnitudes. As in antiferromagnetism, the adjacent magnetic spins align antiparallel and however, since the adjacent spins are of different magnitudes, the resulting material exhibits a net magnetic moment in the absence of an applied magnetic field.

Although the four major class of magnetism account for the majority of observed magnetic behaviors, many other classes of magnetism exist. Many of these classes are subtle variations of the previously described major classes of magnetism. For example, a three dimensional metamagnet is a two dimensional ferromagnet that orders antiferromagnetically in the third dimension upon application of low magnetic fields and ferromagnetically upon application of high magnetic field. [1, 2]

1.4: MAGNETIC ANISOTROPY ENERGY:

The concept of magnetic anisotropy energy was first explained by Van Vleck. It is a very important energy scale which is useful for designing molecular scale magnetic memory devices [3]. In the case of hysteresis loop, we know that if we apply sufficient magnetic field to produce complete saturation inside the magnetic materials and then start reducing the field back to zero, we will find that at zero applied field some residual magnetization = “remnant induction” will remain and it will take a significant field “coercive field” to completely demagnetize the material.

The reason behind the remnant induction or coercive field is the Magnetic Anisotropy Energy. Materials with high magnetic anisotropy usually have high coercivity that is they are hard to demagnetize. These are called hard magnetic materials and are used to make permanent magnet.

Materials with low magnetic anisotropy usually have low coercivity that is they are easy to demagnetize. These are called soft magnetic materials and are used for making transformers and inductors.

Magnetic materials are said to have magneto crystalline anisotropy if it takes more energy to magnetize in any specific direction then the others. So there is a dependence of the magnetic properties on the direction of the applied field with respect to the crystal lattice. It turns out that depending on the orientation of the field with respect to the crystal lattice one would need a lower or higher magnetic field to reach the saturation magnetization. So based on this we can define two type of axis which are called easy axis and hard axis.

Easy axis is the direction inside a crystal, along which small applied magnetic field is sufficient to reach the saturation magnetization.

Hard axis is the direction inside a crystal, along which large applied magnetic field is needed to reach the saturation magnetization.

Finally we can define magneto-crystalline anisotropy energy is the energy necessary to deflect the magnetic moment in a single crystal from the easy to the hard direction. These easy axis and hard axis arise from the interaction of the spin magnetic moment with the crystal lattice (Spin-orbit coupling) [4]. For a material with a single easy axis perpendicular to the hard axes (e.g. Co) the energy associated with the magnetic anisotropy can be shown in the figure bellow.

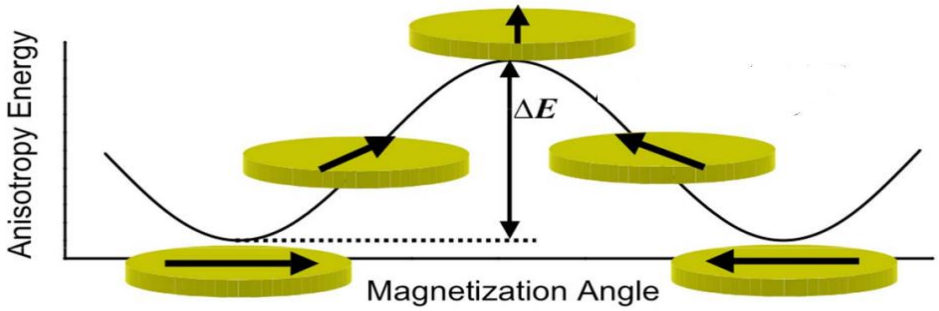

Figure 1.3: Magnetic anisotropy energy with respect to magnetization angle.

Here we can see that if the magnetization is along the easy axis, the energy is minimized and if the magnetization is in the hard axis the energy is much higher. So the difference between the energy associated with easy and hard axis is called magnetic anisotropy energy.

The main purpose of this thesis work is to determine the magnetic anisotropy energy and magnetic moment of different magnetic molecules. We also investigate the most favorable ones in energy by comparing the ferromagnetic and anti-ferromagnetic cases.

CHAPTER 2: THEORY

2.1: DENSITY FUNCTIONAL THEORY

The density functional theory (DFT) is presently the most successful and also the most promising approach to compute the electronic structure of matter. Its applicability ranges from atoms, molecules and solids to nuclei and quantum and classical fluids. In its original formulation, the density functional theory provides the ground state properties of a system, and the ground state electron density plays a key role [5].

DFT says that if we know the ground state density of electrons we can know everything, no wave function are needed. The electron density is defined as,

$$\rho\,(\boldsymbol{r_1}) = \int\ \psi^*\,(\boldsymbol{r_1}, \boldsymbol{r_2}, \dots\dots \boldsymbol{r_N}),\psi\,(\boldsymbol{r_1}, \boldsymbol{r_2}, \dots\dots \boldsymbol{r_N}) dr_2\, dr_3 \dots\dots\dots dr_N\ ,$$

where ψ is the many electron wave function.

The conventional approach uses the wave function ψ as the central quantity since ψ contains the full information of the system. However, ψ is very complicated quantity that cannot be probed experimentally. It depends on 4N variables (3 spatial and 1 spin), N being the number of electrons.

2.1.1: The First Hohenberg-Kohn Theorem

The first Hohenberg-Kohn theorem demonstrates that the ground state electron density uniquely determines the Hamiltonian operator and thus all the properties of the system. Thus $\rho\ (\boldsymbol{r})$ determines the total number of electrons N, and electron-nuclear interaction $V(\boldsymbol{r})$ and all the properties of the ground state. For example, the kinetic energy T[ρ], potential energy V[ρ], and the total energy E[ρ]. Now we can write the total energy as,

$$E[\rho] = V[\rho] + \mathrm{T}[\rho] + E_{ee}[\rho],$$

where $V[\rho]$ is the electron-nuclear potential, T[ρ] is the kinetic energy, and $E_{ee}[\rho]$ is the electron-electron interaction.

2.1.2: The Functional Relation Between ρ and H

The classical expression for $V[\rho]$ can be written as,

$$\int \rho\,(\boldsymbol{r})\, V(\boldsymbol{r}) d^3r = V[\rho],$$

which gives the average value of the electron nuclear interaction potential.

The kinetic energy and the electron-electron interaction can be expressed in terms of ρ.The classical Coulomb electron-electron interaction energy can be written as,

$$\frac{e^{\,2}}{2}\int \rho\,(\boldsymbol{r}')\,\rho\,(\boldsymbol{r})\,\frac{1}{|\boldsymbol{r}-\boldsymbol{r}'|}\,d\boldsymbol{r}'d\boldsymbol{r},$$

to obtain an expression of kinetic in terms of ρ. At the simplest level one can use a uniform electron gas model. The kinetic energy for electrons in a box,

$$E = (\frac{h^2}{8mL^2})(n_x^2 + n_y^2 + n_z^2),$$

within a 1/8 sphere in n_x, n_y, n_z space of radius R. We can express this volume as,

$$\varphi(E) = \frac{1}{8}\frac{4\pi}{3}R^3 = \frac{\pi}{6}\left(\frac{8mL^2E}{h^2}\right)^{\frac{3}{2}},$$

which is also the number of quantum states. The number of states in the range E and E+dE are ,

$$g(E) = \frac{d\,\varphi(E)}{dE} = \frac{\pi}{4}\left(\frac{8mL^2}{h^2}\right)^{\frac{3}{2}} E^{1/2}$$

The energy of the state with two electrons in each of the lowest orbitals up to the Fermi energy E_F is,

$$E_0 = 2\int g(E)\,E dE$$

$$= \frac{8\pi}{5}(\frac{2m}{h^2})^{3/2}L^3{E_F}^{5/2}$$

And the number of electron N is,

$$N = 2\int g(E)\,dE$$

$$= \frac{8\pi}{3}\left(\frac{2m}{h^2}\right)^{3/2} L^3 {E_F}^{3/2}$$

Solving for E_F in terms of N, one can express E_0 in terms of N and can be expressed as,

$$E_0 = \left(\frac{3h^2}{10m}\right)\left(\frac{3}{8\pi}\right)^{\frac{2}{3}} L^3 \left(\frac{N}{L^3}\right)^{5/3}$$

But we know that,

$$\rho = \frac{N}{L^3}$$

Thus the kinetic energy be computed within the local density approximation (LDA) by using this form,

$$T_{TF} = \left(\frac{3h^2}{10m}\right)\left(\frac{3}{8\pi}\right)^{\frac{2}{3}} L^3 \int [\rho(\boldsymbol{r})]^{5/3}\, d^3r$$

$$= C_F \int [\rho(\boldsymbol{r})]^{5/3}\, d^3r,$$

where ($C_F = 2.8712\ atomic\ units$) and the total energy could be expressed in terms of ρ as,

$$E_{0,TF}[\rho] = C_F \int [\rho(\boldsymbol{r})]^{\frac{5}{3}} d^3r + \int \rho\,(\boldsymbol{r})\, V(\boldsymbol{r}) d^3r + \frac{e^{\,2}}{2}\int \rho\,(\boldsymbol{r}')\,\rho\,(\boldsymbol{r})\,\frac{1}{|\boldsymbol{r}-\boldsymbol{r}'|}\, d^3r' d^3r,$$

This is so called **Thomas-Fermi model** and it is the most elementary LDA within the DFT. But the expression lacks exchange energy, that is, contributions to the energy due to spin interactions. The Thomas-Fermi model is too elementary to correctly describe the complex interactions in the many electron systems. .

Dirac augmented Thomas-Fermi functionals with a simple exchange functional,

$$E_{ex,Dirac}[\rho] = -C_x \int [\rho(\boldsymbol{r})]^{4/3}\, d^3r,$$

where $C_x = 0.7386\ au.$

To account for the fact that $\rho(\boldsymbol{r})$ varies strongly in some regions. So, Becke introduced a gradient-correction to Dirac exchange,

$$E_{ex}(Beck88) = E_{ex,Dirac}[\rho] - \gamma \int X^2\,[\rho(\boldsymbol{r})]^{\frac{4}{3}}\left(1 + 6\gamma X\ sinh^{-1}(X)\right)^{-1} dr,$$

where X=$\rho^{-4/3}\boldsymbol{\nabla}|\rho|$ and $\gamma = 0.0042$.

This exchange functional can be augmented to the Thomas-Fermi functional. Weizsacker improved the accuracy of the Thomas-Fermi kinetic energy functional by including a gradient correction to the kinetic energy,

$$\delta T_{weizsacker} = \left(\frac{1}{72}\right)\left(\frac{\hbar}{m}\right)\int \frac{|\boldsymbol{\nabla}\rho(\boldsymbol{r})|^2}{\rho(\boldsymbol{r})}\,d\boldsymbol{r}$$

Further improvement can be obtained by including the correlation energy. By analyzing the uniform electron gas, the correlation energy could be solved analytically in the low ρ and high ρ limits. By interpolating between these limits various approximation for the local **correlation functional** have been suggested. Such as,

$$E_c[\rho] = \int \rho(\boldsymbol{r})\,\epsilon_c[\rho]dr,$$

$$\epsilon_c(\rho) = \frac{A}{2}\{\ln\left(\frac{x}{X}\right) + \frac{2b}{Q}tan^{-1}\left(\frac{Q}{(2x+b)}\right) - \frac{bx_0}{X_0}\left[\ln\left(\frac{(x-x_0)^2}{X}\right) + \frac{2(b+2x_0)}{Q}tan^{-1}\left(\frac{Q}{(2x+b)}\right)\right]\},$$

where $x = r_s^{1/2}$, $X = x^2 + bx + c$, $X_0 = x_0^2 + bx_0 + c$ and $Q = (4c - b^2)^{1/2}$,

A=0.0621814, x_0=-0.409286, b=13.0720 and c=42.7198.

The parameter r_s is how ρ enters since $\frac{4}{3}\pi {r_s}^3$ is equal to 1/ ρ. The numerical values of the parameters are determined by fitting to the data base of the atomic energies.

So one can write the total energy (kinetic, nuclear interaction, Coulomb, exchange, correlation) in terms of $\rho(\boldsymbol{r})$,

$$E_{0,TF}[\rho] = C_F \int [\rho(\boldsymbol{r})]^{\frac{5}{3}} d^3r + \int \rho\,(\boldsymbol{r})\, V(\boldsymbol{r}) d^3r + \frac{e^{\,2}}{2} \int \rho\,(\boldsymbol{r}')\, \rho\,(r)\, \frac{1}{|\boldsymbol{r}-\boldsymbol{r}'|}\, d^3r' d^3r,$$

$$E_{ex}(Beck88) = E_{ex,Dirac}[\rho] - \gamma \int X^2\, [\rho(\boldsymbol{r})]^{\frac{4}{3}} \left(1 + 6\gamma X\, sinh^{-1}(X)\right)^{-1} dr,$$

$$\delta T_{weizsacker} = \left(\frac{1}{72}\right)\left(\frac{\hbar}{m}\right) \int \frac{|\boldsymbol{\nabla}\rho(\boldsymbol{r})|^2}{\rho(\boldsymbol{r})}\, dr,$$

$$E_c[\rho] = \int \rho(\boldsymbol{r})\, \epsilon_c[\rho] dr,$$

$$\epsilon_c(\rho) = \frac{A}{2}\left\{\ln\left(\frac{x}{X}\right) + \frac{2b}{Q}\, tan^{-1}\left(\frac{Q}{(2x+b)}\right) - \frac{bx_0}{X_0}\left[\ln\left(\frac{(x-x_0)^2}{X}\right) + \frac{2(b+2x_0)}{Q}\, tan^{-1}\left(\frac{Q}{(2x+b)}\right)\right]\right\}.$$

Although this was an important first step, the Thomas–Fermi equation's accuracy is limited because the resulting expression for the kinetic energy is only approximate. However, the Thomas–Fermi–Dirac theory remained rather inaccurate for most applications. The largest source of error was in the representation of the kinetic energy. In 1962, Edward Teller showed that Thomas–Fermi theory cannot describe molecular bonding – the energy of any molecule calculated with TF theory is higher than the sum of the energies of the constituent atoms. More generally, the total energy of a molecule decreases when the bond lengths are uniformly increased. This can be overcome by improving the expression for the kinetic energy [6]

2.1.3: Kohn-Sham Equation

To obtain the kinetic energy exactly, Kohn and Sham introduced an orbital like equation,

$$\left[-\frac{\hbar^2}{2m}\boldsymbol{\nabla}^2 - \sum_A Z_A \frac{e^2}{|\boldsymbol{r}-\boldsymbol{R_A}|} + e^2 \int \rho\,(\boldsymbol{r}')\, \frac{1}{|\boldsymbol{r}-\boldsymbol{r}'|}\, dr' + U_{xc}(\boldsymbol{r})\right] \varphi_i = \epsilon_i \varphi_i,$$

φ_i is the Kohn-Sham orbital which is the solution of the above equation. First term of the equation is the kinetic energy of the electron, 2nd term is the nucleus-electron interaction, 3rd term is the Coulomb

potential and the last term is the exchange- correlation potential. The exchange-correlation potential is obtained by taking a functional derivative of the earlier expression for the exchange-correlation energy.

$$U_{xc}(\boldsymbol{r}) = \frac{\delta E_{xc}[\rho]}{\delta \rho(\boldsymbol{r})}$$

Practical implementation of the Kohn-Sham procedure is as follows:

1. Atomic basis functions of the nuclides are chosen.
2. Molecular orbital is expressed as a linear combination of the basis functions times the co-efficient,

$$\varphi_j = \sum_a C_{ja}\, \chi_a,$$

where χ_a are the basis functions and C_{ja} are the co-efficients.

3. The electron density is obtained by summing the orbital densities of all occupied orbitals.

$$\rho = \textstyle\sum_{j=occ} n_j\, |\varphi_i(\boldsymbol{r})|^2.$$

4. This density is used to determine the Kohn-Sham potential

$$V_{eff(\boldsymbol{r})} = -\sum_A Z_A \frac{e^2}{|\boldsymbol{r} - \boldsymbol{R_A}|} + e^2 \int \rho\,(\boldsymbol{r}') \frac{1}{|\boldsymbol{r} - \boldsymbol{r}'|} dr' + U_{xc}(\boldsymbol{r})$$

5. Using the effective potential determined in the previous step, the Kohn-Sham equations are solved again

$$\left[-\frac{\hbar^2}{2m} \boldsymbol{\nabla}^2 - \textstyle\sum_A Z_A \frac{e^2}{|\boldsymbol{r} - \boldsymbol{R_A}|} + e^2 \int \rho\,(\boldsymbol{r}') \frac{1}{|\boldsymbol{r} - \boldsymbol{r}'|} dr' + U_{xc}(\boldsymbol{r}) \right] \varphi_i = \epsilon_i \varphi_i,$$

to find the new eigenfunctions $\{\varphi_i\}$ and new eigenvalues $\{\epsilon_i\}$.

6. This new $\{\varphi_i\}$ are used to find new density, which is used to find the new set of Kohn-Sham equation. This process is continued until the convergence is reached.

The total energy at every step during the cycle is obtained using the following (Kohn-Sham) energy expression.

$$E[\rho] = \sum_{j=occ} n_j < \varphi_i \left| -\frac{\hbar^2}{2m}\boldsymbol{\nabla}^2 \right| \varphi_i > + \int \rho\,(\boldsymbol{r})\, V(\boldsymbol{r}) d^3r + \frac{e^2}{2}\int \rho\,(\boldsymbol{r}')\,\rho\,(\boldsymbol{r})\frac{1}{|\boldsymbol{r}-\boldsymbol{r}'|} d^3r' d^3r + E_{xc}[\rho],$$

The Kohn-Sham formalism is, in principle, exact but the exchange correlation functional E_{xc} is unknown. The practical applications require approximations to the E_{xc}. Several approximate forms exists. The development of accurate density functionals is very active area of research. In our present study, we approximate E_{xc} at the level of generalized gradient approximation (GGA) using the Perdew-Burke-Ernzerhof (PBE) parameterization. [7]

2.2: ORIGIN OF MAGNETIC ANISOTROPY ENERGY:

The main cause of magnetic anisotropy energy is the spin-orbit coupling. In quantum physics, the spin–orbit interaction (also called spin–orbit effec**t** or spin–orbit coupling) is an interaction of a particle's spin with its motion. The first and best known example of this is that spin–orbit interaction causes shifts in an electron's atomic energy levels due to electromagnetic interaction between the electron's spin and the magnetic field generated by the electron's orbit around the nucleus [8]. This interaction is weaker than the Coulomb interaction and is responsible for the fine-structure of atomic lines.

The electron has a spin **s**, as well as orbital angular momentum **l**. For each angular momentum, there is an associated magnetic moment. These are spin magnetic moment μ_s and the magnetic moment associated with the orbital motion is μ_l. Spin-orbit coupling is the interaction between μ_s and μ_l.

The magnetic moment μ_l is defined as,

$$\mu_l = IA,$$

where 'I' is the current created by the orbital motion of electron and 'A' is the area of the orbit.

$\boldsymbol{\mu_l}$ is a vector perpendicular to plane of the orbit and it is linked to the orbital angular momentum. We know that time period of the orbital motion of electrons is

$$T = \frac{2\pi}{\omega}.$$

And the current 'I' can be expressed as,

$$I = -\frac{e}{T} = -\frac{e\omega}{2\pi}$$

Now the magnetic moment μ_l will be,

$$\mu_l = -\frac{e\omega}{2\pi}\pi r^2 = -\frac{1}{2}e\omega r^2$$

The orbital angular momentum can be defined as,

$$\left|\bar{l}\right| = |\bar{r} \times \bar{p}| = mvr = m\omega r^2$$

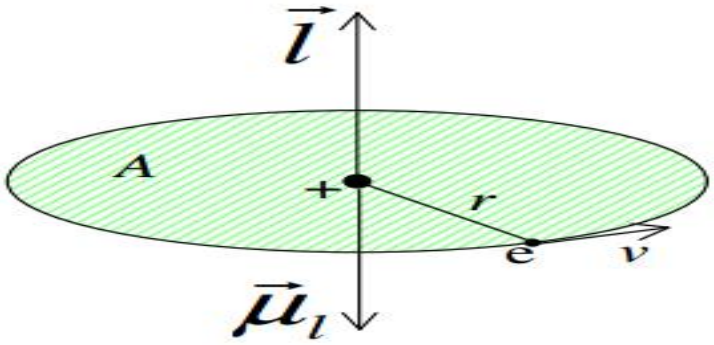

Figure 2.1: Orbital motion of electron.

Finally the $\bar{\mu_l}$ is written as,

$$\bar{\mu_l} = -\frac{e}{2m}\bar{l}$$

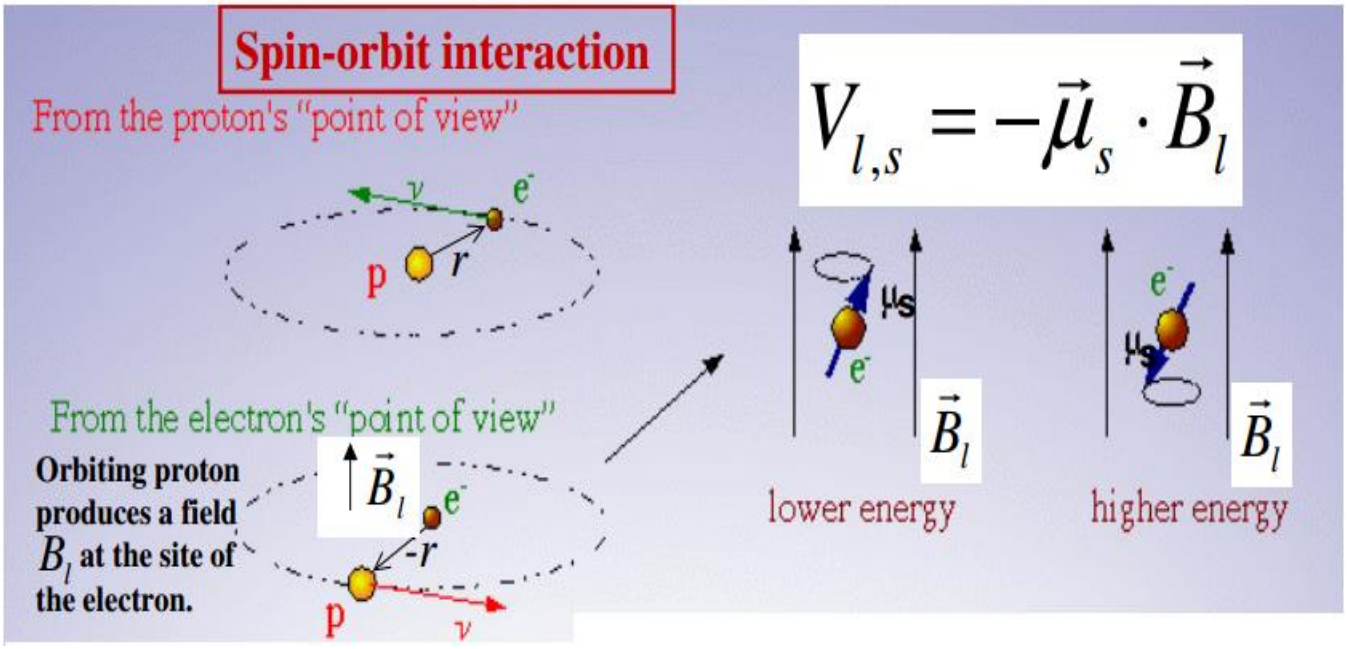

Figure 2.2: Physical picture of spin-orbit interaction.

In the above figure, from the electron point of view the proton is moving around the electron and produces a magnetic field $\boldsymbol{B_l}$ at the side of the electron. So the spin magnetic moment $\boldsymbol{\mu_s}$ interact with the magnetic field $\boldsymbol{B_l}$created by the orbital motion. This interaction energy can be expressed as

$$V_{l,s} = -\boldsymbol{\mu_s}.\boldsymbol{B_l}$$

Note that this is not the only magnetic interaction that is taking place in an atom. The nucleus also has a spin, hence a magnetic moment. The nuclear magnetic moment interacts with the magnetic field produced by the orbiting electron. This interaction is much weaker than the spin-orbit interaction considered here. [9].

So the spin $\boldsymbol{\mu_s}$ has two possible orientation with respect to the field 'parallel', with lower energy and anti-parallel with higher energy. In the case of molecular system, the lower energy and larger energy are associated with the easy axis and hard axis. For such systems the anisotropy barrier is related to the

shift of the total energy because of the spin orbit coupling and the magnetic anisotropy energy is originated.

2.3: CALCULATION OF MAGNETIC ANISOTROPY ENERGY

In this section we provide Pederson and Khanna formalism to compute the magnetic anisotropy energy. This approach is implemented in the NRLMOL code used here for calculations.

Magnetic anisotropy energy originates primarily due to spin-orbit coupling and is typically on the order of microhartee. In the classical explanation of spin-orbit coupling an electron moving with velocity **v** and accounting for the fact that electron is not spinless, the interaction energy is given by,

$$U(\boldsymbol{r},\boldsymbol{p},\boldsymbol{S}) = -\frac{1}{2c^2}\,\boldsymbol{S}.\boldsymbol{P}\times\boldsymbol{\nabla}\varphi(\boldsymbol{r}), \tag{1}$$

where $\varphi(\boldsymbol{r})$ is the Coulomb potential, $\boldsymbol{P}$ is the momentum operator.

The determination of spin-orbit coupling matrix element is a necessary ingredient to the numerical solution of the Schrodinger equation. To determine the generalized spin-orbit interaction from Eq. (1) it is necessary to calculate matrix element of the form,

$$\begin{aligned} U_{j,\sigma,k,\sigma'} &= \langle f_j\chi_\sigma|U(\boldsymbol{r},\boldsymbol{p},\boldsymbol{S})|f_k\chi_{\sigma'}\rangle \\ &= \textstyle\sum_x \frac{-1}{i2c^2}\langle f_j|[\boldsymbol{\nabla}\times\boldsymbol{\nabla}\varphi(\boldsymbol{r})]_x|f_k\rangle\langle\chi_\sigma|S_x|\chi_{\sigma'}\rangle \\ &= \textstyle\sum_x \frac{1}{i}\langle f_j|V_x|f_k\rangle\,\langle\chi_\sigma|S_x|\chi_{\sigma'}\rangle, \end{aligned}$$

with the operator V_x defined according to

$$\langle f_j|V_x|f_k\rangle = \frac{-1}{2c^2}\langle\, f_j|\,\frac{d}{dy}\frac{d\varphi}{dz} - \frac{d}{dz}\frac{d\varphi}{dy}\,|f_k\,\rangle\,. \tag{2}$$

We know that,

$$\langle f_i | \frac{d\varphi}{dy}\frac{d}{dz} | f_j \rangle = \int d^3r \frac{d}{dy}\left[f_i \varphi \frac{df_j}{dz}\right] - \langle \frac{df_i}{dy} | \varphi | \frac{df_j}{dz} \rangle - \langle f_i | \varphi | \frac{d^2 f_j}{dzdy} \rangle,$$

using the above identity in Eq. 3 we get

$$\langle f_j | V_x | f_k \rangle = \frac{1}{2c^2}\left(\langle \frac{df_j}{dz} | \varphi | \frac{df_k}{dy} \rangle - \langle \frac{df_j}{dy} | \varphi | \frac{df_k}{dz} \rangle\right) \quad (4)$$

The matrix elements for V_y and V_z are determined by the cyclical permutation.

Let us assume that, in the absence of a magnetic field and spin-orbit coupling, we have determined the wave functions $\psi_{i\sigma}$ within a self-consistent field (SCF) approximation. The SCF wave functions satisfy

$$H \mid \psi_{i\sigma} > = \epsilon_{i\sigma} | \psi_{i\sigma} >,$$

where $|\psi_{i\sigma} >$ is a product of a spatial function and spinor according to $\mid \psi_{i\sigma} > = \varphi_{i\sigma}(\boldsymbol{r})\chi_\sigma$.

With the inclusion of spin-orbit coupling and the introduction of a magnetic of field the perturbed wave functions satisfy,

$$\left[H + \left(\frac{\boldsymbol{V}}{i} + \frac{1}{c}\boldsymbol{B}\right) . \boldsymbol{S}\right] | \psi'_{i\sigma} > = \epsilon'_{i\sigma} | \psi'_{i\sigma} >.$$

Here, the operator $\boldsymbol{V}$ is defined according to Eq.4 and the magnetic field (**B**) is assumed to be uniform.

Now let,

$$\boldsymbol{W} = \left(\frac{\boldsymbol{V}}{i} + \frac{1}{c}\boldsymbol{B}\right)$$

According to the second order perturbation theory, the Hamiltonian matrix is perturbed by the following equations,

$$\Delta = \Delta_1 + \Delta_2$$

In absence of applied magnetic field, the first order energy shift is,

$$\Delta_1 = \sum_{i\sigma} S_i^{\sigma\sigma} \sum_k < \varphi_{k\sigma}|W_i|\varphi_{k\sigma} >$$

The first order energy shift vanishes due to the operator $-i\,\boldsymbol{V}.\boldsymbol{S}$ and the first order correction to the orbital is purely imaginary.

The second order energy shift is,

$$\Delta_2 = \sum_{\sigma\sigma'} \sum_{ij} W_{ij}^{\sigma\sigma'} S_i^{\sigma\sigma'} S_j^{\sigma'\sigma}, \qquad (5)$$

where,

$$S_i^{\sigma\sigma'} = < \chi_\sigma|S_i|\chi'_\sigma >,$$

and

$$W_{ij}^{\sigma\sigma'} = W_{ji}^{\sigma\sigma'^*} = \sum_{ij} \frac{< \varphi_{k\sigma}|W_i|\varphi_{l\sigma'} >< \varphi_{k\sigma'}|W_j|\varphi_{l\sigma} >}{\epsilon_{k\sigma} - \epsilon_{l\sigma'}}$$

In Eq.5 here the 1st sum is running over spin-up and spin-down states. The second sum is over all the co-ordinate levels (x,y,z).

The *W* matrices are simplified to,

$$W_{ij}^{\sigma\sigma'} = -\sum_{kl} \frac{< \sigma_{k\sigma}|V_i|\sigma_{l\sigma'} >< \sigma_{l\sigma'}|V_j|\sigma_{k\sigma} >}{\epsilon_{k\sigma} - \epsilon_{l\sigma'}} + \frac{B_i B_j}{c^2} \sum_{kl} \frac{< \sigma_{k\sigma}|\sigma_{l\sigma'} >< \sigma_{l\sigma'}|\sigma_{k\sigma} >}{\epsilon_{k\sigma} - \epsilon_{l\sigma'}}$$

At zero magnetic field,

$$W_{ij}^{\sigma\sigma'} \to M_{ij}^{\sigma\sigma'} = -\sum_{kl} \frac{< \sigma_{k\sigma}|V_i|\sigma_{l\sigma'} >< \sigma_{l\sigma'}|V_j|\sigma_{k\sigma} >}{\epsilon_{k\sigma} - \epsilon_{l\sigma'}}.$$

In the above equations χ_σ and χ'_σ are any set of spinors. $\varphi_{k\sigma}$ and $\varphi_{l\sigma'}$ are the occupied and unoccupied states respectively. $\epsilon's$ are the corresponding energies.

So the second-order shift in the energy of the system in the absence of a magnetic field can be rewritten as,

$$\Delta_2 = \sum_{ij} \gamma_{ij} \langle S_i \rangle \langle S_j \rangle.$$

The anisotropy energy can be determined after diagonalization of the anisotropy tensor (γ). The value of γ can be calculated within the density functional framework using second- order perturbation theory and in terms of Kohn-Sham orbitals. It is given by,

$$\gamma = \left(\frac{2}{\Delta N^2}\right)(M_{zz}^{11} + M_{zz}^{22} + M_{xx}^{12} + M_{xx}^{21} - M_{xx}^{11} - M_{xx}^{22} - M_{zz}^{12} - M_{zz}^{21}),$$

Where, ΔN is the number of unpaired electrons. Once the anisotropy tensor is diagonalized the second-order energy shift can be rewritten as,

$$\Delta_2 = \frac{1}{3}(\gamma_{xx} + \gamma_{yy} + \gamma_{zz})S(S+1) + \frac{1}{3}\left[\gamma_{zz} - \frac{1}{2}(\gamma_{xx} + \gamma_{yy})\right] \times [3S_z^2 - S(S+1)] + \frac{1}{2}(\gamma_{xx} - \gamma_{yy})(S_x^2 - S_y^2$$

The anisotropy Hamiltonian splits 2S+1 spin states and can be expressed as

$$H = DS_z^2 + E(S_x^2 - S_y^2).$$

The value of D and E in the above equation can be directly obtained from the γ_{xx}, γ_{yy}, γ_{zz} and therefore the magnetic anisotropy energy can be obtained. [3, 10, 11, 12].

2.4: COMPUTATIONAL METHOD

Our density functional-based calculation were performed with the all-electron Gaussian-orbital based Naval Research Laboratory Molecular Orbital Library (NRLMOL) program using the Perdew-Burke-Ernzerhof (PBE) generalized -gradient approximation for the exchange and correlation functional. NRLMOL combines large Gaussian orbital basis sets, numerically precise variational integration and an analytic solution of Poisson's equation to accurately determine the self-consistent potentials, secular matrix, total energies and Hellmann-Feynman-Pulay forces. The exponents for the Single Gaussian has fully optimized.

This computational method approach described earlier has been implemented in the NRLMOL and was previously used to calculate the magnetic anisotropy energy of Mn_{12}, Mn_{10}, $Cr[N(Si(CH_3)_3)_2]_3$ clusters and also the 'D' and 'E' parameter . The predictions of the magnetic anisotropy energies by this approach provide very good agreement with the experimentally measured second-order anisotropy energies. [10, 13]

Table 2.1: Comparison between the calculated density functional based second-order anisotropy energy with the experimental values

Cluster	**Second-order Anisotropy Energy (K)**	**Experimental Values (K)**
Mn_{12}	55.7	55.6
Mn_{10}	9.5	7.7
$Cr[N(Si(CH_3)_3)_2]_3$	5.6	6

Table 2.2: Comparison between the calculated and experimental magnetic anisotropy parameters for the single molecule magnets

Molecule	S	D (K)		E (K)	
		Theory	Experimental	Theory	Experimental
$Mn_{12}O_{12}(O_2CH)_{16}(H_2O)_4$	10	-0.56	-0.56	--	--
$[Mn_{10}O_4$(2,2'-biphenoxide)$_4Br_{12}]^{4-}$	13	-0.06	-0.05	--	--
$Co_4(CH_2C_5H_4N)_4(CH_3OH)_4Cl_4$	6	-0.64	-5.6	--	--
$Fe_4(OCH_2)_6(C_4H_9ON)_6$	5	-0.56	-0.57	0.06	0.05
$Cr[N(Si(CH_3)_3)_2]_3$	3/2	-2.49	-2.66	--	--

CHAPTER 3: RESULTS AND DISCUSSION

Synthesis and characterization of the $[As@Ni_{12}@As_{20}]^{3-}$ ion has been reported earlier. It contains interpenetrating reciprocal platonic polyhedra that is an undistorted As_{20} pentagonal dodecahedron and an arsenic centered Ni_{12} icosahedron [14]. We have first optimized the geometry of the $As@Ni_{12}@As_{20}$ cluster earlier, which we will henceforth call the parent cluster. The optimized geometry was verified with the experimental one by comparing various bond lengths in the cluster. We used the same basis set and exchange-correlation functional (PBE) in the present calculations also. The table below is reproduced from our earlier calculations, which shows the comparison of our calculated bond lengths with the experimental bond lengths. In addition other electronic structure properties (HOMO-LUMO gap, Magnetic Moment, Magnetic Anisotropy Energy) are given in the table 3.1 [15].

Table 3.1: Data for $As@Ni_{12}@As_{20}$ system

Systems	H-L gap (eV)	M.M μ_B	M.A.E (K)	As-As Å	As-As Å (Expt)	Ni-Ni Å	As-Ni Å	As-Ni Å (Expt)	Energy (Hartee)
$As@Ni_{12}@As_{20}$	**0.12**	**3**	**0.00**	**2.80**	**2.75**	**2.67**	**2.44**	**2.40**	**-65047.469248**

The parent cluster in the neutral state has a magnetic moment of $3\mu_B$. The icosahedral symmetry leads orbital degeneracy in the parent cluster. Both the HOMO and LUMO of the parent cluster belong to the minority spin with a small gap of 0.115 between them. In the parent cluster the HOMO and LUMO are of Hu and T1u symmetry, respectively. The HOMO orbital is centered around the Ni ions whereas the LUMO orbital has contribution from the Ni p and the central As p states. This cluster is symmetric which results in a very small value of magnetic anisotropy.

We have constructed the starting geometries of the Mn doped clusters from the optimized parent geometry. The doping is substitutional such that Mn atoms replace the Ni atoms. We doped the parent cluster by up to 10 Mn atoms. Depending on the number of dopant Mn atoms, the substitutional doping can result in a large number of isomers as there are multiple possible configurations of doping sites.

Furthermore, each configuration can have multiple spin states and spin ordering which leads to a larger number of conformers for each doped cluster. The NRLMOL code optimizes the spin moment for a given spin ordering. To simplify the calculations, we have first considered all possible sites for substitutional doping for a given number of Mn dopants in the ferromagnetic state. For example, for $As@Mn_2Ni_{10}@As_{20}$ there are 4 possible ferromagnetic isomers forming a family of $As@As_{10}Mn_2@As_{20}$ cluster. We chose the lowest energy isomer from each family for further study on the ferrimagnetic spin state. For the lowest energy isomer, all possible anti ferromagnetic spin states were studied. Below we describe each family of the Mn doped clusters studied here.

3.1: $As@Ni_{11}Mn@As_{20}$

In the parent $As@Ni_{12}@As_{20}$ system, all Ni atoms as well as all the As atoms that form the outer dodecahedral cage are equivalent by symmetry. Since all Ni atoms are equivalent one only needs to replace one of the 12 Ni atoms by Mn atom. Thus, there is only one resultant structure. The optimized structure of $As@Ni_{12}@As_{20}$ is shown in Figure 3.1 below.

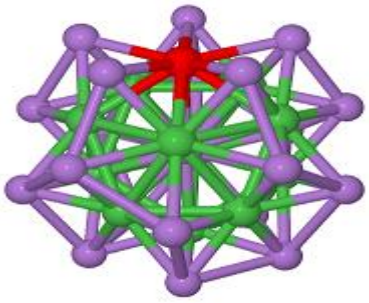

Figure 3.1: Picture of $As@Ni_{11}Mn_1@As_{20}$

As evident from the figure, the As_{20} cage in this case is distorted due to the expansion of the As-As bond lengths near Mn. Compared to As_{20} cage in the parent $As_{21}Ni_{12}$ cluster, near the Mn atom the As-As bond is elongated by 0.16 Å (2.96 vs. 2.80 Å) on average.

The net spin moment in this molecule is $6\mu_B$. Our calculation on the charge density inside a sphere placed on the Mn shows that the spin charge on the Mn ion is $3\mu_B$. The HOMO-LUMO gap is reduced to 0.07eV compared to the parent $As_{21}Ni_{12}$. The presence of Mn atoms as well as the distortion of the cage breaks the symmetry of the system, resulting in magnetic anisotropy energy of 10.40 K. The small HOMO-LUMO gap indicates that the cluster is chemically active and will likely to change its spin state upon chemical interaction with the environment.

3.2: $As@Ni_{10}Mn_2@As_{20}$

In the parent $As@Ni_{12}@As_{20}$ system, two Mn atoms were introduced by replacing two of the 12 Ni atoms. There are three unique resultant possible structures of the $As@Ni_{10}Mn_2@As_{20}$ system. The optimized structures of $As@Ni_{10}Mn_2@As_{20}$ systems in the ferromagnetic state are given below.

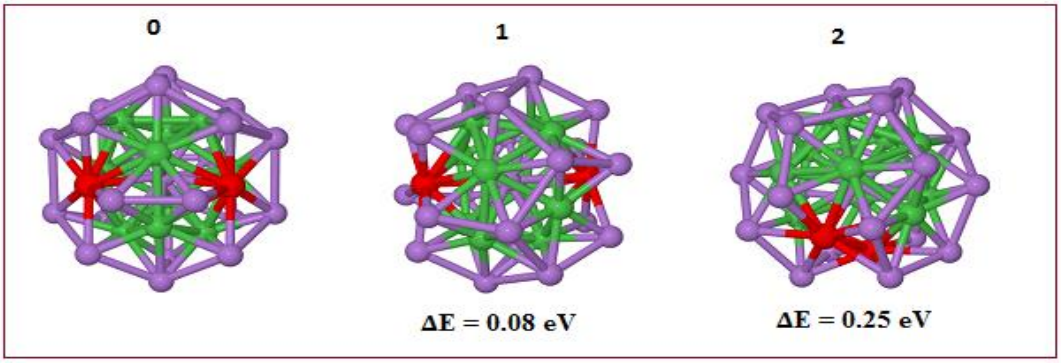

Figure 3.2: All possible combination of $As@Ni_{10}Mn_2@As_{20}$ cluster according to their energy.

In the Mn_2 doped cages also we find that the As-As bonds near the Mn ion are elongated. The As-As bond lengths vary from 2.65 Å to 3.35 Å in these clusters. On an average the As-As bond length is increased by 0.09 Å for all the resultant structures.

The net spin moment, HOMO-LUMO gaps, average bond lengths of As-As, Ni-Ni, As-Ni, As-Mn, Ni-Mn in the Mn2 doped isomers are given in the Table 3.2. In the table the most favorable (lowest energy) cluster is indicated by red color. The lowest energy isomer has a net magnetic moment of 9 μ_B.

The net spin on each of the Mn ions is $3\mu_B$ and the average spin on the Ni ions is 0.25 μ_B, which in the ferromagnetic state leads to a net moment of 9 μ_B. There are two low-lying isomers with a total energy difference of 0.08 eV and 0.25 eV. The presence of Mn atoms breaks the symmetry of the system, resulting in magnetic anisotropy energy compared to the parent cluster. The lowest energy cluster has MAE on the order of 20 K. The cluster also has a gap of 0.25 eV, which indicates that the cluster is chemically more stable compared to the single Mn doped system.

Table 3.2: Data for all possible combination of $As@Ni_{10}Mn_2@As_{20}$ cluster.

Systems	**H-L gap (eV)**	**M.M μ_B**	**M.A.E (K)**	**As-As** Å	**Ni-Ni** Å	**As-Ni** Å	**As-Mn** Å	**Ni-Mn** Å	**Energy (Hartee)**
$As_{21}Ni_{10}Mn_2$_0	0.25	9	20.4	2.75	2.67	2.44	2.55	2.75	-64332.76103
$As_{21}Ni_{10}Mn_2$_1	0.25	7	18.8	2.71	2.68	2.44	2.57	2.79	-64332.75191
$As_{21}Ni_{10}Mn_2$_2	0.31	7	14.8	2.71	2.69	2.44	2.55	2.78	-64332.75795

3.2.1: Ferrimagnetic Investigation of $As@Ni_{10}Mn_2@As_{20}$

The most favorable ferromagnetic cluster ($As_{21}Ni_{10}Mn_2$_0) from the above table is chosen for studying different spin ordering of the Mn atoms. Since there are only two Mn atoms in this cluster, only one antiferromagnetic ordering is possible. The antiferromagnetic spin ordering results in a structure that is slightly higher in energy by 0.1 eV. The magnetic moment of the AFM cluster is $1\mu_B$. The anisotropy in magnetism vanishes in the AFM cluster. The magnetic anisotropy energy (MAE), magnetic moment (M.M), HOMO-LUMO gap (H-L gap) and the deviation in energy ($E-E_{FM}$) from the ferromagnetic ($As_{21}Ni_{10}Mn_2$_0) cluster is given in Table 3.3. In the table below '0' stands for spin down and '1' stand for spin up.

Table 3.3: Data for different spin orientation of $As21Ni_{10}Mn_2$_0 system

Systems	**MAE (K)**	**M.M (μ_B)**	**H-L gap (eV)**	**$E-E_{FM}$ (eV)**
S.01	0.00	1	0.23	0.09

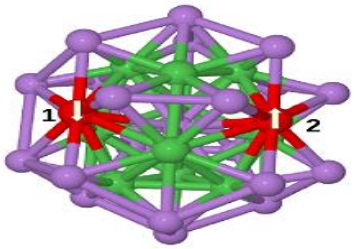

Figure 3.3: Spin ordering (S.01) of Mn atom in $As@Ni_{10}Mn_2@As_{20}$ system

3.3: $As@Ni_9Mn_3@As_{20}$:

In the $As@Ni_9Mn_3@As_{20}$ system three Mn atoms are doped by replacing three of the 12 Ni atom of the parent $As@Ni_{12}@As_{20}$ system. There are 9 unique combinations of the $As@Ni_9Mn_3@As20$ system is possible. The optimized structures of the 9 combinations of $As@Ni_9Mn_3@As_{20}$ systems are shown in the Fig. 3.4 below.

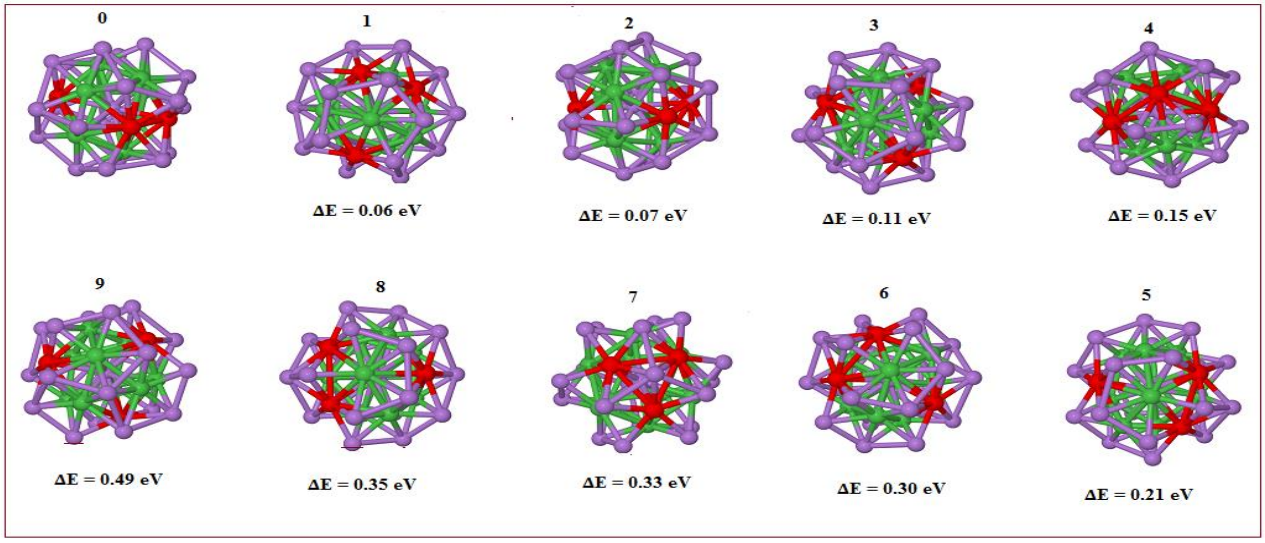

Figure 3.4: All possible combination of $As@Ni_9Mn_3@As_{20}$ cluster according to their energy.

As evident from the figure, the As_{20} cage in this case is also significantly distorted. In the above structures near the Mn atom the As-As bonds vary from 2.69 Å to 3.54 Å. For all the possible clusters As-As bond length is increased by 0.09 Å on an average compared to As20 cage in As21Ni12 system.

The HOMO-LUMO gap, net spin moment, average bond lengths of As-As, Ni-Ni, As-Ni, As-Mn, Ni-Mn and total energy differences with the lowest energy structure are presented in the Table 3.4. All the clusters are in these calculations are in the ferromagnetic state. Due to the breaking of symmetry of the parent cage, magnetic anisotropy energy becomes significant. The MAEs for all the investigated clusters in the ferromagnetic state are presented in Table 3.4. The HOMO-LUMO gap is large in these clusters and the magnetic moment is all clusters except one is 12 μB. The magnetic moment is 10 μB for the cluster in which all the three Mn ions are adjacent. The anisotropy energy is also least (2.7K) for this cluster. The largest MAE is 37 K for the lowest energy ferromagnetic structure in which the distances between the Mn ions are 0.264, 0.536, 0.472 Angstroms. We find that clusters in which the average Mn-Mn distances are on the order of 3 Angstroms, the anisotropy energy is also lower. This is due to the reduced interactions between the Mn ions.

Table 3.4: Calculated data for all the possible combination of $As@Ni_9Mn_3@As_{20}$ cluster.

Systems	**H-L gap (eV)**	**M.M μ_B**	**M.A.E (K)**	**As-As Å**	**As-Ni Å**	**Ni-Mn Å**	**As-Mn Å**	**Mn-Mn Å**	**Ni-Ni Å**	**Energy (Hartee)**
$As_{21}Ni_9Mn_3$_0	0.33	12	37.40	2.71	2.44	2.78	2.55	2.64	2.67	-63975.38476
$As_{21}Ni_9Mn_3$_1_	0.29	12	28.62	2.71	2.44	2.79	2.56	2.62	2.65	-63975.38237
$As_{21}Ni_9Mn_3$_2	0.34	12	24.92	2.72	2.45	2.74	2.53	---	2.70	-63975.38233
$As_{21}Ni_9Mn_3$_3	0.5	12	33.64	2.72	2.44	2.78	2.53	----	2.68	-63975.3806
$As_{21}Ni_9Mn_3$_4	0.24	12	22.36	2.73	2.44	2.79	2.56	2.71	2.65	-63975.37917
$As_{21}Ni_9Mn_3$_5	0.25	12	11.63	2.69	2.44	2.73	2.53	3.12	2.67	-63975.37467
$As_{21}Ni_9Mn_3$_6	0.25	12	11.67	2.69	2.45	2.74	2.53	3.13	2.69	-63975.37366
$As_{21}Ni_9Mn_3$_7	0.26	10	2.73	2.80	2.45	2.68	2.47	2.66	2.75	-63975.37245
$As_{21}Ni_9Mn_3$_8	0.25	12	11.03	2.69	2.45	2.73	2.53	3.12	2.69	-63975.37179
$As_{21}Ni_9Mn_3$_9	0.52	12	33.41	2.73	2.44	2.78	2.54	----	2.68	-63975.36678

In the above table among all the combinations of the cluster the most favorable (lowest energy) cluster is found to be As21Ni9Mn3_0 system which is indicated by red color.

3.3.1: Ferrimagnetic States of As@Ni_9Mn_3@As_{20}

The most favorable ferromagnetic cluster ($As_{21}Ni_9Mn_3$_0) from Table 3.4 is chosen for studying different ferromagnetic spin ordering of the Mn atoms. There are three such spin ordering apart from the ferromagnetic structure as shown in Table 3.5. The corresponding magnetic anisotropy energy (MAE), magnetic moment (M.M), HOMO-LUMO gap (H-L gap) and the deviation in energy from the ferromagnetic ($As_{21}Ni_9Mn_3$_4) cluster are given below. We find one ferrimagnetically ordered structure S.110, which is almost at the same total energy as the ferromagnetic structure. This isomer has a magnetic moment of 4 μB but has a larger HOMO-LUMO gap of 0.47 eV. The MAE is half of the ferromagnetic structure. The physical picture of the S.110 system is shown below. Another similar isomer S.101 also has same magnetic moment and gap but slightly higher MAE. These studies show that these clusters are chemically stable as indicated by their HOMO-LUMO gaps but can span several spin states at low temperature with an energy difference of a few tenths of meV.

Table 3.5: Data for all possible spin ordering of Mn atom in the $As_{21}Ni_9Mn_3$_0 system

Systems	**MAE (K)**	**M.M (μ_B)**	**H-L gap (eV)**	**E-E_{FM} (eV)**
S.110 ↑↑↓	18.633	4	0.47	-0.15
S.101 ↑↓↑	27.572	4	0.43	-0.10
S.100 ↑↓↓	31.369	2	0.18	0.19

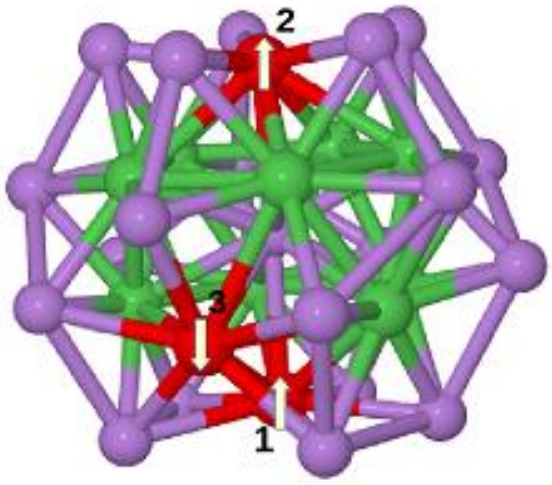

Figure 3.5: Spin ordering (S.110) of Mn atom in $As@Ni_9Mn_3@As_{20}$ system

3.4: $As@Ni_8Mn_4@As_{20}$

For the $As@Ni_8Mn_4@As_{20}$ system there are 6 possible unique structures which can be generated from $As@Ni_8Mn_4@As_{20}$ system by replacing four Ni atoms by Mn atoms. The optimized structures of $As@Ni_8Mn4@As_{20}$ in the ferromagnetic state are shown in Fig. 3.6. The As cage is distorted in these clusters in which the As-As bonds near the Mn ions vary from 2.61 to 3.41 Å. On average, the As-As bonds near Mn atoms increase by 0.12 Å compared to As_{20} cage in parent $As_{21}Ni_{12}$ system. The various calculated electronic and structural properties of these clusters such as HOMO-LUMO gaps, magnetic moments, various bond lengths and magnetic anisotropy energies are presented in Table 3. 6. The symmetry of the parent cluster is broken resulting in magnetic anisotropy energies in these isomers. The spin magnetic moments in these isomers range from 13 to 15 μB within a range of 0.45 eV in total energy. The HOMO-LUMO gap in the lowest energy structure is 0.16 eV and the MAE is 33K. However, as discussed below the ferromagnetic state is higher in energy compared to an anti-ferromagnetic state.

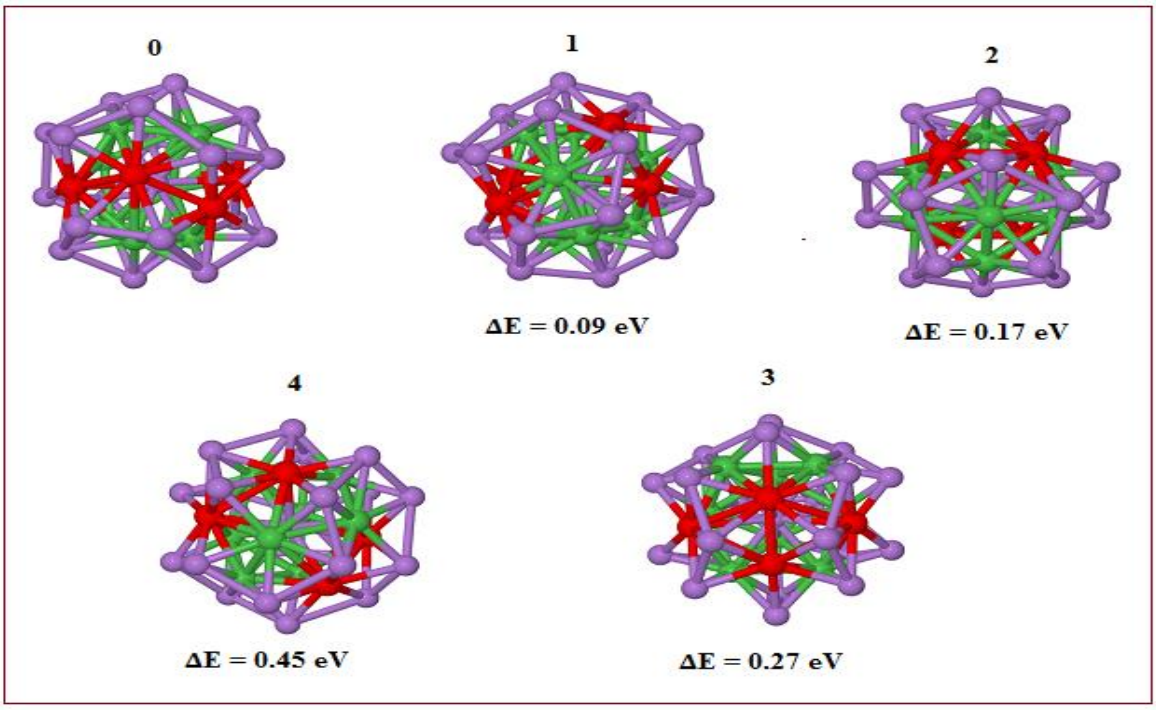

Figure 3.6: All possible combination of $As@Ni_8Mn_4@As_{20}$ system.

Table 3.6: Data for all possible combination of $As@Ni_8Mn_4@As_{20}$ cluster.

Systems	**H-L gap (eV)**	**M.M μ_B**	**M.A.E (K)**	**As-As Å**	**As-Ni Å**	**Ni-Mn Å**	**As-Mn Å**	**Mn-Mn Å**	**Ni-Ni Å**	**Energy (Hartee)**
$As_{21}Ni_8Mn_4$_0	0.16	15	32.82	2.72	2.44	2.77	2.56	2.69	2.65	-63618.01696
$As_{21}Ni_8Mn_4$_1	0.27	15	49.19	2.70	2.45	2.78	2.56	2.64	2.65	-63618.01353
$As_{21}Ni_8Mn_4$_2	0.24	15	57.78	2.68	2.44	2.82	2.55	2.63	2.65	-63618.0105
$As_{21}Ni_8Mn_4$_3	0.21	13	12.12	2.68	2.46	2.68	2.53	2.90	2.73	-63618.00693
$As_{21}Ni_8Mn_4$_4	0.17	15	29.54	2.67	2.45	2.72	2.53	3.07	2.72	-63618.00025

In the above table among all the combinations of the cluster the most favorable (lowest energy) cluster is found to be $As_{21}Ni_8Mn_4$_0 which is indicated by red color. These systems are considered as Ferromagnetic as they have all the spins in the same directions.

3.4.1 Ferrimagnetic Investigation of $As@Ni_8Mn_4@As_{20}$

There are four different spin ordered state for the lowest energy structure from the ferromagnetic calculation. The corresponding Magnetic Anisotropy Energy (MAE), Magnetic Moment (M.M), HOMO-LUMO gap (H-L gap) and the deviation in energy from the ferromagnetic ($As_{21}Ni_8Mn_4$_0) cluster for all the spin ordered isomers are given in Table 3.7. A spin S=1/2 (S.0011) state is lower than the ferromagnetic state by 0.2 eV. The physical picture of the S.0011 system is shown below. In this picture Mn1, Mn2 have spin down and Mn3, Mn4 has spin up.

Table 3.7: Data for all possible spin ordering of Mn atom in the $As_{21}Ni_8Mn_4$_0 system

Systems	**MAE (K)**	**M.M μ_B**	**H-L gap (eV)**	**E-E_{FM} (eV)**
S.0011 ↓↓↑↑	0	1	0.45	-0.20
S.0001 ↓↓↓↑	22.32	5	0.22	0.04
S.0010 ↓↓↑↓	22.16	5	0.22	0.04
S.0100 ↓↑↓↓	32.38	7	0.14	0.36

In the above table it can be seen that the first two system S.0011 has lower energy than the ferromagnetic system.

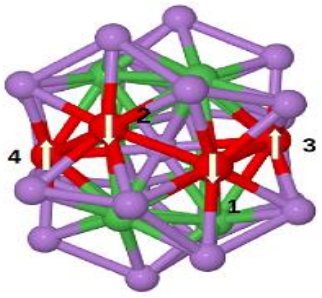

Figure 3.7: Spin ordering (S.0011) of Mn atom in $As@Ni_8Mn_4@As_{20}$ system

3.5: $As@Ni_7Mn_5@As_{20}$

In the parent $As@Ni_{12}@As_{20}$ system, we have doped five Mn atom by replacing any five of the 12 Ni atoms. There are 7 possible resultant isomers of the $As@Ni_7Mn_5@As_{20}$ system. The optimized

structures of the $As@Ni_7Mn_5@As_{20}$ isomers in ferromagnetic state are shown in the Fig. 3.8. Due to the presence of the Mn atoms in the above structures near the Mn atom the As-As bond is increased by 0.05 Å on an average compared to As_{20} cage in $As_{21}Ni_{12}$ system.

The net spin moment and HOMO-LUMO gap of all the above structures are calculated. The presence of Mn atoms breaks the symmetry of the system, resulting the larger magnetic anisotropy compared to the parent cluster. Moreover overall average bond lengths of As-As, Ni-Ni, As-Ni, As-Mn, Ni-Mn in the whole clusters are also computed. In the table below all the detailed information are given.

A comparison of the As-As bond in the doped clusters with that of the parent cluster shows that the As-As bonds are shorter in the doped clusters. Moreover, the binding energy of the cluster increases as the number of the Mn atoms increases. Thus, the doping has a stabilizing effect on the cluster.

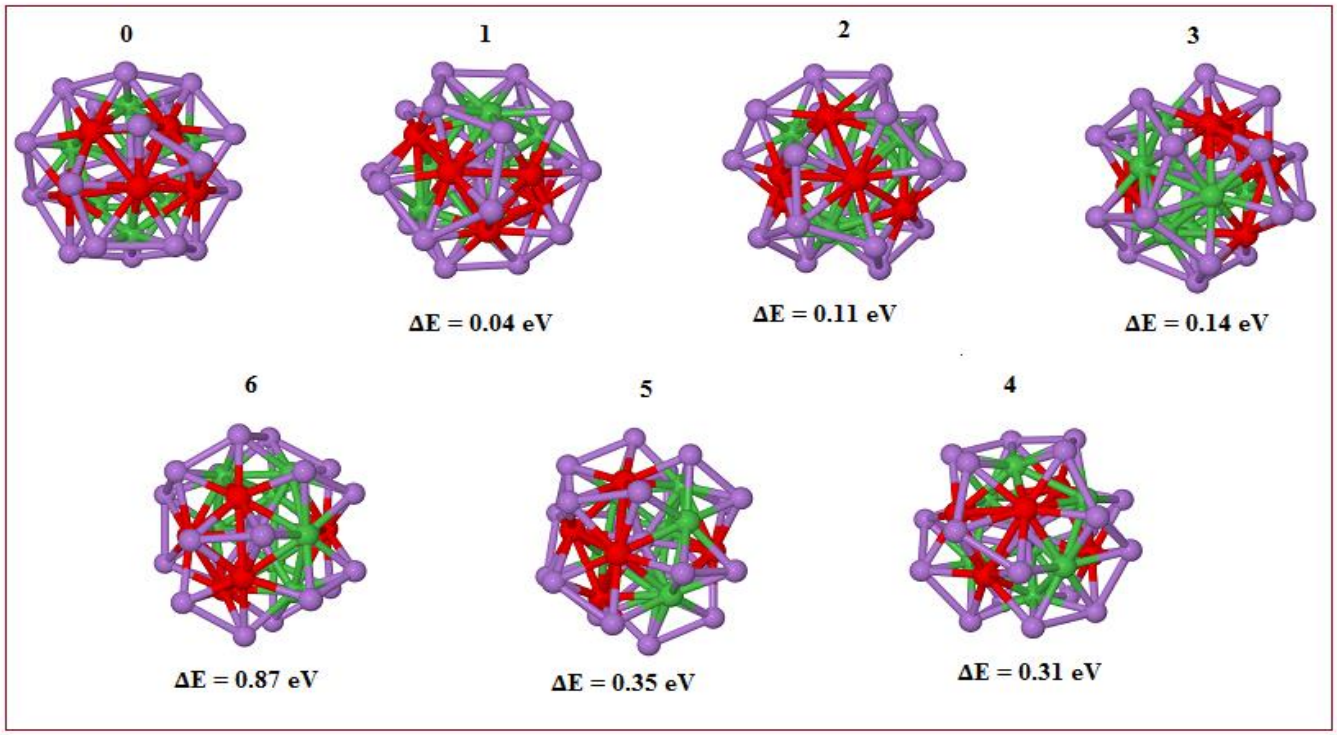

Figure 3.8: All possible combination of $As@Ni_7Mn_5@As_{20}$ cluster according to their energy.

Table 3.8: Data for all possible combination of $As@Ni_7Mn_5@As_{20}$ cluster.

Systems	**H-L gap (eV)**	**M.M μ_B**	**M.A.E (K)**	**As-As Å**	**As-Ni Å**	**Ni-Mn Å**	**As-Mn Å**	**Mn-Mn Å**	**Ni-Ni Å**	**Energy (Hartee)**
$As_{21}Ni_7Mn_5$_0	0.22	14	17.20	2.71	2.44	2.76	2.53	2.64	2.67	-63260.64776
$As_{21}Ni_7Mn_5$_1	0.11	16	19.67	2.69	2.45	2.72	2.54	2.77	2.70	-63260.64615
$As_{21}Ni_7Mn_5$_2	0.21	16	21.14	2.67	2.45	2.76	2.55	2.68	2.65	-63260.64364
As21Ni7Mn5_3	0.11	18	36.74	2.68	2.46	2.75	2.55	2.74	2.67	-63260.64279
As21Ni7Mn5_4	0.12	18	49.27	2.63	2.47	2.73	2.53	2.88	2.72	-63260.63624
As21Ni7Mn5_5	0.24	16	26.93	2.66	2.46	2.75	2.53	2.83	2.71	-63260.63473
As21Ni7Mn5_6	0.22	15	19.43	2.65	2.46	2.75	2.53	2.83	2.71	-63260.61562

In the above table among all the combinations of the cluster, the most favorable one (lowest energy) is found to be $As_{21}Ni_7Mn_5$_0 system which is indicated by red color.

3.5.1 Ferrimagnetic Investigation of $As@Ni_7Mn_5@As_{20}$:

In the $As@Ni_7Mn_5@As_{20}$ cluster it is evident that there are five Mn atoms. The most favorable ferromagnetic cluster ($As_{21}Ni_7Mn_5$_0) from the above table is chosen for different spin ordering of the Mn atoms. All the possible spin ordering of the Mn atoms in this cluster are studied and the corresponding Magnetic Anisotropy Energy (MAE), Magnetic Moment (M.M), HOMO-LUMO gap (H-L gap) and the deviation in energy from the ferromagnetic ($As_{21}Ni_7Mn_5$_0) cluster is also computed.

Table 3.9: Data for different spin ordering of Mn atoms for the $As@Ni_7Mn_5@As_{20}$ system

Systems	**MAE (K)**	**M.M μ_B**	**H-L gap (eV)**	**E-E_{FM} (eV)**
S.01010 ↓↑↓↑↓	11.05	2	0.32	-0.03
S.01001 ↓↑↓↓↑	19.64	2	0.25	0.02
S.01011 ↓↑↓↑↑	7.96	2	0.26	0.00
S.00011 ↓↓↓↑↑	19.79	2	0.32	0.10
S.01000 ↓↑↓↓↓	24.47	10	0.22	0.11
S.00100 ↓↓↑↓↓	21.48	10	0.24	0.13
S.00010 ↓↓↓↑↓	18.94	6	0.3	0.14
S.00110 ↓↓↑↑↓	28.80	4	0.15	0.15
S.00001 ↓↓↓↓↑	20.34	8	0.21	0.24
S.00111 ↓↓↑↑↑	13.08	2	0.18	0.26
S.00101 ↓↓↑↓↑	18.62	4	0.14	0.26
S.01100 ↓↑↑↓↓	8.20	6	0.2	0.32
S.00110 ↓↓↑↑↓	28.80	4	0.15	0.15

In the above table it is evident that the first system (S.01010) have slightly lower energy than the ferromagnetic system. The physical picture of the S.01010 system is shown below. In this picture Mn1, Mn3 and Mn5 have down spin and Mn2, Mn4 have up spin. There are in total three spin states with net magnetic moment 2 μB, which are almost degenerate with the ferromagnetic state. The very small energy difference indicates vanishingly small exchange-interactions between some of the spins. As a result the system can transit from one spin state to another of these states with a small penalty in terms of energy.

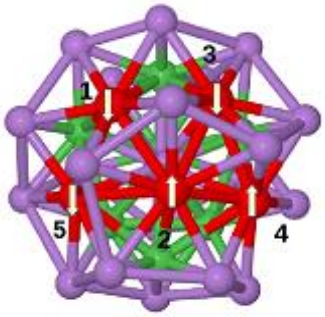

Figure 3.9: Spin ordering (S.01010) of Mn atom in $As@Ni_7Mn_5@As_{20}$ system

3.6: $As@Ni_6Mn_6@As_{20}$:

In the parent $As@Ni_{12}@As_{20}$ system six Mn atoms are doped by replacing any six of the 12 Ni atoms. There are 3 possible resultant isomers of the $As@Ni_6Mn_6@As_{20}$ system. The optimized structure of ferromagnetic $As@Ni_6Mn_6@As_{20}$ isomers are shown in the figure below and the electronic and structural properties of the systems are presented in Table 3.10.

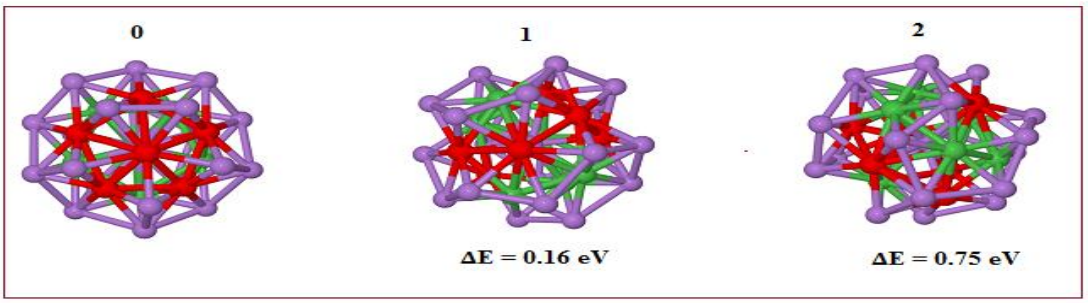

Figure 3.10: All possible combination of $As@Ni_6Mn_6@As_{20}$ cluster according to their energy.

On an average the As-As bond length is increased by 0.02 Å compared to the As_{20} cage in the parent $As_{21}Ni_{12}$ system. The spin magnetic moment of these isomers varies from 15 to 21 μB in these clusters. The lowest structure has six Mn atoms forming a pentagonal pyramid. The magnetic anisotropy energy of the lowest energy isomer is 7K. The binding energy of the six Mn doped cluster increases to 5.48 eV from 4.81 eV in the parent cluster. The gap of 0.25 eV suggests the cluster to be chemically stable. The As-Ni bonds in the parent cluster are shorter compared to the As-Mn bonds. On the other hand As-As bonds are shorter which results in significant distortion of the cluster.

Table 3.10: Data for ferromagnetic isomers of $As@Ni_6Mn_6@As_{20}$ cluster.

Systems	**H-L gap (eV)**	**M.M μ_B**	**M.A.E (K)**	**As-As Å**	**As-Ni Å**	**Ni-Mn Å**	**As-Mn Å**	**Mn-Mn Å**	**Ni-Ni Å**	**Energy (Hartee)**
$As_{21}Ni_6Mn_6$_0	0.25	15	7.20	2.75	2.45	2.71	2.50	2.68	2.70	-62903.27183
$As_{21}Ni_6Mn_6$_1	0.16	21	44.73	2.66	2.47	2.74	2.55	2.80	2.70	-62903.26591
$As_{21}Ni_6Mn_6$_2	0.01	18	31.67	2.68	2.74	2.75	2.54	2.85	2.69	-62903.24426

In the above table it is found that the most favorable (lowest energy) cluster is $As_{21}Ni_6Mn_6$_0.

3.6.1 Ferrimagnetic Investigation of $As@Ni_6Mn_6@As_{20}$

The presence of six Mn atoms in the cluster leads to 32 spin states in total. The most favorable ferromagnetic cluster ($As_{21}Ni_6Mn_6$_0) from the above table is chosen for studying different spin ordering of the Mn atoms. To reduce the computational costs, the anti-ferromagnetic states are first done as single point calculations. Then the lowest 10 isomers are chosen and further optimized. All the possible spin ordering of the Mn atoms in this cluster and the corresponding magnetic anisotropy energy (MAE), magnetic moment (M.M), HOMO-LUMO gap (H-L gap) and the deviation in energy from the ferromagnetic ($As_{21}Ni_7Mn_5$_0) cluster are presented in Table 3.11. As can be seen from the table some of the spin ordered states have zero magnetic moment. Some of the states are almost metallic in character with very small HOMO-LUMO gaps. For ease of reading, the ferromagnetic state is also presented in this table.

Table 3.11: Data for different spin orientation of Mn atoms in $As_{21}Ni_6Mn_6$_0 system from single point calculations.

Systems	**MAE (K)**	**M.M (μ_B)**	**H-L gap (eV)**	**E-E_{FM} (eV)**
S.000000 ↓↓↓↓↓↓	7.09	15	0.25	0.00
S.001000 ↓↓↑↓↓↓	9.92	11	0.09	0.20
S.000100 ↓↓↓↑↓↓	11.23	11	0.13	0.20
S.010000 ↓↑↓↓↓↓	4.73	13	0.12	0.28
S.000110 ↓↓↓↑↑↓	17.55	5	0.19	0.30
S.001010 ↓↓↑↓↑↓	17.84	5	0.19	0.30
S.000001 ↓↓↓↓↓↑	39.20	11	0.08	0.34
S.010100 ↓↑↓↑↓↓	29.18	5	0.13	0.38
S.011111 ↓↑↑↑↑↑	16.14	9.03	0.02	0.38
S.000111 ↓↓↓↑↑↑	0.00	1	0.1	0.41
S.001011 ↓↓↑↓↑↑	0.00	1	0.07	0.41
S.000010 ↓↓↓↓↑↓	29.04	9	0.06	0.42
S.010111 ↓↑↓↑↑↑	18.05	3	0.05	0.42
S.011110 ↓↑↑↑↑↓	26.86	5	0.1	0.43
S.001110 ↓↓↑↑↑↓	0.00	1	0.05	0.45
S.010001 ↓↑↓↓↓↑	23.08	7	0.05	0.45

S.011000 ↓↑↑↓↓↓	20.29	7	0.11	0.46
S.010101 ↓↑↓↑↓↑	0.00	1	0.14	0.46
S.000101 ↓↓↓↑↓↑	20.19	7	0.13	0.47
S.001001 ↓↓↑↓↓↑	20.20	7	0.13	0.47
S.001111 ↓↓↑↑↑↑	9.25	3	0.09	0.47
S.011011 ↓↑↑↓↑↑	29.08	3	0.09	0.49
S.001100 ↓↓↑↑↓↓	4.28	7	0.11	0.54
S.010110 ↓↑↓↑↑↓	0.00	1	0.09	0.56
S.000011 ↓↓↓↓↑↑	19.81	5	0.07	0.58
S.011001 ↓↑↑↓↓↑	42.07	3	0.11	0.58
S.011010 ↓↑↑↓↑↓	0.00	1	0.07	0.61
S.010010 ↓↑↓↓↑↓	18.19	5	0.12	0.65
S.010011 ↓↑↓↓↑↑	0.00	1	0.07	0.66
S.011101 ↓↑↑↑↓↓	39.24	3	0.04	0.68
S.011100 ↓↑↑↑↓↓	0.00	1	0.07	0.69
S.001101 ↓↓↑↑↓↑	0.00	1	0.08	0.78

The spin ordering of the clusters in the above table are arranged according to their energy. From the table it is evident that the ferromagnetic or antiferromagnetic states are much higher in energy compared to the ferromagnetic state. The lowest 10 spin ordered states of the cluster are selected and optimized by running several iteration in order to find the lower energy clusters compared to the ferromagnetic one.

Table 3.12: Data for the first 10 different spin-ordering of Mn atom in $As_{21}Ni_6Mn_6$_0 system

Systems	**MAE (K)**	**M.M (μ_B)**	**H-L gap (eV)**	**E-E_{FM} (eV)**
S.010100 ↓↑↓↑↓↓	12.62	5	0.32	-0.29
S.000110 ↓↓↓↑↑↓	9.93	5	0.4	-0.25
S.001010 ↓↓↑↓↑↓	10.13	5	0.4	-0.25
S.000100 ↓↓↓↑↓↓	9.34	9	0.15	-0.20
S.001000 ↓↓↑↓↓↓	8.65	9	0.12	-0.14
S.010000 ↓↑↓↓↓↓	16.50	11	0.18	-0.06
S.000111 ↓↓↓↑↑↑	0.00	1	0.22	0.01
S.000000 ↓↓↓↓↓↓	4.85	15	0.25	0.02
S.000001 ↓↓↓↓↓↑	39.45	9	0.03	0.04
S.011111 ↓↑↑↑↑↑	20.15	9	0.0	0.02

In the above table it is evident that the first six clusters have lower energy compared to the ferromagnetic case. The cluster with spin ordering S.010100 has the lowest energy and it can be considered

as the most favorable cluster of the $As@Ni_6Mn_6@As_{20}$ system which has magnetic anisotropy energy of 12.6 K. The picture of the spin ordering S.010100 is given below. Similar to the other clusters studied here, this cluster also has several closely spaced spin states with nearly same magnetic moment. It can be mentioned here that the bare Mn6 cluster also has a ferromagnetic spin arrangement but the preferred structure is octahedral with a magnetic moment of 9 μB. Experimentally determined value of magnetic moment of the bare Mn6 cluster ranges from 2-4 μB at temperature of 50K. The magnetic anisotropy energy of the bare Mn6 cluster is 0K compared to the 12K of the $As@Mn_6Ni_6@As_{20}$ cluster. The spin moment on the individual Mn ions in $As@Ni_6Mn_6@As_{20}$ ranges from 2 – 3 μB compared to the 3.7 μB in the bare Mn6 cluster. These comparisons show that the bonding of the Mn ions with the As and Ni atoms reduces the individual spin moments.

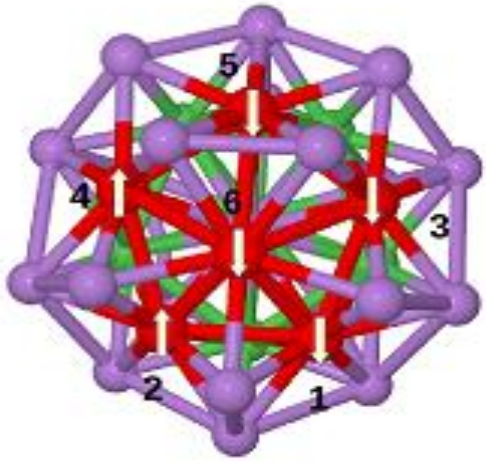

Figure 3.11: Spin ordering (S.010100 ↓ ↑ ↓ ↑ ↓ ↓) of Mn atom in $As@Ni_6Mn_6@As_{20}$ system.

3.7: $As@Ni_5Mn_7@As_{20}$

In the parent $As@Ni_{12}@As_{20}$ system seven Mn atoms are doped by replacing seven of the 12 Ni atoms. Five such stable ferromagnetic isomers of the $As@Ni_5Mn_7@As_{20}$ system are obtained. These optimized isomers are shown in Fig. 3.12 and their properties are listed in Table 3.13. Due to the presence of the Mn atoms in the above structures near the Mn atom the As-As bond is varied from 3.37 Å to 2.49 Å. An average increment of 0.03 Å is seen for the As-As bonds compared to the parent cluster. The

favorable (lowest energy) cluster ($As_{21}Ni_5Mn_7$_0) is indicated by the red color in the table. The lowest energy cluster is stable with a HOMO-LUMO gap of 0.20 eV and has a magnetic moment of 22 μB. This cluster has magnetic anisotropy energy of 27K. One of the isomers ($As_{21}Ni_5Mn_7$_5) has very low gap between the HOMO and LUMO. So this system can be considered as metallic.

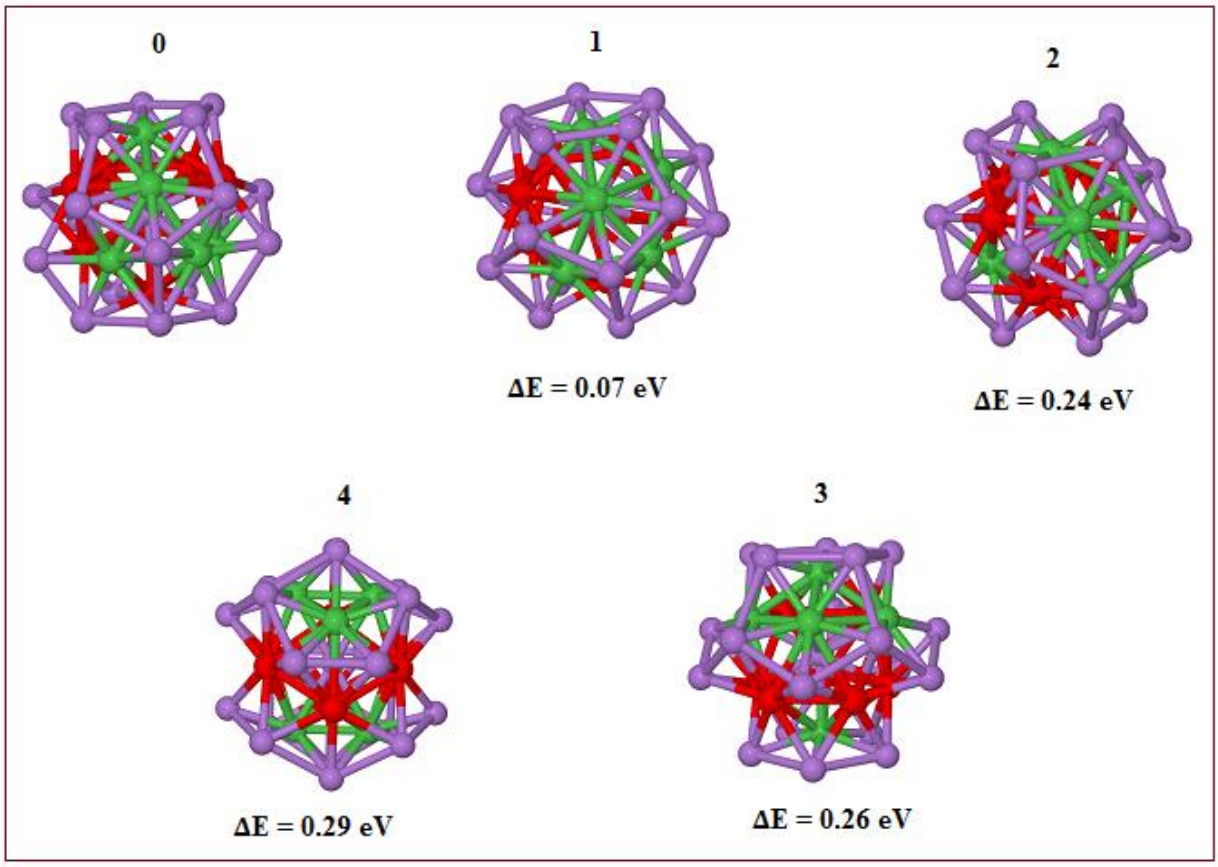

Figure 3.12: All possible combination of $As@Ni_5Mn_7@As_{20}$ cluster according to their energy.

It is evident from the figure that As_{20} cage is broken. Due to the presence of the Mn atoms in the above structures near the Mn atom the As-As bond is varied from 3.37 Å to 2.49 Å. On an average the bond length is increased by 0.03 Å compared to As20 cage in $As_{21}Ni_{12}$ system.

The net spin moment and HOMO-LUMO gap of all the above structures are calculated. Due to the breaking of symmetry, the resulting magnetic anisotropy compared to the parent cluster become larger.

Average bond lengths of As-As, Ni-Ni, As-Ni, As-Mn, Ni-Mn in the whole clusters are also computed. In the table below all the detailed information are given.

Table 3.13: Data for all the possible combination of $As@Ni_5Mn_7@As_{20}$ cluster.

Systems	**H-L gap (eV)**	**M.M μ_B**	**M.A.E (K)**	**As-As Å**	**As-Ni Å**	**Ni-Mn Å**	**As-Mn Å**	**Mn-Mn Å**	**Ni-Ni Å**	**Energy (Hartee)**
$As_{21}Ni_5Mn_7$_0	0.2	22	27.41	2.65	2.46	2.76	2.55	2.73	2.65	-62545.91441
$As_{21}Ni_5Mn_7$_1	0.24	18	10.55	2.69	2.44	2.74	2.51	2.68	2.67	-62545.9117
$As_{21}Ni_5Mn_7$_2	0.1	18	27.30	2.69	2.45	2.73	2.51	2.67	2.68	-62545.90552
$As_{21}Ni_5Mn_7$_3	0.19	18	22.58	2.69	2.45	2.73	2.51	2.67	2.68	-62545.90485
$As_{21}Ni_5Mn_7$_4	0.04	20	35.97	2.68	2.44	2.78	2.55	2.70	2.59	-62545.90392

3.7.1: Ferrimagnetic Investigation of $As@Ni_5Mn_7@As_{20}$

The most favorable ferromagnetic cluster ($As_{21}Ni_5Mn_7$_0) from the above table is chosen for studying different ferromagnetic spin ordering of the Mn atoms. As the number of the Mn atoms increases, the number of possible ferromagnetic isomers also increases. To keep the computations tractable, we first performed a single point calculation on all the possible spin ordered isomers. The corresponding magnetic anisotropy energy (MAE), magnetic moment (M.M), HOMO-LUMO gap (H-L gap) and the deviation in energy from the ferromagnetic ($As_{21}Ni_5Mn_7$_0) cluster are presented in Table 3.14. We have included the ferromagnetic state in the table for the sake of completion.

Table 3.14: Data for different spin configuration of Mn atom in the $As_{21}Ni_5Mn_7$_0 system

Systems	**Systems**	**MAE (K)**	**M.M (μ_B)**	**H-L gap (eV)**	**E-E_{FM} (eV)**
S.0000000	↓↓↓↓↓↓↓	27.5	22.0	0.2	0.0
S.0111110	↓↑↑↑↑↑↓	26.3	8.0	0.1	0.1
S.0011000	↓↓↑↑↓↓↓	28.1	8.0	0.3	0.2
S.0001000	↓↓↓↑↓↓↓	30.0	14.0	0.1	0.2
S.0100000	↓↑↓↓↓↓↓	22.1	16.0	0.1	0.2
S.0000010	↓↓↓↓↓↑↓	33.7	14.0	0.2	0.3
S.0011010	↓↓↑↑↓↑↓	0.0	0.0	0.2	0.3
S.0111100	↓↑↑↑↑↓↓	16.8	2.0	0.1	0.3
S.0100110	↓↑↓↓↑↑↓	40.1	4.0	0.2	0.4
S.0000110	↓↓↓↓↑↑↓	30.7	8.0	0.2	0.4
S.0100100	↓↑↓↓↑↓↓	21.6	10.0	0.2	0.4
S.0110110	↓↑↑↓↑↑↓	26.6	2.0	0.1	0.4
S.0000100	↓↓↓↓↑↓↓	29.2	16.0	0.2	0.4
S.0111000	↓↑↑↑↓↓↓	22.8	4.0	0.1	0.4
S.0011110	↓↓↑↑↑↑↓	38.2	2.0	0.0	0.4
S.0010000	↓↓↑↓↓↓↓	35.4	14.0	0.1	0.4
S.0110000	↓↑↑↓↓↓↓	26.7	8.0	0.1	0.4
S.0011111	↓↓↑↑↑↑↑	27.0	8.0	0.2	0.4
S.0011100	↓↓↑↑↑↓↓	15.5	4.0	0.2	0.5
S.0110100	↓↑↑↓↑↓↓	43.4	4.0	0.1	0.5
S.0000001	↓↓↓↓↓↓↑	54.1	16.0	0.2	0.5

S.0001010	↓↓↓↑↓↑↓	46.9	8.0	0.0	0.5
S.0000011	↓↓↓↓↓↑↑	29.9	10.0	0.1	0.5
S.0100010	↓↑↓↓↓↑↓	23.3	8.0	0.2	0.5
S.0011011	↓↓↑↑↓↑↑	31.9	4.0	0.2	0.5
S.0010010	↓↓↑↓↓↑↓	42.7	8.0	0.1	0.6
S.0100111	↓↑↓↓↑↑↑	0.0	0.0	0.1	0.6
S.0111101	↓↑↑↑↑↓↑	24.0	8.0	0.2	0.6
S.0110111	↓↑↑↓↑↑↑	15.4	6.0	0.1	0.6
S.0101110	↓↑↓↑↑↑↓	30.9	2.0	0.2	0.6
S.0101000	↓↑↓↑↓↓↓	46.0	9.9	0.0	0.6
S.0000111	↓↓↓↓↑↑↑	31.3	4.0	0.1	0.6
S.0001110	↓↓↓↑↑↑↓	28.8	4.0	0.0	0.6
S.0010110	↓↓↑↓↑↑↓	28.6	4.0	0.2	0.6
S.0001100	↓↓↓↑↑↓↓	34.3	10.0	0.1	0.6
S.0111011	↓↑↑↑↓↑↑	29.8	8.0	0.2	0.6
S.0001001	↓↓↓↑↓↓↑	30.5	8.0	0.2	0.7
S.0011001	↓↓↑↑↓↓↑	35.7	4.0	0.1	0.7
S.0001011	↓↓↓↑↓↑↑	38.8	4.0	0.1	0.7
S.0010100	↓↓↑↓↑↓↓	25.1	10.0	0.1	0.7
S.0101100	↓↑↓↑↑↓↓	22.9	4.0	0.1	0.7
S.0010111	↓↓↑↓↑↑↑	0.0	0.0	0.1	0.7
S.0100101	↓↑↓↓↑↓↑	28.8	6.0	0.2	0.7
S.0111001	↓↑↑↑↓↓↑	39.4	2.0	0.1	0.7

S.0100011	↓↑↓↓↓↑↑	31.9	4.0	0.2	0.7
S.0110101	↓↑↑↓↑↓↑	0.0	0.0	0.2	0.8
S.0001111	↓↓↓↑↑↑↑	0.0	0.0	0.1	0.8
S.0100001	↓↑↓↓↓↓↑	20.1	10.0	0.0	0.8
S.0111010	↓↑↑↑↓↑↓	58.8	2.0	0.1	0.8
S.0010011	↓↓↑↓↓↑↑	16.5	4.0	0.1	0.8
S.0101111	↓↑↓↑↑↑↑	21.4	6.0	0.1	0.8
S.0010001	↓↓↑↓↓↓↑	40.7	10.0	0.2	0.8
S.0011101	↓↓↑↑↑↓↑	0.0	0.0	0.1	0.8
S.0101010	↓↑↓↑↓↑↓	13.8	2.0	0.2	0.8
S.0110011	↓↑↑↓↓↑↑	38.5	2.0	0.1	0.8
S.0000101	↓↓↓↓↑↓↑	46.3	12.0	0.1	0.9
S.0110001	↓↑↑↓↓↓↑	44.4	6.0	0.0	0.9
S.0101011	↓↑↓↑↓↑↑	21.5	2.0	0.1	1.0
S.0101001	↓↑↓↑↓↓↑	27.6	4.0	0.1	1.0
S.0010101	↓↓↑↓↑↓↑	30.6	6.0	0.1	1.0
S.0001101	↓↓↓↑↑↓↑	20.7	6.0	0.1	1.1
S.0101101	↓↑↓↑↑↓↑	0.0	0.2	0.0	1.1

The spin ordering of Mn atoms in the cluster are arranged according to their energy. The first 10 spin ordering of the cluster are selected and again optimized in order to find the lower energy clusters compare to the ferromagnetic one. These optimized clusters are again investigated by computing MAE, M.M, H-L gap and $E\text{-}E_{FM}$ which are shown in the table below.

Table 3.15: Data for the lowest 10 spin ordered isomers of Mn atoms in the $As@Ni_5Mn_7@As_{20}$ cluster

Systems		MAE (K)	M.M (μ_B)	H-L gap (eV)	E-E_{FM} (eV)
S.0111110	↓↑↑↑↑↑↓	24.5	8.0	0.4	-0.2
S.0011010	↓↓↑↑↓↑↓	0.0	0.0	0.3	-0.2
S.0011000	↓↓↑↑↓↓↓	26.2	8.0	0.4	-0.2
S.0100100	↓↑↓↓↑↓↓	21.6	10.0	0.2	-0.2
S.0100000	↓↑↓↓↓↓↓	24.4	16.0	0.3	-0.1
S.0000110	↓↓↓↓↑↑↓	24.4	8.0	0.3	-0.1
S.0111100	↓↑↑↑↑↓↓	15.8	2.0	0.2	-0.1
S.0000000	↓↓↓↓↓↓↓	25.5	22.0	0.3	0.0
S.0000010	↓↓↓↓↓↑↓	32.0	14.0	0.2	0.0
S.0100110	↓↑↓↓↑↑↓	19.8	4.0	0.2	0.0
S.0001000	↓↓↓↑↓↓↓	27.1	14.0	0.2	0.0

It is evident from the table that the first seven clusters have lower energy compare to the ferromagnetic case. The cluster with spin ordering S.0111110 has the lowest energy and it can be considered as the most favorable cluster of the $As@Ni_5Mn_7@As_{20}$ system which has the magnetic anisotropy energy of 24.5 K. In the S.0111110 spin ordering cluster, two of the Mn atoms have spin down (0) and the other Mn atoms have up spin (1). Similar to the other clusters studied in this work, the Mn7 doped cluster also has several very low-lying isomers. Thus the magnetic state even in low temperature can be transient. Moreover, the anisotropy energy is about 25K which shows that the zero field splitting is small.

3.8: $As@Ni_4Mn_8@As_{20}$

In the parent $As@Ni_{12}@As_{20}$ system eight Mn atoms are doped by replacing eight of the 12 Ni atoms. There are 8 unique possible resultant structures of the $As@Ni_4Mn_8@As_{20}$ systems which are shown in the figure below.

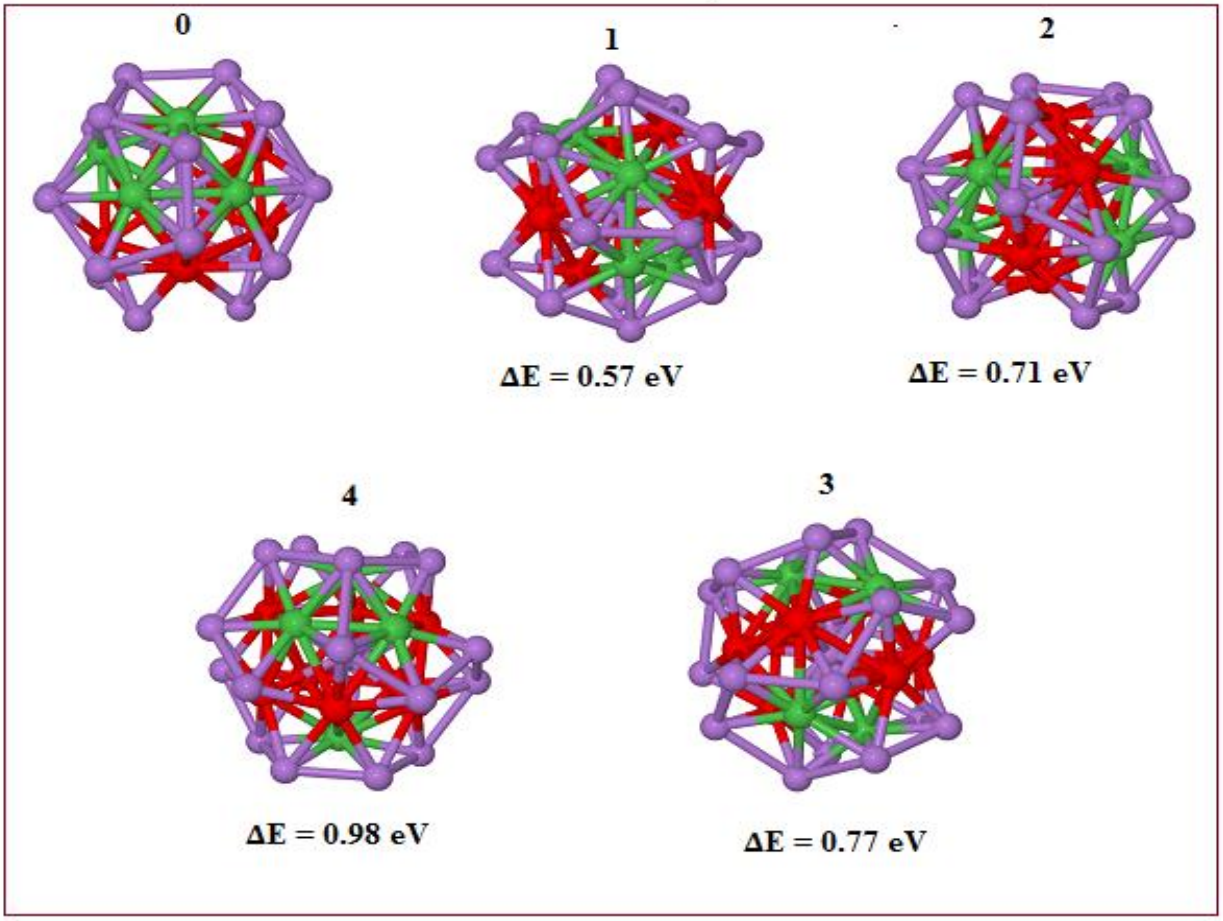

Figure 3.13: All possible combination of $As@Ni_4Mn_8@As_{20}$ cluster according to their energy.

It is evident from the figure that As_{20} cage is broken from the parent molecule. Due to the presence of the Mn atoms in the above structures near the Mn atom the As-As bond is varied from 3.39 Å to 2.42 Å. On an average the bond length is increased by 0.17 Å compared to As_{20} cage in $As_{21}Ni_{12}$ system.

The net spin moment and HOMO-LUMO gap of all the above structures are calculated. Due to the breaking of symmetry, the resulting magnetic anisotropy compared to the parent cluster become larger.

Average bond lengths of As-As, Ni-Ni, As-Ni, As-Mn, Ni-Mn in the whole clusters are also computed. In the table below all the detailed information are given.

Table 3.16: Data for all possible combination of $As@Ni_4Mn_8@As_{20}$ cluster.

Systems	**H-L gap (eV)**	**M.M μ_B**	**M.A.E (K)**	**As-As Å**	**As-Ni Å**	**Ni-Mn Å**	**As-Mn Å**	**Mn-Mn Å**	**Ni-Ni Å**	**Energy (Hartee)**
$As_{21}Ni_4Mn_8$_0	0.27	21	25.19	2.63	2.45	2.75	2.52	2.71	2.68	-62188.55912
$As_{21}Ni_4Mn_8$_1	0.19	21	35.19	2.65	2.46	2.73	2.52	2.68	2.73	-62188.53794
$As_{21}Ni_4Mn_8$_2	0.17	17	20.96	2.71	2.45	2.74	2.50	2.66	2.66	-62188.53286
$As_{21}Ni_4Mn_8$_3	0.17	17	20.94	2.71	2.45	2.74	2.50	2.66	2.67	-62188.53064
$As_{21}Ni_4Mn_8$_4	0.04	21	12.85	2.68	2.45	2.73	2.51	2.69	2.70	-62188.52288

The most favorable (lowest energy) cluster in the above table is $As_{21}Ni_4Mn_8$_0.

3.8.1 Ferrimagnetic Investigation of $As@Ni_4Mn_8@As_{20}$

In the $As@Ni_4Mn_8@As_{20}$ cluster it is evident that there are eight Mn atoms. The most favorable ferromagnetic cluster ($As_{21}Ni_4Mn_8$_1) from the above table is chosen for studying different spin ordering of the Mn atoms. All the possible spin ordering of the Mn atoms in this cluster are studied and the corresponding Magnetic Anisotropy Energy (MAE), Magnetic Moment (M.M), HOMO-LUMO gap (H-L gap) and the deviation in energy from the ferromagnetic ($As_{21}Ni_4Mn_8$_0) cluster is also computed.

Table 3.17: Data for different spin configuration of Mn atom in $As_{21}Ni_4Mn_8$_0 system

Systems		**MAE (K)**	**M.M μ_B**	**H-L gap(eV)**	**E-E_{FM} (eV)**
S.00000000	↓↓↓↓↓↓↓↓	25.2	21.0	0.3	0.0
S.00000010	↓↓↓↓↓↓↑↓	25.6	15.0	0.1	0.4
S.00001000	↓↓↓↓↑↓↓↓	19.7	15.0	0.1	0.5
S.00000001	↓↓↓↓↓↓↓↑	24.7	17.0	0.1	0.5

S.00010000	↓↓↓↑↓↓↓↓	30.4	15.0	0.1	0.5
S.00001010	↓↓↓↓↑↓↑↓	28.0	11.0	0.0	0.6
S.00000011	↓↓↓↓↓↓↑↑	34.1	11.0	0.1	0.6
S.01101010	↓↑↑↓↑↓↑↓	0.0	1.0	0.2	0.7
S.00100000	↓↓↑↓↓↓↓↓	25.4	17.0	0.1	0.7
S.00010001	↓↓↓↑↓↓↓↑	26.0	9.0	0.1	0.7
S.00011000	↓↓↓↑↑↓↓↓	41.2	11.0	0.1	0.7
S.00000100	↓↓↓↓↓↑↓↓	31.0	17.0	0.1	0.7
S.00001001	↓↓↓↓↑↓↓↑	13.2	9.0	0.1	0.7
S.01100101	↓↑↑↓↓↑↓↑	23.7	3.0	0.1	0.7
S.00010010	↓↓↓↑↓↓↑↓	38.4	11.0	0.1	0.7
S.01000000	↓↑↓↓↓↓↓↓	30.3	17.0	0.1	0.7
S.01000001	↓↑↓↓↓↓↓↑	30.1	11.0	0.2	0.7
S.01101101	↓↑↑↓↑↑↓↑	23.9	3.5	0.0	0.7
S.01101011	↓↑↑↓↑↓↑↑	30.6	7.0	0.2	0.7
S.01000010	↓↑↓↓↓↓↑↓	24.5	11.0	0.2	0.7
S.01100001	↓↑↑↓↓↓↓↑	31.0	7.0	0.2	0.7
S.00000101	↓↓↓↓↓↑↓↑	32.1	11.0	0.2	0.7
S.01001011	↓↑↓↓↑↓↑↑	0.0	1.0	0.1	0.8
S.00011010	↓↓↓↑↑↓↑↓	19.5	3.0	0.1	0.8
S.01111100	↓↑↑↑↑↑↓↓	21.3	5.0	0.1	0.8
S.01001000	↓↑↓↓↑↓↓↓	16.7	11.0	0.1	0.8
S.01001001	↓↑↓↓↑↓↓↑	17.9	7.0	0.1	0.8
S.01111001	↓↑↑↑↑↓↓↑	22.8	5.0	0.1	0.8
S.00100010	↓↓↑↓↓↓↑↓	22.7	11.0	0.2	0.8
S.01101100	↓↑↑↓↑↑↓↓	0.0	1.0	0.2	0.8
S.00010100	↓↓↓↑↓↑↓↓	26.8	11.0	0.1	0.8
S.00101101	↓↓↑↓↑↑↓↑	0.0	1.0	0.2	0.8
S.00001011	↓↓↓↓↑↓↑↑	21.2	3.0	0.1	0.8
S.01110001	↓↑↑↑↓↓↓↑	0.0	1.0	0.2	0.8
S.00101000	↓↓↑↓↑↓↓↓	26.4	11.0	0.2	0.8

S.00100101	↓↓↑↓↓↑↓↑	21.6	7.0	0.2	0.8
S.01000011	↓↑↓↓↓↓↑↑	18.5	5.0	0.1	0.8
S.00001100	↓↓↓↓↑↑↓↓	26.0	11.0	0.1	0.8
S.01101001	↓↑↑↓↑↓↓↑	34.4	2.5	0.0	0.8
S.00101010	↓↓↑↓↑↓↑↓	21.5	5.0	0.1	0.8
S.01110101	↓↑↑↑↓↑↓↑	126.8	-3.0	0.0	0.8
S.01010000	↓↑↓↑↓↓↓↓	41.0	11.0	0.1	0.8
S.01111110	↓↑↑↑↑↑↑↓	46.8	-9.0	0.1	0.9
S.00110100	↓↓↑↑↓↑↓↓	21.6	7.0	0.2	0.9
S.01011000	↓↑↓↑↑↓↓↓	18.3	5.0	0.1	0.9
S.01011001	↓↑↓↑↑↓↓↑	0.0	-1.0	0.2	0.9
S.00100001	↓↓↑↓↓↓↓↑	22.0	11.0	0.1	0.9
S.00010101	↓↓↓↑↓↑↓↑	35.3	7.0	0.1	0.9
S.01010001	↓↑↓↑↓↓↓↑	20.0	5.0	0.1	0.9
S.01101110	↓↑↑↓↑↑↑↓	23.9	-3.0	0.1	0.9
S.00111101	↓↓↑↑↑↑↓↑	35.8	-5.0	0.1	0.9
S.01111000	↓↑↑↑↑↓↓↓	0.0	1.0	0.1	0.9
S.01001010	↓↑↓↓↑↓↑↓	22.2	7.0	0.0	0.9
S.00011100	↓↓↓↑↑↑↓↓	20.5	5.0	0.2	0.9
S.00110000	↓↓↑↑↓↓↓↓	39.6	11.0	0.1	0.9
S.00010011	↓↓↓↑↓↓↑↑	17.5	3.0	0.1	0.9
S.01100111	↓↑↑↓↓↑↑↑	42.3	-3.0	0.0	0.9
S.00010110	↓↓↓↑↓↑↑↓	22.9	7.0	0.1	0.9
S.00000110	↓↓↓↓↓↑↑↓	27.0	13.0	0.1	0.9
S.00101001	↓↓↑↓↑↓↓↑	18.2	7.0	0.1	0.9
S.00100011	↓↓↑↓↓↓↑↑	24.2	5.0	0.2	0.9
S.00001110	↓↓↓↓↑↑↑↓	21.6	7.0	0.2	0.9
S.01111010	↓↑↑↑↑↓↑↓	31.1	-7.0	0.2	0.9
S.01100000	↓↑↑↓↓↓↓↓	29.8	13.0	0.1	0.9
S.00111100	↓↓↑↑↑↑↓↓	0.0	1.0	0.1	0.9
S.01100011	↓↑↑↓↓↓↑↑	0.0	1.0	0.1	0.9

S.00001101	↓↓↓↓↑↑↓↑	28.0	5.0	0.2	0.9
S.00010111	↓↓↓↑↓↑↑↑	0.0	1.0	0.1	0.9
S.00110110	↓↓↑↑↓↑↑↓	0.0	1.0	0.2	1.0
S.00110101	↓↓↑↑↓↑↓↑	0.0	1.0	0.1	1.0
S.01110100	↓↑↑↑↓↑↓↓	16.5	3.0	0.1	1.0
S.01000101	↓↑↓↓↓↑↓↑	26.6	7.0	0.1	1.0
S.01011010	↓↑↓↑↑↓↑↓	0.0	1.1	0.0	1.0
S.00110010	↓↓↑↑↓↓↑↓	26.6	5.0	0.2	1.0
S.01111011	↓↑↑↑↑↓↑↑	31.7	-11.0	0.0	1.0
S.01011101	↓↑↓↑↑↑↓↑	31.9	3.2	0.0	1.0
S.00000111	↓↓↓↓↓↑↑↑	33.2	7.0	0.1	1.0
S.01001101	↓↑↓↓↑↑↓↑	0.0	1.0	0.1	1.0
S.00100100	↓↓↑↓↓↑↓↓	27.7	11.0	0.1	1.0
S.00011110	↓↓↓↑↑↑↑↓	0.0	1.0	0.1	1.0
S.00101011	↓↓↑↓↑↓↑↑	0.0	1.0	0.1	1.0
S.01000100	↓↑↓↓↓↑↓↓	24.3	11.0	0.1	1.0
S.01100100	↓↑↑↓↓↑↓↓	18.1	9.0	0.2	1.0
S.00111000	↓↓↑↑↑↓↓↓	29.2	7.0	0.1	1.1
S.00100111	↓↓↑↓↓↑↑↑	25.8	3.0	0.1	1.1
S.01110000	↓↑↑↑↓↓↓↓	29.7	7.0	0.1	1.1
S.01010101	↓↑↓↑↓↑↓↑	44.2	3.0	0.1	1.1
S.00111001	↓↓↑↑↑↓↓↑	0.0	1.0	0.1	1.1
S.01010010	↓↑↓↑↓↓↑↓	39.5	5.0	0.1	1.1
S.01011111	↓↑↓↑↑↑↑↑	16.4	-9.0	0.1	1.1
S.01001100	↓↑↓↓↑↑↓↓	38.5	5.0	0.1	1.1
S.00110001	↓↓↑↑↓↓↓↑	39.6	7.0	0.1	1.1
S.00011001	↓↓↓↑↑↓↓↑	24.7	4.9	0.0	1.1
S.01100010	↓↑↑↓↓↓↑↓	33.3	7.0	0.1	1.1
S.00111110	↓↓↑↑↑↑↑↓	26.8	3.1	0.0	1.1
S.00101111	↓↓↑↓↑↑↑↑	26.0	-3.0	0.1	1.1
S.00101100	↓↓↑↓↑↑↓↓	14.1	7.0	0.1	1.1

S.00011101	↓↓↓↑↑↑↓↑	0.0	-1.0	0.1	1.1
S.00110111	↓↓↑↑↓↑↑↑	33.0	-3.0	0.0	1.1
S.01011100	↓↑↓↑↑↑↓↓	0.0	1.0	0.1	1.1
S.01010100	↓↑↓↑↓↑↓↓	37.0	5.0	0.1	1.1
S.01110110	↓↑↑↑↓↑↑↓	0.0	-1.0	0.1	1.1
S.00111010	↓↓↑↑↑↓↑↓	0.0	-1.0	0.1	1.1
S.01110011	↓↑↑↑↓↓↑↑	18.8	-5.0	0.1	1.2
S.00100110	↓↓↑↓↓↑↑↓	22.5	9.0	0.1	1.2
S.01000111	↓↑↓↓↓↑↑↑	31.0	3.0	0.1	1.2
S.01100110	↓↑↑↓↓↑↑↓	14.2	3.0	0.1	1.2
S.00101110	↓↓↑↓↑↑↑↓	23.0	3.0	0.1	1.2
S.01010011	↓↑↓↑↓↓↑↑	0.0	-1.0	0.1	1.2
S.01010110	↓↑↓↑↓↑↑↓	0.0	1.0	0.1	1.2
S.01000110	↓↑↓↓↓↑↑↓	22.5	9.0	0.1	1.2
S.01110010	↓↑↑↑↓↓↑↓	0.0	1.0	0.1	1.2
S.00011111	↓↓↓↑↑↑↑↑	34.6	5.0	0.0	1.3
S.01001110	↓↑↓↓↑↑↑↓	12.7	3.0	0.1	1.3
S.00110011	↓↓↑↑↓↓↑↑	0.0	1.0	0.1	1.3
S.00111011	↓↓↑↑↑↓↑↑	35.8	5.2	0.0	1.3
S.01011011	↓↑↓↑↑↓↑↑	29.9	6.1	0.0	1.4

The spin ordering of Mn atoms in the cluster are arranged according to their energy as shown in the table above. The lowest 10 different spin ordering of the cluster are selected and again optimized by running several iteration in order to find the lower energy clusters compare to the ferromagnetic one. These optimized clusters are again investigated by computing MAE, M.M, H-L gap and $E\text{-}E_{FM}$ which are shown in the table below.

Table 3.18: Data for the first 10 lower energy spin ordering of the $As@Ni_4Mn_8@As_{20}$ cluster

Systems		MAE (K)	M.M μ_B	H-L gap (eV)	E-E_{FM} (eV)
S.00000010	↓ ↓ ↓ ↓ ↓ ↓ ↑ ↓	21.4	15.0	0.2	0.1
S.00001010	↓ ↓ ↓ ↓ ↑ ↓ ↑ ↓	16.9	9.0	0.1	0.2
S.00010000	↓ ↓ ↓ ↑ ↓ ↓ ↓ ↓	27.1	15.0	0.1	0.3
S.00010001	↓ ↓ ↓ ↑ ↓ ↓ ↓ ↑	14.7	9.0	0.1	0.4
S.00011000	↓ ↓ ↓ ↑ ↑ ↓ ↓ ↓	20.5	9.0	0.1	0.4
S.00100000	↓ ↓ ↑ ↓ ↓ ↓ ↓ ↓	30.7	17.0	0.2	0.4
S.00000001	↓ ↓ ↓ ↓ ↓ ↓ ↓ ↑	32.2	15.0	0.1	0.6
S.00000011	↓ ↓ ↓ ↓ ↓ ↓ ↑ ↑	19.6	9.0	0.1	0.1
S.00001000	↓ ↓ ↓ ↓ ↑ ↓ ↓ ↓	18.1	15.0	0.2	0.2

It is evident that all the clusters with different spin orientation of the Mn atoms investigated in the above table have the larger energy then the ferromagnetic one. So it can be concluded that ferromagnetic spin ordering is the most favorable one for the $As@Ni_5Mn_7@As_{20}$ system with magnetic anisotropy energy 25.19 K.

3.9: $As@Ni_3Mn_9@As_{20}$

In the parent $As@Ni_{12}@As_{20}$ system nine Mn atoms are doped by replacing any nine of the 12 Ni atoms. There are 12 unique possible resultant structures of the $As@Ni_3Mn_9@As_{20}$ system. The optimized structure of $As@Ni_4Mn_8@As_{20}$ is shown in the figure below.

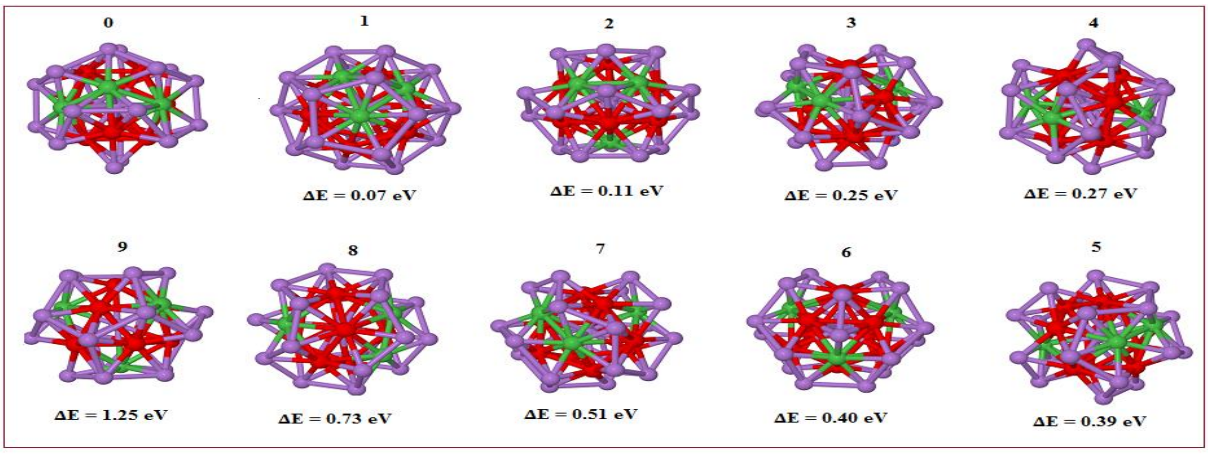

Figure 3.14: All possible combination of $As@Ni_3Mn_9@As_{20}$ cluster according to their energy.

It is evident from the figure that As_{20} cage is broken from the parent molecule. Due to the presence of the Mn atoms in the above structures near the Mn atom the As-As bond is varied, ranging from 3.36 Å to 2.46 Å. On an average the As-As bond length is increased by 0.02 Å compared to As20 cage in $As_{21}Ni_{12}$ system.

The net spin moment and HOMO-LUMO gap of all the above structures are calculated. Due to the breaking of symmetry, the resulting magnetic anisotropy compared to the parent cluster become larger. Average bond lengths of As-As, Ni-Ni, As-Ni, As-Mn, Ni-Mn in the whole clusters are also computed. In the table below all the detailed information are given.

Table 3.19: Data for all possible combination of $As@Ni_3Mn_9@As_{20}$ cluster.

Systems	**H-L gap (eV)**	**M.M μ_B**	**M.A.E (K)**	**As-As** Å	**As-Ni** Å	**Ni-Mn** Å	**As-Mn** Å	**Mn-Mn** Å	**Ni-Ni** Å	**Energy (Hartee)**
$As_{21}Ni_3Mn_9$_0	0.27	20	32.68	2.69	2.45	2.76	2.50	2.67	2.63	-61831.18229
$As_{21}Ni_3Mn_9$_1	0.26	18	13.41	2.80	2.45	2.68	2.47	2.66	2.75	-61831.17975
$As_{21}Ni_3Mn_9$_2	0.20	20	12.03	2.65	2.45	2.75	2.51	2.67	2.60	-61831.17821
$As_{21}Ni_3Mn_9$_3	0.21	20	12.38	2.65	2.45	2.75	2.50	2.67	2.60	-61831.17285
$As_{21}Ni_3Mn_9$_4	0.17	18	24.43	2.71	2.45	2.73	2.49	2.67	2.70	-61831.17235
$As_{21}Ni_3Mn_9$_5	0.01	20	24.13	2.69	2.45	2.74	2.50	2.67	2.65	-61831.16776
$As_{21}Ni_3Mn_9$_6	0.22	20	18.41	2.70	2.46	2.74	2.50	2.68	----	-61831.1675
$As_{21}Ni_3Mn_9$_7	0.02	18	21.59	2.72	2.46	2.74	2.49	2.68	2.64	-61831.16325
$As_{21}Ni_3Mn_9$_8	0.06	20	20.20	2.70	2.46	2.74	2.49	2.67	2.65	-61831.15534
$As_{21}Ni_3Mn_9$_9	0	12	25.53	2.78	2.48	2.72	2.48	2.66	----	-61831.13599

In the above table the most favorable (lowest energy) cluster is found to be $As_{21}Ni_3Mn_9$_0 which is indicated by red color. It can be noted that the $As_{21}Ni_3Mn_9$_5, $As_{21}Ni_3Mn_9$_7 systems have very small/no gap between the HOMO and LUMO. So that these clusters can be considered as metallic systems.

3.9.1: Ferrimagnetic Investigation of $As@Ni_3Mn_9@As_{20}$

In the $As@Ni_3Mn_9@As_{20}$ cluster it is evident that there are nine Mn atoms. The most favorable ferromagnetic cluster ($As_{21}Ni_3Mn_9$_0) from the above table is chosen for studying different spin ordering of the Mn atoms. All the possible spin ordering of the Mn atoms in this cluster are studied and the corresponding Magnetic Anisotropy Energy (MAE), Magnetic Moment (M.M), HOMO-LUMO gap (H-L gap) and the deviation in energy from the ferromagnetic ($As_{21}Ni_4Mn_8$_1) cluster is also computed.

Table 3.20: Data for different spin configuration of Mn atom in $As_{21}Ni_3Mn_9$_0 system

Systems		**MAE (K)**	**M.M μ_B**	**H-L gap**	**E-E_{FM} (eV)**
S.000000000	↓↓↓↓↓↓↓↓↓	29.7	20.0	0.3	0.1
S.000000100	↓↓↓↓↓↓↑↓↓	34.1	18.0	0.2	0.2
S.000100000	↓↓↓↑↓↓↓↓↓	15.7	14.0	0.2	0.2
S.011001111	↓↑↑↓↓↑↑↑↑	25.2	6.0	0.3	0.2
S.010100000	↓↑↓↑↓↓↓↓↓	9.7	10.0	0.2	0.2
S.000100100	↓↓↓↑↓↓↑↓↓	21.7	12.0	0.2	0.3
S.001000000	↓↓↑↓↓↓↓↓↓	18.9	16.0	0.1	0.3
S.000000001	↓↓↓↓↓↓↓↓↑	42.5	18.0	0.1	0.3
S.001000100	↓↓↑↓↓↓↑↓↓	16.6	14.0	0.2	0.3
S.000000010	↓↓↓↓↓↓↓↑↓	29.6	18.0	0.1	0.3
S.000010000	↓↓↓↓↑↓↓↓↓	5.0	16.0	0.1	0.3
S.010101000	↓↑↓↑↓↑↓↓↓	9.6	6.0	0.1	0.3

S.000001000	↓↓↓↓↓↑↓↓↓	38.1	16.0	0.1	0.3
S.011101011	↓↑↑↑↓↑↓↑↑	11.2	6.0	0.1	0.3
S.011001101	↓↑↑↓↓↑↑↓↑	28.1	2.0	0.1	0.4
S.010100100	↓↑↓↑↓↓↑↓↓	28.4	6.0	0.2	0.4
S.010101001	↓↑↓↑↓↑↓↓↑	9.2	2.0	0.1	0.4
S.011101110	↓↑↑↑↓↑↑↑↓	22.3	6.0	0.1	0.4
S.011101101	↓↑↑↑↓↑↑↓↑	32.9	6.1	0.0	0.4
S.011111101	↓↑↑↑↑↑↑↓↑	23.5	12.0	0.2	0.4
S.000100010	↓↓↓↑↓↓↓↑↓	28.2	12.0	0.2	0.4
S.011101001	↓↑↑↑↓↑↓↓↑	19.5	2.4	0.0	0.4
S.011001011	↓↑↑↓↓↑↓↑↑	36.9	0.0	0.1	0.4
S.011000000	↓↑↑↓↓↓↓↓↓	13.2	12.0	0.1	0.4
S.000110000	↓↓↓↑↑↓↓↓↓	19.5	12.0	0.1	0.4
S.001000101	↓↓↑↓↓↓↑↓↑	2.1	8.0	0.1	0.4
S.000000110	↓↓↓↓↓↓↑↑↓	14.2	14.0	0.1	0.4
S.011100100	↓↑↑↑↓↓↑↓↓	26.4	2.0	0.1	0.4
S.000101100	↓↓↓↑↓↑↑↓↓	34.8	6.0	0.2	0.4
S.001001101	↓↓↑↓↓↑↑↓↑	10.0	4.0	0.2	0.4
S.000000101	↓↓↓↓↓↓↑↓↑	20.2	14.0	0.1	0.4
S.000001011	↓↓↓↓↓↑↓↑↑	18.7	8.0	0.1	0.4
S.011000100	↓↑↑↓↓↓↑↓↓	25.0	8.0	0.1	0.5
S.010111000	↓↑↓↑↑↑↓↓↓	19.5	2.0	0.2	0.5
S.000010001	↓↓↓↓↑↓↓↓↑	40.7	14.0	0.1	0.5

S.010101010	↓↑↓↑↓↑↓↑↓	11.8	2.0	0.1	0.5
S.010100010	↓↑↓↑↓↓↓↑↓	5.2	8.0	0.1	0.5
S.000101000	↓↓↓↑↓↑↓↓↓	11.9	12.0	0.1	0.5
S.010000000	↓↑↓↓↓↓↓↓↓	11.6	16.0	0.1	0.5
S.010100001	↓↑↓↑↓↓↓↓↑	10.3	8.0	0.1	0.6
S.011100001	↓↑↑↑↓↓↓↓↑	21.4	2.0	0.1	0.6
S.011111110	↓↑↑↑↑↑↑↑↓	2.6	10.0	0.1	0.6
S.010000100	↓↑↓↓↓↓↑↓↓	24.7	12.0	0.2	0.6
S.010111001	↓↑↓↑↑↑↓↓↑	6.7	2.0	0.1	0.6
S.011101010	↓↑↑↑↓↑↓↑↓	14.6	2.0	0.0	0.6
S.011001000	↓↑↑↓↓↑↓↓↓	9.0	8.0	0.1	0.6
S.010101110	↓↑↓↑↓↑↑↑↓	7.4	2.0	0.1	0.6
S.011100101	↓↑↑↑↓↓↑↓↑	24.8	2.4	0.0	0.6
S.011001010	↓↑↑↓↓↑↓↑↓	9.3	4.0	0.2	0.6
S.011100010	↓↑↑↑↓↓↓↑↓	6.0	2.0	0.1	0.6
S.011000111	↓↑↑↓↓↓↑↑↑	26.6	0.0	0.1	0.6
S.001001100	↓↓↑↓↓↑↑↓↓	12.0	8.0	0.1	0.6
S.000101011	↓↓↓↑↓↑↓↑↑	38.1	4.0	0.1	0.6
S.001010111	↓↓↑↓↑↓↑↑↑	15.4	2.0	0.2	0.6
S.010001001	↓↑↓↓↓↑↓↓↑	27.3	8.0	0.1	0.6
S.000010110	↓↓↓↓↑↓↑↑↓	10.9	8.0	0.2	0.6
S.010000001	↓↑↓↓↓↓↓↓↑	24.4	14.0	0.1	0.6
S.011111100	↓↑↑↑↑↑↑↓↓	27.4	6.0	0.1	0.6

S.011100111	↓↑↑↑↓↓↑↑↑	31.1	6.0	0.1	0.6
S.000011001	↓↓↓↓↑↑↓↓↑	26.8	10.0	0.1	0.6
S.001101101	↓↓↑↑↓↑↑↓↑	15.7	2.0	0.2	0.6
S.011000110	↓↑↑↓↓↓↑↑↓	2.2	4.0	0.1	0.6
S.001001011	↓↓↑↓↓↑↓↑↑	31.9	4.0	0.1	0.6
S.010001011	↓↑↓↓↓↑↓↑↑	13.6	4.0	0.0	0.6
S.010001111	↓↑↓↓↓↑↑↑↑	7.4	2.0	0.2	0.6
S.000111001	↓↓↓↑↑↑↓↓↑	7.8	2.0	0.1	0.6
S.001001001	↓↓↑↓↓↑↓↓↑	18.9	10.0	0.1	0.6
S.011000011	↓↑↑↓↓↓↓↑↑	24.9	4.0	0.1	0.6
S.011100110	↓↑↑↑↓↓↑↑↓	36.5	2.0	0.1	0.6
S.000000111	↓↓↓↓↓↓↑↑↑	19.7	8.0	0.1	0.6
S.011110100	↓↑↑↑↑↓↑↓↓	29.7	2.4	0.0	0.6
S.011010101	↓↑↑↓↑↓↑↓↑	5.7	0.0	0.1	0.6
S.010010000	↓↑↓↓↑↓↓↓↓	17.9	12.0	0.1	0.6
S.010000010	↓↑↓↓↓↓↓↑↓	17.2	14.0	0.1	0.6
S.000001110	↓↓↓↓↓↑↑↑↓	15.7	8.0	0.1	0.6
S.001011101	↓↓↑↓↑↑↑↓↑	33.2	0.0	0.1	0.6
S.011010100	↓↑↑↓↑↓↑↓↓	2.3	4.0	0.1	0.6
S.000100110	↓↓↓↑↓↓↑↑↓	35.1	8.0	0.1	0.6
S.001110100	↓↓↑↑↑↓↑↓↓	19.6	4.0	0.2	0.6
S.000101110	↓↓↓↑↓↑↑↑↓	21	4	0	1
S.001000011	↓↓↑↓↓↓↓↑↑	15	8	0	1

S.010001000	↓↑↓↓↓↑↓↓↓	27	14	0	1
S.011011001	↓↑↑↓↑↑↓↓↑	32	-2	0	1
S.010111111	↓↑↓↑↑↑↑↑↑	16	-10	0	1
S.001001010	↓↓↑↓↓↑↓↑↓	27	8	0	1
S.010100011	↓↑↓↑↓↓↓↑↑	40	4	0	1
S.011001100	↓↑↑↓↓↑↑↓↓	9	4	0	1
S.001010001	↓↓↑↓↑↓↓↓↑	11	10	0	1
S.010111010	↓↑↓↑↑↑↓↑↓	13	-2	0	1
S.011110000	↓↑↑↑↑↓↓↓↓	25	4	0	1
S.011100011	↓↑↑↑↓↓↓↑↑	44	-2	0	1
S.011111011	↓↑↑↑↑↑↓↑↑	13	-8	0	1
S.000100101	↓↓↓↑↓↓↑↓↑	16	8	0	1
S.001010110	↓↓↑↓↑↓↑↑↓	12	4	0	1
S.010111011	↓↑↓↑↑↑↓↑↑	15	-6	0	1
S.000111101	↓↓↓↑↑↑↑↓↑	1	0	0	1
S.010100101	↓↑↓↑↓↓↑↓↑	31	4	0	1
S.011001110	↓↑↑↓↓↑↑↑↓	23	2	0	1
S.001110000	↓↓↑↑↑↓↓↓↓	18	8	0	1
S.011011011	↓↑↑↓↑↑↓↑↑	31	-4	0	1
S.000011011	↓↓↓↓↑↑↓↑↑	21	4	0	1
S.011010001	↓↑↑↓↑↓↓↓↑	17	4	0	1
S.000010101	↓↓↓↓↑↓↑↓↑	15	10	0	1
S.001111111	↓↓↑↑↑↑↑↑↑	22	-10	0	1

S.011010000	↓↑↑↓↑↓↓↓↓	29	10	0	1
S.010100110	↓↑↓↑↓↓↑↑↓	16	4	0	1
S.000110001	↓↓↓↑↑↓↓↓↑	4	6	0	1
S.001101001	↓↓↑↑↓↑↓↓↑	13	2	0	1
S.000111000	↓↓↓↑↑↑↓↓↓	8	10	0	1
S.010100111	↓↑↓↑↓↓↑↑↑	38	0	0	1
S.010001101	↓↑↓↓↓↑↑↓↑	17	4	0	1
S.010111101	↓↑↓↑↑↑↑↓↑	9	-4	0	1
S.000011111	↓↓↓↓↑↑↑↑↑	13	0	0	1
S.001101000	↓↓↑↑↓↑↓↓↓	12	8	0	1
S.000100011	↓↓↓↑↓↓↓↑↑	38	8	0	1
S.000111111	↓↓↓↑↑↑↑↑↑	2	-4	0	1
S.001011011	↓↓↑↓↑↑↓↑↑	37	0	0	1
S.000110010	↓↓↓↑↑↓↓↑↓	14	6	0	1
S.000111100	↓↓↓↑↑↑↑↓↓	23	4	0	1
S.000111011	↓↓↓ ↑ ↑ ↑↓ ↑ ↑	20.0	2.0	0.1	0.8
S.001100001	↓↓ ↑ ↑↓↓↓↓ ↑	35.5	6.0	0.1	0.8
S.011110001	↓ ↑ ↑ ↑ ↑↓↓↓ ↑	39.1	2.0	0.1	0.8
S.000011010	↓↓↓↓ ↑ ↑↓ ↑↓	31.0	8.0	0.2	0.8
S.010000101	↓ ↑↓↓↓↓ ↑↓ ↑	21.6	8.0	0.1	0.8
S.010010001	↓ ↑↓↓ ↑↓↓↓ ↑	21.3	8.0	0.2	0.8
S.001011000	↓↓ ↑↓ ↑ ↑↓↓↓	25.8	8.0	0.1	0.8
S.011010110	↓ ↑ ↑↓ ↑↓ ↑ ↑↓	19.6	2.0	0.2	0.8

S.001101100	↓↓ ↑ ↑↓ ↑ ↑↓↓	8.9	4.0	0.1	0.8
S.010001010	↓ ↑↓↓↓ ↑↓ ↑↓	47.9	9.9	0.0	0.8
S.000011101	↓↓↓↓ ↑ ↑ ↑↓ ↑	9.5	6.0	0.1	0.8
S.001100010	↓↓ ↑ ↑↓↓↓ ↑↓	29.3	6.0	0.1	0.8
S.001001110	↓↓ ↑↓↓ ↑ ↑ ↑↓	45.8	5.6	0.0	0.8
S.001010010	↓↓ ↑↓ ↑↓↓ ↑↓	1.4	8.0	0.1	0.8
S.000010111	↓↓↓↓ ↑↓ ↑ ↑ ↑	7.0	4.0	0.1	0.8
S.010011011	↓ ↑↓↓ ↑ ↑↓ ↑ ↑	24.0	2.0	0.2	0.8
S.001111101	↓↓ ↑ ↑ ↑ ↑ ↑↓ ↑	17.3	4.0	0.1	0.8
S.010110100	↓ ↑↓ ↑ ↑↓ ↑↓↓	6.6	6.0	0.1	0.8
S.010011001	↓ ↑↓↓ ↑ ↑↓↓ ↑	16.3	4.0	0.1	0.8
S.010111100	↓ ↑↓ ↑ ↑ ↑ ↑↓↓	7.7	0.0	0.1	0.8
S.010011000	↓ ↑↓↓ ↑ ↑↓↓↓	33.8	8.0	0.1	0.8
S.001100101	↓↓ ↑ ↑↓↓ ↑↓ ↑	42.4	4.0	0.1	0.8
S.000010011	↓↓↓↓ ↑↓↓ ↑ ↑	40.0	10.0	0.1	0.8
S.010110010	↓ ↑↓ ↑ ↑↓↓ ↑↓	17.9	2.0	0.1	0.8
S.001011001	↓↓ ↑↓ ↑ ↑↓↓ ↑	11.6	6.0	0.1	0.8
S.000100111	↓↓↓ ↑↓↓ ↑ ↑ ↑	28.6	4.0	0.1	0.8
S.000011100	↓↓↓↓ ↑ ↑ ↑↓↓	30.1	10.0	0.1	0.8
S.011010111	↓↑ ↑↓ ↑↓ ↑ ↑ ↑	14.7	4.0	0.0	0.8
S.011111010	↓↑ ↑ ↑ ↑ ↑↓ ↑↓	14.9	4.0	0.1	0.8
S.010000011	↓ ↑↓↓↓↓↓ ↑ ↑	49.1	10.0	0.1	0.8
S.000111010	↓↓↓ ↑ ↑ ↑↓ ↑↓	14.3	4.0	0.1	0.8

S.010111110	↓ ↑↓ ↑ ↑ ↑ ↑ ↑↓	19.0	4.4	0.0	0.8
S.010011111	↓ ↑↓↓ ↑ ↑ ↑ ↑ ↑	23.0	4.0	0.1	0.8
S.001101110	↓↓ ↑ ↑↓ ↑ ↑ ↑↓	17.8	0.0	0.1	0.8
S.010000110	↓ ↑↓↓↓↓ ↑ ↑↓	8.4	8.0	0.1	0.8
S.001110101	↓↓ ↑ ↑ ↑↓ ↑↓ ↑	12.3	2.0	0.1	0.8
S.001100110	↓↓ ↑ ↑↓↓ ↑ ↑↓	30.4	4.0	0.1	0.8
S.001011100	↓↓ ↑↓ ↑ ↑ ↑↓↓	30.8	5.5	0.0	0.8
S.011011000	↓ ↑ ↑↓ ↑ ↑↓↓↓	23.9	4.0	0.1	0.9
S.001100111	↓↓ ↑ ↑↓↓ ↑ ↑ ↑	26.0	0.0	0.1	0.9
S.001101011	↓ ↓ ↑↑↓ ↑↓ ↑↑	42.9	0.0	0.1	0.9
S.010110001	↓ ↑↓ ↑↑↓ ↓ ↓ ↑	30.8	4.0	0.0	0.9
S.010001100	↓ ↑↓ ↓ ↓ ↑↑↓ ↓	29.5	8.0	0.1	0.9
S.011011100	↓ ↑↑↓ ↑↑↑↓ ↓	12.1	0.0	0.1	0.9
S.001101010	↓ ↓ ↑↑↓ ↑↓ ↑↓	10.2	4.0	0.0	0.9
S.000110101	↓ ↓ ↓ ↑↑↓ ↑↓ ↑	14.8	4.0	0.1	0.9
S.000111110	↓ ↓ ↓ ↑↑↑↑↑↓	18.6	0.0	0.1	0.9
S.011011110	↓ ↑↑↓ ↑↑↑↑↓	8.0	4.0	0.1	0.9
S.001011110	↓ ↓ ↑↓ ↑↑↑↑↓	31.9	0.0	0.1	0.9
S.001111100	↓ ↓ ↑↑↑↑↑↓ ↓	18.9	0.0	0.1	0.9
S.000011110	↓ ↓ ↓ ↓ ↑↑↑↑↓	30.9	6.0	0.1	0.9
S.010110101	↓ ↑↓ ↑↑↓ ↑↓ ↑	33.9	0.0	0.1	0.9
S.000110110	↓ ↓ ↓ ↑↑↓ ↑↑↓	13.8	3.8	0.0	0.9
S.010010100	↓ ↑↓ ↓ ↑↓ ↑↓ ↓	8.7	10.0	0.1	0.9

S.010110110	↓ ↑↓ ↑↑↓ ↑↑↓	14.8	2.0	0.2	0.9
S.010001110	↓ ↑↓ ↓ ↓ ↑↑↑↓	26.8	6.0	0.1	0.9
S.010000111	↓ ↑↓ ↓ ↓ ↓ ↑↑↑	33.0	6.0	0.1	0.9
S.001111000	↓ ↓ ↑↑↑↑↓ ↓ ↓	21.1	4.0	0.1	0.9
S.001111110	↓ ↓ ↑↑↑↑↑↑↓	16.0	4.0	0.1	0.9
S.001110110	↓ ↓ ↑↑↑↓ ↑↑↓	17.8	2.0	0.1	0.9
S.001111001	↓ ↓ ↑↑↑↑↓ ↓ ↑	5.1	0.0	0.1	0.9
S.011010010	↓ ↑↑↓ ↑↓ ↓ ↑↓	8.2	3.2	0.0	1.0
S.001011010	↓ ↓ ↑↓ ↑↑↓ ↑↓	26.5	4.0	0.1	1.0
S.011010011	↓ ↑↑↓ ↑↓ ↓ ↑↑	25.4	2.0	0.1	1.0
S.011011010	↓ ↑↑↓ ↑↑↓ ↑↓	25.9	0.0	0.1	1.0
S.001010011	↓ ↓ ↑↓ ↑↓ ↓ ↑↑	47.5	6.0	0.1	1.0
S.001110001	↓ ↓ ↑↑↑↓ ↓ ↓ ↑	16.6	2.0	0.2	1.0
S.010010010	↓ ↑↓ ↓ ↑↓ ↓ ↑↓	32.8	10.0	0.1	1.0
S.010011010	↓ ↑↓ ↓ ↑↑↓ ↑↓	13.4	4.0	0.1	1.0
S.010011101	↓ ↑↓ ↓ ↑↑↑↓ ↑	11.1	2.0	0.1	1.0
S.001100011	↓ ↓ ↑↑↓ ↓ ↓ ↑↑	46.7	4.0	0.1	1.0
S.000110111	↓ ↓ ↓ ↑↑↓ ↑↑↑	3.8	2.0	0.1	1.0
S.011110011	↓ ↑↑↑↑↓ ↓ ↑↑	44.2	4.0	0.1	1.0
S.010110011	↓ ↑↓ ↑↑↓ ↓ ↑↑	62.1	0.0	0.1	1.0
S.010010101	↓ ↑↓ ↓ ↑↓ ↑↓ ↑	16.1	6.0	0.1	1.0
S.010110111	↓ ↑↓ ↑↑↓ ↑↑↑	28.0	4.0	0.0	1.1
S.001111011	↓ ↓ ↑↑↑↑↓ ↑↑	20.9	4.0	0.1	1.1

S.001110111	↓ ↓ ↑ ↑ ↑ ↓ ↑ ↑ ↑	9.2	4.3	0.0	1.1
S.001111010	↓ ↓ ↑ ↑ ↑ ↑ ↓ ↑ ↓	12.7	0.0	0.1	1.1
S.010010011	↓ ↑ ↓ ↓ ↑ ↓ ↓ ↑ ↑	19.2	4.0	0.1	1.1
S.001110010	↓ ↓ ↑ ↑ ↑ ↓ ↓ ↑ ↓	28.3	4.0	0.1	1.1
S.000110011	↓ ↓ ↓ ↑ ↑ ↓ ↓ ↑ ↑	19.7	4.0	0.1	1.1
S.010011110	↓ ↑ ↓ ↓ ↑ ↑ ↑ ↑ ↓	12.0	0.0	0.1	1.1
S.010011100	↓ ↑ ↓ ↓ ↑ ↑ ↑ ↓ ↓	5.6	6.0	0.1	1.1
S.010010110	↓ ↑ ↓ ↓ ↑ ↓ ↑ ↑ ↓	10.2	6.0	0.1	1.2
S.010010111	↓ ↑ ↓ ↓ ↑ ↓ ↑ ↑ ↑	27.0	2.0	0.1	1.2
S.001110011	↓ ↓ ↑ ↑ ↑ ↓ ↓ ↑ ↑	31.3	0.0	0.1	1.3

The spin ordering of Mn atoms in the cluster are arranged according to their energy as shown in the table above. The first 10 cluster with different spin ordering are selected and again optimized by running several iteration in order to find the lower energy clusters compare to the ferromagnetic one. These optimized clusters are again investigated by computing MAE, M.M, H-L gap and E-E_{FM} which are shown in the table below.

Table 3.21: Data for the lowest ten spin ordering of the $As@Ni_3Mn_9@As_{20}$ cluster

Systems		**MAE (K)**	**M.M**	**H-L gap**	**E-E_{FM} (eV)**
S.011001111	↓ ↑ ↑ ↓ ↓ ↑ ↑ ↑ ↑	23.2	6.0	0.4	-0.4
S.000100100	↓ ↓ ↓ ↑ ↓ ↓ ↑ ↓ ↓	27.0	12.0	0.2	-0.3
S.000000100	↓ ↓ ↓ ↓ ↓ ↓ ↑ ↓ ↓	24.1	18.0	0.2	-0.2
S.010100000	↓ ↑ ↓ ↑ ↓ ↓ ↓ ↓ ↓	12.3	10.0	0.2	-0.1
S.000100000	↓ ↓ ↓ ↑ ↓ ↓ ↓ ↓ ↓	19.8	14.0	0.2	-0.1
S.000010000	↓ ↓ ↓ ↓ ↑ ↓ ↓ ↓ ↓	26.7	16.0	0.2	0.0
S.001000000	↓ ↓ ↑ ↓ ↓ ↓ ↓ ↓ ↓	31.2	16.0	0.2	0.0
S.000000000	↓ ↓ ↓ ↓ ↓ ↓ ↓ ↓ ↓	32.6	20.0	0.3	0.0
S.000000001	↓ ↓ ↓ ↓ ↓ ↓ ↓ ↓ ↑	31.2	16.0	0.2	0.1
S.000000010	↓ ↓ ↓ ↓ ↓ ↓ ↓ ↑ ↓	45.6	16.0	0.1	0.3
S.001000100	↓ ↓ ↑ ↓ ↓ ↓ ↑ ↓ ↓	15.0	12.0	0.1	0.3

In the above table it is evident that the first eight clusters have lower energy compare to the ferromagnetic case. The cluster with spin ordering S.011001111 has the lowest energy and it can be considered as the most favorable cluster of the $As@Ni_3Mn_9@As_{20}$ system which has magnetic anisotropy energy of 23.22 K. In the S.011001111 spin ordering, three of the Mn atoms have spin down (0) and the other six Mn atoms have up spin (1).

3.10: $As@Ni_2Mn_{10}@As_{20}$

In the parent $As@Ni_{12}@As_{20}$ system ten Mn atoms are doped by replacing any ten of the 12 Ni atoms. There are 4 unique possible resultant structures of the $As@Ni_2Mn_{10}@As_{20}$ system which are shown in the figure below.

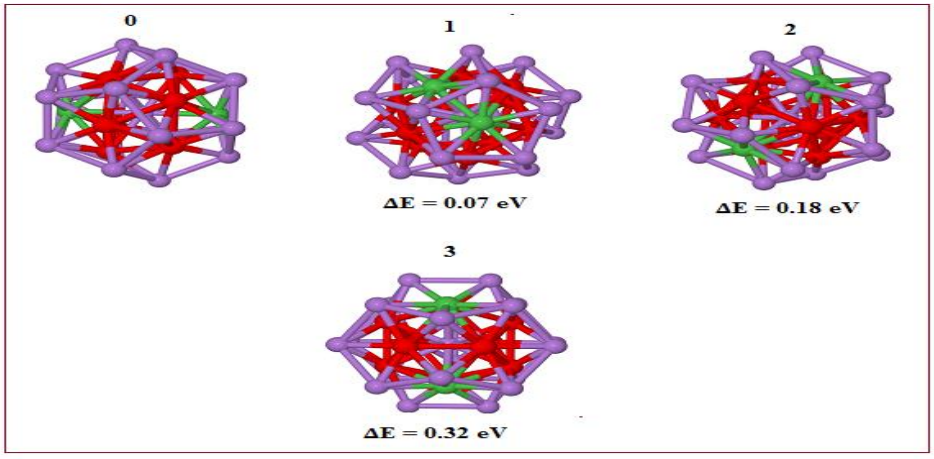

Figure 3.15: All possible combination of $As@Ni_2Mn_{10}@As_{20}$ cluster.

It is evident from the figure that As_{20} cage is broken from the parent molecule. Due to the presence of the Mn atoms in the above structures near the Mn atom the As-As bond is varied from 3.2 Å to 2.64 Å. On an average the As-As bond length is increased by 0.01 Å compared to As20 cage in $As_{21}Ni_{12}$ system.

The net spin moment and HOMO-LUMO gap of all the above structures are calculated. Due to the breaking of symmetry, the resulting magnetic anisotropy compared to the parent cluster become larger.

Average bond lengths of As-As, Ni-Ni, As-Ni, As-Mn, Ni-Mn in the whole clusters are also computed. In the table below all the detailed information are given

Table 3.22: Data for all possible combination of $As@Ni_2Mn_{10}@As_{20}$ cluster.

Systems	**H-L gap (eV)**	**M.M μ_B**	**M.A.E (K)**	**As-As** Å	**As-Ni** Å	**Ni-Mn** Å	**As-Mn** Å	**Mn-Mn** Å	**Ni-Ni** Å	**Energy (Hartee)**
$As_{21}Ni_2Mn_{10}$_0	0.27	19	40.88	2.81	2.47	2.72	2.48	2.65	-----	-61473.81674
$As_{21}Ni_2Mn_{10}$_1	0.11	19	22.50	2.78	2.46	2.72	2.48	2.67	2.70	-61473.81415
$As_{21}Ni_2Mn_{10}$_2	0.2	19	21.20	2.73	2.47	2.73	2.48	2.66	-----	-61473.80988
$As_{21}Ni_2Mn_{10}$_3	0.22	19	20.16	2.73	2.46	2.73	2.48	2.66	-----	-61473.80789
$As_{21}Ni_2Mn_{10}$_4	0.02	18	25.45	2.76	2.47	2.73	2.48	2.66	-----	-61473.80465

The lowest energy molecules is $As_{21}Ni_2Mn_{10}$_0 which is indicated by red color in the above table. It can also be noted that $As_{21}Ni_2Mn_{10}$_4 system have very small/no gap between the HOMO and LUMO. So that this cluster can be considered as a metallic system. The pictures of all these clusters are given below according to lowest to highest energy.

3.10.1: Ferrimagnetic Investigation of $As@Ni_2Mn_{10}@As_{20}$:

In the $As@Ni_2Mn_{10}@As_{20}$ cluster it is evident that there are ten Mn atoms. The most favorable ferromagnetic cluster ($As_{21}Ni_2Mn_{10}$_0) from the above table is chosen for studying different spin ordering of the Mn atoms. All the possible spin ordering of the Mn atoms in this cluster are studied and the corresponding Magnetic Anisotropy Energy (MAE), Magnetic Moment (M.M), HOMO-LUMO gap (H-L gap) and the deviation in energy from the ferromagnetic ($As_{21}1Ni_4Mn_8$_1) cluster is also computed.

Table 3.23: Data for different spin configuration of Mn atom in $As_{21}Ni_2Mn_{10}$_0 system

Systems		**MAE (K)**	**M.M μ_B**	**H-L gap (eV)**	**E-E_{FM} (eV)**
S.0000000010	↓↓↓↓↓↓↓↓↑ ↓	25.5	15.0	0.1	0.1
S.0000100000	↓↓↓↓↑ ↓↓↓↓↓	25.5	15.0	0.1	0.1
S.0000010000	↓↓↓↓↓↑ ↓↓↓↓	25.4	15.0	0.1	0.1
S.0101110101	↓↑ ↓↑ ↑ ↑ ↓↑ ↓↑	22.0	3.0	0.1	0.2
S.0101010111	↓↑ ↓↑ ↓↑ ↓↑ ↑ ↑	22.0	3.0	0.1	0.2
S.0001000000	↓↓↓↑ ↓↓↓↓↓↓	26.0	15.0	0.1	0.2
S.0000001000	↓↓↓↓↓↓↑ ↓↓↓	26.0	15.0	0.1	0.2
S.0010000000	↓↓↑ ↓↓↓↓↓↓↓	26.0	15.0	0.1	0.2
S.0000000100	↓↓↓↓↓↓↓↑ ↓↓	25.3	15.0	0.1	0.2
S.0100000000	↓↑ ↓↓↓↓↓↓↓↓	24.8	15.0	0.1	0.2
S.0000100001	↓↓↓↓↑ ↓↓↓↓↑	41.8	13.0	0.2	0.2
S.0000010010	↓↓↓↓↓↑ ↓↓↑ ↓	41.4	13.0	0.2	0.2
S.0111110100	↓↑ ↑ ↑ ↑ ↑ ↓↑ ↓↓	21.0	3.0	0.2	0.2
S.0101001111	↓↑ ↓↑ ↓↓↑ ↑ ↑ ↑	22.5	3.0	0.2	0.2
S.0101000101	↓↑ ↓↑ ↓↓↓↑ ↓↑	149.7	4.8	0.0	0.2
S.0101010100	↓↑ ↓↑ ↓↑ ↓↑ ↓↓	150.0	4.8	0.0	0.2
S.0101100101	↓↑ ↓↑ ↑ ↓↓↑ ↓↑	0.0	1.0	0.1	0.2
S.0101010110	↓↑ ↓↑ ↓↑ ↓↑ ↑ ↓	0.0	1.0	0.1	0.2
S.0101010101	↓↑ ↓↑ ↓↑ ↓↑ ↓↑	0.0	1.0	0.1	0.2
S.0001000100	↓↓↓↑ ↓↓↓↑ ↓↓	24.5	13.0	0.0	0.2

S.0010001000	↓↓↑ ↓↓↓↑ ↓↓↓	24.9	13.0	0.0	0.2
S.0000100010	↓↓↓↓↑ ↓↓↓↑ ↓	36.0	13.0	0.1	0.3
S.0000010001	↓↓↓↓↓↑ ↓↓↓↑	36.0	13.0	0.1	0.3
S.0010000100	↓↓↑ ↓↓↓↓↑ ↓↓	43.0	13.0	0.2	0.3
S.0101110100	↓↑ ↓↑ ↑ ↑ ↓↑ ↓↓	0.0	1.0	0.1	0.3
S.0001001000	↓↓↓↑ ↓↓↑ ↓↓↓	43.0	13.0	0.2	0.3
S.0101000111	↓↑ ↓↑ ↓↓↓↑ ↑ ↑	0.0	1.0	0.1	0.3
S.0111010100	↓↑ ↑ ↑ ↓↑ ↓↑ ↓↓	0.0	1.0	0.1	0.3
S.0101001101	↓↑ ↓↑ ↓↓↑ ↑ ↓↑	0.0	1.0	0.1	0.3
S.0101110001	↓↑ ↓↑ ↑ ↑ ↓↓↓↑	0.0	1.0	0.1	0.3
S.0100010111	↓↑ ↓↓↓↑ ↓↑ ↑ ↑	0.0	1.0	0.1	0.3
S.0011110100	↓↓↑ ↑ ↑ ↑ ↓↑ ↓↓	0.0	1.0	0.1	0.3
S.0001001111	↓↓↓↑ ↓↓↑ ↑ ↑ ↑	0.0	1.0	0.1	0.3
S.0010001111	↓↓↑ ↓↓↓↑ ↑ ↑ ↑	0.0	1.0	0.1	0.3
S.0011111000	↓↓↑ ↑ ↑ ↑ ↑ ↓↓↓	0.0	1.0	0.1	0.3
S.0100000111	↓↑ ↓↓↓↓↓↑ ↑ ↑	42.6	5.0	0.0	0.3
S.0100000001	↓↑ ↓↓↓↓↓↓↓↑	13.2	13.0	0.1	0.3
S.0100010000	↓↑ ↓↓↓↑ ↓↓↓↓	12.9	13.0	0.1	0.3
S.0000001111	↓↓↓↓↓↓↑ ↑ ↑ ↑	65.5	4.8	0.0	0.3
S.0011110000	↓↓↑ ↑ ↑ ↑ ↓↓↓↓	71.4	4.8	0.0	0.3
S.0001000010	↓↓↓↑ ↓↓↓↓↑ ↓	32.6	13.0	0.1	0.3
S.0000000011	↓↓↓↓↓↓↓↓↑ ↑	31.1	11.0	0.1	0.3
S.0000100100	↓↓↓↓↑ ↓↓↑ ↓↓	34.9	13.0	0.1	0.3

S.0111110000	↓↑ ↑ ↑ ↑ ↑ ↓↓↓↓	0.0	1.0	0.1	0.3
S.0100001111	↓↑ ↓↓↓↓↑ ↑ ↑ ↑	0.0	1.0	0.2	0.3
S.0000011000	↓↓↓↓↓↑ ↑ ↓↓↓	33.2	13.0	0.1	0.3
S.0010000001	↓↓↑ ↓↓↓↓↓↓↑	34.9	13.0	0.1	0.3
S.0011111111	↓↓↑ ↑ ↑ ↑ ↑ ↑ ↑ ↑	35.5	11.0	0.0	0.3
S.0101000100	↓↑ ↓↑ ↓↓↓↑ ↓↓	26.4	7.0	0.1	0.3
S.0101110111	↓↑ ↓↑ ↑ ↑ ↓↑ ↑ ↑	26.2	7.0	0.1	0.3
S.0000001001	↓↓↓↓↓↓↑ ↓↓↑	30.8	13.0	0.0	0.3
S.0000000110	↓↓↓↓↓↓↓↑ ↑ ↓	28.1	13.0	0.0	0.3
S.0000010100	↓↓↓↓↓↑ ↓↑ ↓↓	33.3	13.0	0.1	0.3
S.0010010000	↓↓↑ ↓↓↑ ↓↓↓↓	30.7	13.0	0.0	0.3
S.0001000001	↓↓↓↑ ↓↓↓↓↓↑	30.6	13.0	0.1	0.3
S.0001100000	↓↓↓↑ ↑ ↓↓↓↓↓	28.3	13.0	0.0	0.3
S.0000101000	↓↓↓↓↑ ↓↑ ↓↓↓	33.4	13.0	0.1	0.3
S.0010000010	↓↓↑ ↓↓↓↓↓↑ ↓	30.6	13.0	0.1	0.3
S.0100000101	↓↑ ↓↓↓↓↓↑ ↓↑	27.3	7.0	0.1	0.3
S.0101010000	↓↑ ↓↑ ↓↑ ↓↓↓↓	27.3	7.0	0.1	0.3
S.0110000000	↓↑ ↑ ↓↓↓↓↓↓↓	35.3	13.0	0.1	0.3
S.0111110101	↓↑ ↑ ↑ ↑ ↑ ↓↑ ↓↑	27.2	7.0	0.1	0.3
S.0101011111	↓↑ ↓↑ ↓↑ ↑ ↑ ↑ ↑	27.2	7.0	0.1	0.3
S.0100001000	↓↑ ↓↓↓↓↑ ↓↓↓	35.3	13.0	0.1	0.3
S.0001110000	↓↓↓↑ ↑ ↑ ↓↓↓↓	26.2	7.0	0.1	0.3
S.0000000111	↓↓↓↓↓↓↓↑ ↑ ↑	24.0	7.0	0.1	0.3

S.0000000101	↓↓↓↓↓↓↓↑ ↓↑	36.5	11.0	0.1	0.3
S.0001010000	↓↓↓↑ ↓↑ ↓↓↓↓	36.6	11.0	0.1	0.3
S.0010100000	↓↓↑ ↓↑ ↓↓↓↓↓	36.6	11.0	0.1	0.3
S.0000001010	↓↓↓↓↓↓↑ ↓↑ ↓	36.5	11.0	0.1	0.3
S.0101000000	↓↑ ↓↑ ↓↓↓↓↓↓	33.3	11.0	0.1	0.4
S.0100000100	↓↑ ↓↓↓↓↓↑ ↓↓	33.3	11.0	0.1	0.4
S.0111110111	↓↑ ↑ ↑ ↑ ↑ ↓↑ ↑ ↑	32.1	11.0	0.1	0.4
S.0101111111	↓↑ ↓↑ ↑ ↑ ↑ ↑ ↑ ↑	32.0	11.0	0.1	0.4
S.0010110000	↓↓↑ ↓↑ ↑ ↓↓↓↓	49.6	8.3	0.0	0.4
S.0000001011	↓↓↓↓↓↓↑ ↓↑ ↑	49.7	8.3	0.0	0.4
S.0001000110	↓↓↓↑ ↓↓↓↑ ↑ ↓	35.5	9.0	0.1	0.4
S.0010001001	↓↓↑ ↓↓↓↑ ↓↓↑	29.9	9.0	0.1	0.4
S.0010011000	↓↓↑ ↓↓↑ ↑ ↓↓↓	29.9	9.0	0.1	0.4
S.0100000010	↓↑ ↓↓↓↓↓↓↑ ↓	31.5	13.0	0.1	0.4
S.0100100000	↓↑ ↓↓↑ ↓↓↓↓↓	31.2	13.0	0.1	0.4
S.0001100100	↓↓↓↑ ↑ ↓↓↑ ↓↓	37.3	9.0	0.1	0.4
S.0111111011	↓↑ ↑ ↑ ↑ ↑ ↑ ↓↑ ↑	34.8	11.0	0.0	0.4
S.0110111111	↓↑ ↑ ↓↑ ↑ ↑ ↑ ↑ ↑	34.8	11.0	0.0	0.4
S.0100010001	↓↑ ↓↓↓↑ ↓↓↓↑	69.8	9.0	0.0	0.4
S.0111101111	↓↑ ↑ ↑ ↑ ↓↑ ↑ ↑ ↑	39.4	11.0	0.0	0.4
S.0111111110	↓↑ ↑ ↑ ↑ ↑ ↑ ↑ ↑ ↓	44.6	11.0	0.0	0.4
S.0000001100	↓↓↓↓↓↓↑ ↑ ↓↓	33.9	13.0	0.1	0.4
S.0011000000	↓↓↑ ↑ ↓↓↓↓↓↓	33.9	13.0	0.1	0.4

S.0001000101	↓↓↓↑ ↓↓↓↑ ↓↑	24.3	9.0	0.1	0.4
S.0001010100	↓↓↓↑ ↓↑ ↓↑ ↓↓	26.7	9.0	0.1	0.4
S.0010001010	↓↓↑ ↓↓↓↑ ↓↑ ↓	26.7	9.0	0.1	0.4
S.0010101000	↓↓↑ ↓↑ ↓↑ ↓↓↓	24.3	9.0	0.1	0.4
S.0100100001	↓↑ ↓↓↑ ↓↓↓↓↑	51.8	9.0	0.1	0.4
S.0100010010	↓↑ ↓↓↓↑ ↓↓↑ ↓	51.8	9.0	0.1	0.4
S.0011000100	↓↓↑ ↑ ↓↓↓↑ ↓↓	63.1	9.0	0.1	0.4
S.0001001100	↓↓↓↑ ↓↓↑ ↑ ↓↓	48.2	9.0	0.1	0.4
S.0010001100	↓↓↑ ↓↓↓↑ ↑ ↓↓	48.2	9.0	0.1	0.4
S.0011001000	↓↓↑ ↑ ↓↓↑ ↓↓↓	48.2	9.0	0.1	0.4
S.0000010110	↓↓↓↓↓↑ ↓↑ ↑ ↓	63.0	9.0	0.1	0.4
S.0101100100	↓↑ ↓↑ ↑ ↓↓↑ ↓↓	29.3	5.0	0.1	0.4
S.0010010010	↓↓↑ ↓↓↑ ↓↓↑ ↓	59.7	9.0	0.1	0.4
S.0000101001	↓↓↓↓↑ ↓↑ ↓↓↑	59.7	9.0	0.1	0.4
S.0101000001	↓↑ ↓↑ ↓↓↓↓↓↑	23.8	9.0	0.1	0.4
S.0101110110	↓↑ ↓↑ ↑ ↑ ↓↑ ↑ ↓	23.4	3.0	0.1	0.4
S.0001100001	↓↓↓↑ ↑ ↓↓↓↓↑	59.5	9.0	0.1	0.4
S.0101000110	↓↑ ↓↑ ↓↓↓↑ ↑ ↓	29.4	5.0	0.1	0.4
S.0101100111	↓↑ ↓↑ ↑ ↓↓↑ ↑ ↑	23.3	3.0	0.1	0.4
S.0100010100	↓↑ ↓↓↓↑ ↓↑ ↓↓	22.2	9.0	0.1	0.4
S.0100001001	↓↑ ↓↓↓↓↑ ↓↓↑	33.2	9.0	0.1	0.4
S.0100010011	↓↑ ↓↓↓↑ ↓↓↑ ↑	37.3	5.0	0.1	0.4
S.0100110001	↓↑ ↓↓↑ ↑ ↓↓↓↑	37.3	5.0	0.1	0.4

S.0110010000	↓↑ ↑ ↓↓↑ ↓↓↓↓	33.2	9.0	0.1	0.4
S.0001110100	↓↓↓↑ ↑ ↑ ↓↑ ↓↓	27.0	5.0	0.1	0.4
S.0111010101	↓↑ ↑ ↑ ↓↑ ↓↑ ↓↑	23.3	3.0	0.1	0.4
S.0100110000	↓↑ ↓↓↑ ↑ ↓↓↓↓	22.1	9.0	0.1	0.4
S.0111100101	↓↑ ↑ ↑ ↑ ↓↓↑ ↓↑	42.8	3.0	0.2	0.4
S.0001000111	↓↓↓↑ ↓↓↓↑ ↑ ↑	21.0	5.0	0.1	0.4
S.0101011101	↓↑ ↓↑ ↓↑ ↑ ↑ ↓↑	23.3	3.0	0.1	0.4
S.0100000011	↓↑↓↓↓↓↓↓↑↑	25.0	9.0	0.1	0.4
S.0010001011	↓↓↑↓↓↓↑↓↑↑	21.0	5.0	0.1	0.4
S.0010111000	↓↓↑↓↑↑↑↓↓↓	27.0	5.0	0.1	0.4
S.0101011110	↓↑↓↑↓↑↑↑↑↓	42.8	-3.0	0.2	0.4
S.0101110011	↓↑↓↑↑↑↓↓↑↑	43.1	-3.0	0.2	0.4
S.0010010100	↓↓↑↓↓↑↓↑↓↓	61.0	9.0	0.1	0.4
S.0010000110	↓↓↑↓↓↓↓↑↑↓	60.8	9.0	0.1	0.4
S.0001001001	↓↓↓↑↓↓↑↓↓↑	61.0	9.0	0.1	0.4
S.0111101101	↓↑↑↑↑↓↑↑↓↑	30.8	-7.0	0.0	0.4
S.0111011110	↓↑↑↑↓↑↑↑↑↓	30.8	-7.0	0.0	0.4
S.0100110111	↓↑↓↓↑↑↓↑↑↑	43.1	-3.0	0.2	0.4
S.0001101000	↓↓↓↑↑↓↑↓↓↓	60.8	9.0	0.1	0.4
S.0101010001	↓↑↓↑↓↑↓↓↓↑	20.3	5.0	0.1	0.4
S.0100010101	↓↑↓↓↓↑↓↑↓↑	22.2	5.0	0.1	0.4
S.0000110010	↓↓↓↓↑↑↓↓↑↓	41.7	9.0	0.1	0.4
S.0000100011	↓↓↓↓↑↓↓↓↑↑	42.0	9.0	0.1	0.4

S.0000010011	↓↓↓↓↓↑↓↓↑↑	42.0	9.0	0.1	0.4
S.0110111011	↓↑↑↓↑↑↑↓↑↑	35.7	-9.0	0.1	0.4
S.0110001000	↓↑↑↓↓↓↑↓↓↓	35.9	9.0	0.1	0.4
S.0101100000	↓↑↓↑↑↓↓↓↓↓	26.7	9.0	0.1	0.4
S.0100000110	↓↑↓↓↓↓↓↑↑↓	26.8	9.0	0.1	0.4
S.0111001101	↓↑↑↑↓↓↑↑↓↑	14.0	-3.0	0.0	0.4
S.0111011100	↓↑↑↑↓↑↑↑↓↓	14.0	-3.0	0.0	0.5
S.0101100001	↓↑↓↑↑↓↓↓↓↑	26.7	5.0	0.1	0.5
S.0100010110	↓↑↓↓↓↑↓↑↑↓	26.7	5.0	0.1	0.5
S.0011100100	↓↓↑↑↑↓↓↑↓↓	30.6	5.0	0.1	0.5
S.0111111101	↓↑↑↑↑↑↑↑↓↑	46.1	-9.0	0.0	0.5
S.0010001101	↓↓↑↓↓↓↑↑↓↑	36.5	5.0	0.1	0.5
S.0001001110	↓↓↓↑↓↓↑↑↑↓	30.5	5.0	0.1	0.5
S.0001100101	↓↓↓↑↑↓↓↑↓↑	36.4	5.0	0.1	0.5
S.0111011111	↓↑↑↑↓↑↑↑↑↑	45.8	-9.2	0.0	0.5
S.0011011000	↓↓↑↑↓↑↑↓↓↓	36.5	5.0	0.1	0.5
S.0001010110	↓↓↓↑↓↑↓↑↑↓	29.7	5.0	0.1	0.5
S.0010101001	↓↓↑↓↑↓↑↓↓↑	28.5	5.0	0.1	0.5
S.0010011010	↓↓↑↓↓↑↑↓↑↓	36.5	5.0	0.1	0.5
S.0111111000	↓↑↑↑↑↑↑↓↓↓	22.1	-3.0	0.1	0.5
S.0110001111	↓↑↑↓↓↓↑↑↑↑	22.1	-3.0	0.1	0.5
S.0000100110	↓↓↓↓↑↓↓↑↑↓	37.1	9.0	0.1	0.5
S.0000011001	↓↓↓↓↓↑↑↓↓↑	39.8	9.0	0.1	0.5

S.0010010001	↓↓↑↓↓↑↓↓↓↑	39.7	9.0	0.1	0.5
S.0100110101	↓↑↓↓↑↑↓↑↓↑	0.0	1.0	0.1	0.5
S.0101010011	↓↑↓↑↓↑↓↓↑↑	0.0	1.0	0.1	0.5
S.0001100010	↓↓↓↑↑↓↓↓↑↓	39.7	9.0	0.1	0.5
S.0011110101	↓↓↑↑↑↑↓↑↓↑	43.7	3.0	0.2	0.5
S.0100001011	↓↑↓↓↓↓↑↓↑↑	21.2	5.0	0.1	0.5
S.0001011111	↓↓↓↑↓↑↑↑↑↑	43.7	3.0	0.2	0.5
S.0011111010	↓↓↑↑↑↑↑↓↑↓	43.7	3.0	0.2	0.5
S.0111110001	↓↑↑↑↑↑↓↓↓↑	22.4	3.0	0.1	0.5
S.0010101111	↓↓↑↓↑↓↑↑↑↑	43.8	3.0	0.2	0.5
S.0100011111	↓↑↓↓↓↑↑↑↑↑	22.4	3.0	0.1	0.5
S.0000001101	↓↓↓↓↓↓↑↑↓↑	23.5	9.0	0.1	0.5
S.0011111110	↓↓↑↑↑↑↑↑↑↓	32.9	7.2	0.0	0.5
S.0111010110	↓↑↑↑↓↑↓↑↑↓	32.9	3.0	0.1	0.5
S.0000001110	↓↓↓↓↓↓↑↑↑↓	23.5	9.0	0.1	0.5
S.0011111101	↓↓↑↑↑↑↑↑↓↑	34.1	7.2	0.0	0.5
S.0011100000	↓↓↑↑↑↓↓↓↓↓	26.2	9.0	0.1	0.5
S.0011010000	↓↓↑↑↓↑↓↓↓↓	23.5	9.0	0.1	0.5
S.0111010000	↓↑↑↑↓↑↓↓↓↓	27.3	5.0	0.1	0.5
S.0101101101	↓↑↓↑↑↓↑↑↓↑	32.8	3.0	0.1	0.5
S.0111000101	↓↑↑↑↓↓↓↑↓↑	0.0	1.0	0.1	0.5
S.0101011100	↓↑↓↑↓↑↑↑↓↓	0.0	1.0	0.1	0.5
S.0100001101	↓↑↓↓↓↓↑↑↓↑	27.1	5.0	0.1	0.5

S.0011101111	↓↓↑↑↑↓↑↑↑↑	32.1	7.2	0.0	0.5
S.0010110010	↓↓↑↓↑↑↓↓↑↓	36.3	5.0	0.1	0.5
S.0001110101	↓↓↓↑↑↑↓↑↓↑	0.0	1.0	0.1	0.5
S.0001001101	↓↓↓↑↓↓↑↑↓↑	29.4	5.0	0.1	0.5
S.0001110001	↓↓↓↑↑↑↓↓↓↑	36.3	5.0	0.1	0.5
S.0111100100	↓↑↑↑↑↓↓↑↓↓	0.0	1.0	0.1	0.5
S.0001010111	↓↓↓↑↓↑↓↑↑↑	0.0	1.0	0.1	0.5
S.0010101011	↓↓↑↓↑↓↑↓↑↑	0.0	1.0	0.1	0.5
S.0010111010	↓↓↑↓↑↑↑↓↑↓	0.0	1.0	0.1	0.5
S.0011010100	↓↓↑↑↓↑↓↑↓↓	29.5	5.0	0.1	0.5
S.0101001110	↓↑↓↑↓↓↑↑↑↓	0.0	1.0	0.1	0.5
S.0110111101	↓↑↑↓↑↑↑↑↓↑	39.8	-9.0	0.1	0.5
S.0111011011	↓↑↑↑↓↑↑↓↑↑	37.1	-9.0	0.1	0.5
S.0010001110	↓↓↑↓↓↓↑↑↑↓	29.2	5.0	0.1	0.5
S.0110000001	↓↑↑↓↓↓↓↓↓↑	41.3	9.0	0.1	0.5
S.0011001111	↓↓↑↑↓↓↑↑↑↑	37.3	-3.0	0.0	0.5
S.0011111100	↓↓↑↑↑↑↑↑↓↓	37.1	-3.0	0.0	0.5
S.0100011000	↓↑↓↓↓↑↑↓↓↓	38.7	9.0	0.1	0.5
S.0011101000	↓↓↑↑↑↓↑↓↓↓	29.3	5.0	0.1	0.5
S.0111001111	↓↑↑↑↓↓↑↑↑↑	27.5	-5.0	0.1	0.5
S.0000100101	↓↓↓↓↑↓↓↑↓↑	40.1	9.0	0.1	0.5
S.0001010010	↓↓↓↑↓↑↓↓↑↓	40.1	9.0	0.1	0.5
S.0010100001	↓↓↑↓↑↓↓↓↓↑	40.1	9.0	0.1	0.5

S.0000011010	↓↓↓↓↓↑↑↓↑↓	40.1	9.0	0.1	0.5
S.0011011111	↓↓↑↑↓↑↑↑↑↑	38.8	-7.7	0.0	0.5
S.0101010010	↓↑↓↑↓↑↓↓↑↓	38.2	5.0	0.1	0.5
S.0000101011	↓↓↓↓↑↓↑↓↑↑	31.2	5.0	0.0	0.5
S.0111111100	↓↑↑↑↑↑↑↑↓↓	30.5	-5.0	0.0	0.5
S.0100100101	↓↑↓↓↑↓↓↑↓↑	33.7	5.0	0.1	0.5
S.0101110010	↓↑↓↑↑↑↓↓↑↓	0.0	1.0	0.1	0.5
S.0000010111	↓↓↓↓↓↑↓↑↑↑	37.7	5.0	0.0	0.5
S.0101001001	↓↑↓↑↓↓↑↓↓↑	29.4	5.0	0.1	0.5
S.0100100111	↓↑↓↓↑↓↓↑↑↑	0.0	1.0	0.1	0.5
S.0111000100	↓↑↑↑↓↓↓↑↓↓	38.9	5.0	0.1	0.5
S.0101001100	↓↑↓↑↓↓↑↑↓↓	38.9	5.0	0.1	0.5
S.0110010100	↓↑↑↓↓↑↓↑↓↓	38.8	5.0	0.1	0.5
S.0001001011	↓↓↓↑↓↓↑↓↑↑	35.7	5.0	0.1	0.5
S.0000110100	↓↓↓↓↑↑↓↑↓↓	29.8	9.0	0.1	0.5
S.0001000011	↓↓↓↑↓↓↓↓↑↑	27.1	9.0	0.1	0.5
S.0010110100	↓↓↑↓↑↑↓↑↓↓	35.7	5.0	0.1	0.5
S.0000111000	↓↓↓↓↑↑↑↓↓↓	27.1	9.0	0.1	0.5
S.0101111101	↓↑↓↑↑↑↑↑↓↑	25.0	-5.0	0.1	0.5
S.0010000111	↓↓↑↓↓↓↓↑↑↑	35.7	5.0	0.1	0.5
S.0010000011	↓↓↑↓↓↓↓↓↑↑	29.8	9.0	0.1	0.5
S.0111110110	↓↑↑↑↑↑↓↑↑↓	24.7	-5.0	0.1	0.5
S.0000010101	↓↓↓↓↓↑↓↑↓↑	29.3	9.0	0.1	0.5

S.0111010111	↓↑↑↑↓↑↓↑↑↑	25.1	-5.0	0.1	0.5
S.0001111000	↓↓↓↑↑↑↑↓↓↓	35.7	5.0	0.1	0.5
S.0010100010	↓↓↑↓↑↓↓↓↑↓	29.3	9.0	0.1	0.5
S.0001010001	↓↓↓↑↓↑↓↓↓↑	30.0	9.0	0.1	0.5
S.0000101010	↓↓↓↓↑↓↑↓↑↓	29.9	9.0	0.1	0.5
S.0101101111	↓↑↓↑↑↓↑↑↑↑	24.7	-5.0	0.1	0.5
S.0010000101	↓↓↑↓↓↓↓↑↓↑	40.2	9.0	0.1	0.5
S.0001001010	↓↓↓↑↓↓↑↓↑↓	40.2	9.0	0.1	0.5
S.0010100100	↓↓↑↓↑↓↓↑↓↓	40.2	9.0	0.1	0.5
S.0001011000	↓↓↓↑↓↑↑↓↓↓	40.2	9.0	0.1	0.5
S.0011110111	↓↓↑↑↑↑↓↑↑↑	30.7	-7.0	0.1	0.5
S.0101111000	↓↑↓↑↑↑↑↓↓↓	0.0	1.0	0.1	0.5
S.0010111111	↑↓↓↑↓↑↑↑↑↑↑	30.7	-7.0	0.1	0.5
S.0110000111	↑↓↑↑↓↓↓↓↑↑↑	0.0	1.0	0.1	0.5
S.0011111011	↑↓↓↑↑↑↑↑↓↑↑	30.7	-7.0	0.1	0.5
S.0001111111	↑↓↓↓↑↑↑↑↑↑↑	30.7	-7.0	0.1	0.5
S.0000011111	↑↓↓↓↓↓↑↑↑↑↑	0.0	1.0	0.1	0.5
S.0101111011	↑↓↑↓↑↑↑↑↓↑↑	30.4	-7.0	0.1	0.5
S.0011110010	↑↓↓↑↑↑↑↓↓↑↓	0.0	1.0	0.1	0.5
S.0011110001	↑↓↓↑↑↑↑↓↓↓↑	0.0	1.0	0.1	0.5
S.0110110111	↑↓↑↑↓↑↑↓↑↑↑	30.4	-7.0	0.1	0.5
S.0101001011	↑↓↑↓↑↓↓↑↓↑↑	0.0	1.0	0.1	0.5
S.0101000010	↑↓↑↓↑↓↓↓↓↑↓	27.5	9.0	0.1	0.5

S.0100100100	↑↓↑↓↓↑↓↓↑↓↓	30.6	9.0	0.1	0.5
S.0010011111	↑↓↓↑↓↓↑↑↑↑↑	13.1	-3.0	0.0	0.5
S.0011110110	↑↓↓↑↑↑↑↓↑↑↓	13.1	-3.0	0.0	0.5
S.0011111001	↑↓↓↑↑↑↑↑↓↓↑	13.1	-3.0	0.0	0.5
S.0110100000	↑↓↑↑↓↑↓↓↓↓↓	29.3	9.0	0.1	0.5
S.0100001010	↑↓↑↓↓↓↓↑↓↑↓	31.1	9.0	0.1	0.5
S.0001101111	↑↓↓↓↑↑↓↑↑↑↑	13.1	-3.0	0.0	0.5
S.0110000100	↑↓↑↑↓↓↓↓↑↓↓	42.2	9.0	0.1	0.5
S.0101001000	↑↓↑↓↑↓↓↑↓↓↓	42.2	9.0	0.1	0.5
S.0110010111	↑↓↑↑↓↓↑↓↑↑↑	12.7	-3.0	0.0	0.5
S.0101111001	↑↓↑↓↑↑↑↑↓↓↑	12.6	-3.0	0.0	0.5
S.0111011101	↑↓↑↑↑↓↑↑↑↓↑	27.5	-5.2	0.0	0.5
S.0001010101	↑↓↓↓↑↓↑↓↑↓↑	27.8	7.0	0.0	0.5
S.0010101010	↑↓↓↑↓↑↓↑↓↑↓	27.8	7.0	0.0	0.5
S.0000011011	↑↓↓↓↓↓↑↑↓↑↑	38.3	7.0	0.1	0.5
S.0000100111	↑↓↓↓↓↑↓↓↑↑↑	38.3	7.0	0.1	0.5
S.0010110001	↑↓↓↑↓↑↑↓↓↓↑	38.3	7.0	0.1	0.5
S.0010111011	↑↓↓↑↓↑↑↑↓↑↑	26.2	-3.0	0.1	0.5
S.0111100111	↑↓↑↑↑↑↓↓↑↑↑	38.1	-7.0	0.1	0.5
S.0001110111	↑↓↓↓↑↑↑↓↑↑↑	26.2	-3.0	0.1	0.5
S.0100110011	↑↓↑↓↓↑↑↓↓↑↑	0.0	1.0	0.1	0.5
S.0101111110	↑↓↑↓↑↑↑↑↑↑↓	38.2	-7.0	0.1	0.5
S.0001110010	↑↓↓↓↑↑↑↓↓↑↓	38.3	7.0	0.1	0.5

S.0111111010	↑↓↑↑↑↑↑↑↓↑↓	35.7	-7.0	0.1	0.6
S.0100001100	↑↓↑↓↓↓↓↑↑↓↓	29.3	9.0	0.1	0.6
S.0101111100	↑↓↑↓↑↑↑↑↑↓↓	28.1	-3.0	0.1	0.6
S.0111000000	↑↓↑↑↑↓↓↓↓↓↓	29.3	9.0	0.1	0.6
S.0111000111	↑↓↑↑↑↓↓↓↑↑↑	28.0	-3.0	0.1	0.6
S.0010011001	↑↓↓↑↓↓↑↑↓↓↑	50.8	7.0	0.1	0.6
S.0001100110	↓ ↓ ↓ ↑↑ ↓ ↓ ↑↑ ↓	50.8	7.0	0.1	0.6
S.0101100110	↓ ↑ ↓ ↑↑ ↓ ↓ ↑↑ ↓	0.0	1.0	0.1	0.6
S.0110001001	↓ ↑↑ ↓ ↓ ↓ ↑ ↓ ↓ ↑	48.6	7.0	0.1	0.6
S.0111110011	↓ ↑↑↑↑↑ ↓ ↓ ↑↑	38.3	7.0	0.1	0.6
S.0110011000	↓ ↑↑ ↓ ↓ ↑↑ ↓ ↓ ↓	48.5	7.0	0.1	0.6
S.0100111111	↓ ↑ ↓ ↓ ↑↑↑↑↑↑	38.3	7.0	0.1	0.6
S.0101000011	↓ ↑ ↓ ↑ ↓ ↓ ↓ ↓ ↑↑	25.9	7.0	0.0	0.6
S.0100100011	↓ ↑ ↓ ↓ ↑ ↓ ↓ ↓ ↑↑	39.2	5.0	0.1	0.6
S.0100110100	↓ ↑ ↓ ↓ ↑↑ ↓ ↑ ↓ ↓	25.9	7.0	0.0	0.6
S.0100110010	↓ ↑ ↓ ↓ ↑↑ ↓ ↓ ↑ ↓	39.2	5.0	0.1	0.6
S.0110110101	↓ ↑↑ ↓ ↑↑ ↓ ↑ ↓ ↑	26.0	3.0	0.1	0.6
S.0111110010	↓ ↑↑↑↑↑ ↓ ↓ ↑ ↓	22.2	3.0	0.1	0.6
S.0101011011	↓ ↑ ↓ ↑ ↓ ↑↑ ↓ ↑↑	26.4	3.0	0.1	0.6
S.0111111001	↓ ↑↑↑↑↑↑ ↓ ↓ ↑	28.1	5.1	0.0	0.6
S.0110011111	↓ ↑↑ ↓ ↓ ↑↑↑↑↑	27.0	5.1	0.0	0.6
S.0100101111	↓ ↑ ↓ ↓ ↑ ↓ ↑↑↑↑	22.2	3.0	0.1	0.6
S.0110001101	↓ ↑↑ ↓ ↓ ↓ ↑↑ ↓ ↑	0.0	1.0	0.1	0.6

S.0111011000	↓ ↑ ↑ ↑ ↓ ↑ ↑ ↓ ↓ ↓	0.0	1.0	0.1	0.6
S.0011001100	↓ ↓ ↑ ↑ ↓ ↓ ↑ ↑ ↓ ↓	39.8	7.0	0.0	0.6
S.0100011001	↓ ↑ ↓ ↓ ↓ ↑ ↑ ↓ ↓ ↑	49.4	7.0	0.1	0.6
S.0110010001	↓ ↑ ↑ ↓ ↓ ↑ ↓ ↓ ↓ ↑	49.4	7.0	0.1	0.6
S.0010011100	↓ ↓ ↑ ↓ ↓ ↑ ↑ ↑ ↓ ↓	58.7	5.0	0.1	0.6
S.0001110110	↓ ↓ ↓ ↑ ↑ ↑ ↓ ↑ ↑ ↓	0.0	1.0	0.1	0.6
S.0010111001	↓ ↓ ↑ ↓ ↑ ↑ ↑ ↓ ↓ ↑	0.0	1.0	0.1	0.6
S.0010011011	↓ ↓ ↑ ↓ ↓ ↑ ↑ ↓ ↑ ↑	0.0	1.0	0.1	0.6
S.0011000110	↓ ↓ ↑ ↑ ↓ ↓ ↓ ↑ ↑ ↓	52.4	5.0	0.1	0.6
S.0011001001	↓ ↓ ↑ ↑ ↓ ↓ ↑ ↓ ↓ ↑	52.3	5.0	0.1	0.6
S.0001101100	↓ ↓ ↓ ↑ ↑ ↓ ↑ ↑ ↓ ↓	52.5	5.0	0.1	0.6
S.0001100111	↓ ↓ ↓ ↑ ↑ ↓ ↓ ↑ ↑ ↑	0.0	1.0	0.1	0.6
S.0100100010	↓ ↑ ↓ ↓ ↑ ↓ ↓ ↓ ↑ ↓	40.8	9.0	0.1	0.6
S.0111101011	↓ ↑ ↑ ↑ ↑ ↓ ↑ ↓ ↑ ↑	56.4	7.0	0.1	0.6
S.0111101110	↓ ↑ ↑ ↑ ↑ ↓ ↑ ↑ ↑ ↓	92.0	7.0	0.0	0.6
S.0110111110	↓ ↑ ↑ ↓ ↑ ↑ ↑ ↑ ↑ ↓	56.5	7.0	0.1	0.6
S.0100011011	↓ ↑ ↓ ↓ ↓ ↑ ↑ ↓ ↑ ↑	0.0	1.0	0.1	0.6
S.0110010010	↓ ↑ ↑ ↓ ↓ ↑ ↓ ↓ ↑ ↓	47.4	5.0	0.1	0.6
S.0100101001	↓ ↑ ↓ ↓ ↑ ↓ ↑ ↓ ↓ ↑	58.5	5.0	0.1	0.6
S.0001101001	↓ ↓ ↓ ↑ ↑ ↓ ↑ ↓ ↓ ↑	49.4	7.0	0.0	0.6
S.0110000101	↓ ↑ ↑ ↓ ↓ ↓ ↓ ↑ ↓ ↑	37.6	7.0	0.1	0.6
S.0111001100	↓ ↑ ↑ ↑ ↓ ↓ ↑ ↑ ↓ ↓	0.0	1.0	0.0	0.6
S.0101011000	↓ ↑ ↓ ↑ ↓ ↑ ↑ ↓ ↓ ↓	37.6	7.0	0.1	0.6

S.0000101101	↓ ↓ ↓ ↓ ↑ ↓ ↑ ↑ ↓ ↑	39.5	5	0.2	0.6
S.0011000101	↓ ↓ ↑ ↑ ↓ ↓ ↓ ↑ ↓ ↑	39.3	5	0.2	0.6
S.0011100001	↓ ↓ ↑ ↑ ↑ ↓ ↓ ↓ ↓ ↑	39.4	5	0.2	0.6
S.0000011110	↓ ↓ ↓ ↓ ↓ ↑ ↑ ↑ ↑ ↓	39.4	5	0.1	0.6
S.0110010101	↓ ↑ ↑ ↓ ↓ ↑ ↓ ↑ ↓ ↑	0	1	0.1	0.6
S.0110001011	↓ ↑ ↑ ↓ ↓ ↓ ↑ ↓ ↑ ↑	0	1	0.1	0.6
S.0010101100	↓ ↓ ↑ ↓ ↑ ↓ ↑ ↑ ↓ ↓	39.3	5	0.2	0.6
S.0011010010	↓ ↓ ↑ ↑ ↓ ↑ ↓ ↓ ↑ ↓	39.5	5	0.2	0.6
S.0011001010	↓ ↓ ↑ ↑ ↓ ↓ ↑ ↓ ↑ ↓	39.3	5	0.2	0.6
S.0001011100	↓ ↓ ↓ ↑ ↓ ↑ ↑ ↑ ↓ ↓	39.3	5	0.2	0.6
S.0110111000	↓ ↑ ↑ ↓ ↑ ↑ ↑ ↓ ↓ ↓	0	1	0.1	0.6
S.0101011001	↓ ↑ ↓ ↑ ↓ ↑ ↑ ↓ ↓ ↑	0	1	0.1	0.6
S.0110000110	↓ ↑ ↑ ↓ ↓ ↓ ↓ ↑ ↑ ↓	39.1	5	0.1	0.6
S.0101101000	↓ ↑ ↓ ↑ ↑ ↓ ↑ ↓ ↓ ↓	39.1	5	0.1	0.6
S.0011100101	↓ ↓ ↑ ↑ ↑ ↓ ↓ ↑ ↓ ↑	0	1	0.1	0.6
S.0001011110	↓ ↓ ↓ ↑ ↓ ↑ ↑ ↑ ↑ ↓	0	1	0.1	0.6
S.0010101101	↓ ↓ ↑ ↓ ↑ ↓ ↑ ↑ ↓ ↑	0	1	0.1	0.6
S.0101101100	↓ ↑ ↓ ↑ ↑ ↓ ↑ ↑ ↓ ↓	0	1	0.1	0.6
S.0111000110	↓ ↑ ↑ ↑ ↓ ↓ ↓ ↑ ↑ ↓	0	1	0.1	0.6
S.0011011010	↓ ↓ ↑ ↑ ↓ ↑ ↑ ↓ ↑ ↓	0	1	0.1	0.6
S.0100101000	↓ ↑ ↓ ↓ ↑ ↓ ↑ ↓ ↓ ↓	42.3	9	0.0	0.6
S.0110000010	↓ ↑ ↑ ↓ ↓ ↓ ↓ ↓ ↑ ↓	42.3	9	0.0	0.6
S.0111100000	↓ ↑ ↑ ↑ ↑ ↓ ↓ ↓ ↓ ↓	27.3	7	0.0	0.6

S.0100001110	↓ ↑ ↓ ↓ ↓ ↓ ↑ ↑ ↑ ↓	27.2	7	0.0	0.6
S.0000101100	↓ ↓ ↓ ↓ ↑ ↓ ↑ ↑ ↓ ↓	41.2	9	0.1	0.6
S.0000011100	↓ ↓ ↓ ↓ ↓ ↑ ↑ ↑ ↓ ↓	38.2	9	0.1	0.6
S.0011000001	↓ ↓ ↑ ↑ ↓ ↓ ↓ ↓ ↓ ↑	41.2	9	0.1	0.6
S.0011000010	↓ ↓ ↑ ↑ ↓ ↓ ↓ ↓ ↑ ↓	41.2	9	0.1	0.6
S.0011001101	↓ ↓ ↑ ↑ ↓ ↓ ↑ ↑ ↓ ↑	65.5	3	0.0	0.6
S.0111010001	↓ ↑ ↑ ↑ ↓ ↑ ↓ ↓ ↓ ↑	0	1	0.1	0.6
S.0011011100	↓ ↓ ↑ ↑ ↓ ↑ ↑ ↑ ↓ ↓	65.5	3	0.0	0.6
S.0011001110	↓ ↓ ↑ ↑ ↓ ↓ ↑ ↑ ↑ ↓	65.6	3	0.0	0.6
S.0011101100	↓ ↓ ↑ ↑ ↑ ↓ ↑ ↑ ↓ ↓	65.5	3	0.0	0.6
S.0100011101	↓ ↑ ↓ ↓ ↓ ↑ ↑ ↑ ↓ ↑	0	1	0.1	0.6
S.0100101011	↓ ↑ ↓ ↓ ↑ ↓ ↑ ↓ ↑ ↑	0	1	0.1	0.6
S.0011000111	↓ ↓ ↑ ↑ ↓ ↓ ↓ ↑ ↑ ↑	0	1	0.1	0.6
S.0001111100	↓ ↓ ↓ ↑ ↑ ↑ ↑ ↑ ↓ ↓	0	1	0.1	0.6
S.0010111100	↓ ↓ ↑ ↓ ↑ ↑ ↑ ↑ ↓ ↓	0	1	0.1	0.6
S.0011001011	↓ ↓ ↑ ↑ ↓ ↓ ↑ ↓ ↑ ↑	0	1	0.1	0.6
S.0111010010	↓ ↑ ↑ ↑ ↓ ↑ ↓ ↓ ↑ ↓	0	1	0.1	0.6
S.0111011010	↓ ↑↑↑↓ ↑ ↓ ↑↓	26.0	5.0	0.2	0.7
S.0100011010	↓ ↑↓ ↓ ↓ ↑↑↓ ↑↓	25.8	5.0	0.2	0.7
S.0100101101	↓ ↑↓ ↓ ↑↓ ↑↑↓ ↑	0.0	1.0	0.1	0.7
S.0111100110	↓ ↑↑↑↑↓ ↓ ↑↑↓	33.2	3.0	0.1	0.7
S.0101101110	↓ ↑↓ ↑↑↓ ↑↑↑↓	32.4	3.0	0.1	0.7
S.0011101101	↓ ↓ ↑↑↑↓ ↑↑↓ ↑	0.0	1.0	0.0	0.7

S.0011011110	↓ ↓ ↑ ↑ ↓ ↑ ↑ ↑ ↑ ↓	0.0	1.1	0.0	0.7
S.0111101100	↓ ↑ ↑ ↑ ↑ ↓ ↑ ↑ ↓ ↓	0.0	1.0	0.0	0.7
S.0101100010	↓ ↑ ↓ ↑ ↑ ↓ ↓ ↓ ↑ ↓	32.4	5.0	0.1	0.7
S.0111001110	↓ ↑ ↑ ↑ ↓ ↓ ↑ ↑ ↑ ↓	0.0	1.0	0.0	0.7
S.0100100110	↓ ↑ ↓ ↓ ↑ ↓ ↓ ↑ ↑ ↓	35.6	5.0	0.1	0.7
S.0010011110	↓ ↓ ↑ ↓ ↓ ↑ ↑ ↑ ↑ ↓	61.6	3.0	0.1	0.7
S.0011010110	↓ ↓ ↑ ↑ ↓ ↑ ↓ ↑ ↑ ↓	60.1	3.0	0.1	0.7
S.0001101101	↓ ↓ ↓ ↑ ↑ ↓ ↑ ↑ ↓ ↑	61.9	3.0	0.1	0.7
S.0011101001	↓ ↓ ↑ ↑ ↑ ↓ ↑ ↓ ↓ ↑	59.8	3.0	0.1	0.7
S.0110001100	↓ ↑ ↑ ↓ ↓ ↓ ↑ ↑ ↓ ↓	27.7	7.0	0.1	0.7
S.0110000011	↓ ↑ ↑ ↓ ↓ ↓ ↓ ↓ ↑ ↑	37.4	5.0	0.1	0.7
S.0100111000	↓ ↑ ↓ ↓ ↑ ↑ ↑ ↓ ↓ ↓	37.4	5.0	0.1	0.7
S.0111001000	↓ ↑ ↑ ↑ ↓ ↓ ↑ ↓ ↓ ↓	29.4	6.5	0.0	0.7
S.0111010011	↓ ↑ ↑ ↑ ↓ ↑ ↓ ↓ ↑ ↑	32.5	3.0	0.1	0.7
S.0110111010	↓ ↑ ↑ ↓ ↑ ↑ ↑ ↓ ↑ ↓	33.8	3.0	0.1	0.7
S.0100111101	↓ ↑ ↓ ↓ ↑ ↑ ↑ ↑ ↓ ↑	33.7	3.0	0.1	0.7
S.0111101000	↓ ↑ ↑ ↑ ↑ ↓ ↑ ↓ ↓ ↓	41.9	3.0	0.1	0.7
S.0110001110	↓ ↑ ↑ ↓ ↓ ↓ ↑ ↑ ↑ ↓	42.0	3.0	0.1	0.7
S.0000110101	↓ ↓ ↓ ↓ ↑ ↑ ↓ ↑ ↓ ↑	34.4	5.0	0.2	0.7
S.0001010011	↓ ↓ ↓ ↑ ↓ ↑ ↓ ↓ ↑ ↑	34.4	5.0	0.2	0.7
S.0000111010	↓ ↓ ↓ ↓ ↑ ↑ ↑ ↓ ↑ ↓	34.3	5.0	0.2	0.7
S.0010100011	↓ ↓ ↑ ↓ ↑ ↓ ↓ ↓ ↑ ↑	34.3	5.0	0.2	0.7
S.0110011010	↓ ↑ ↑ ↓ ↓ ↑ ↑ ↓ ↑ ↓	0.0	1.0	0.1	0.7

S.0110101001	↓ ↑ ↑ ↓ ↑ ↓ ↑ ↓ ↓ ↑	0.0	1.0	0.1	0.7
S.0101100011	↓ ↑ ↓ ↑ ↑ ↓ ↓ ↓ ↑ ↑	50.0	3.0	0.0	0.7
S.0010010111	↓ ↓ ↑ ↓ ↓ ↑ ↓ ↑ ↑ ↑	41.2	3.0	0.1	0.7
S.0100110110	↓ ↑ ↓ ↓ ↑ ↑ ↓ ↑ ↑ ↓	49.9	3.0	0.0	0.7
S.0001101011	↓ ↓ ↓ ↑ ↑ ↓ ↑ ↓ ↑ ↑	41.2	3.0	0.1	0.7
S.0010110110	↓ ↓ ↑ ↓ ↑ ↑ ↓ ↑ ↑ ↓	41.2	3.0	0.1	0.7
S.0000110110	↓ ↓ ↓ ↓ ↑ ↑ ↓ ↑ ↑ ↓	24.2	6.7	0.0	0.7
S.0001111001	↓ ↓ ↓ ↑ ↑ ↑ ↑ ↓ ↓ ↑	41.2	3.0	0.1	0.7
S.0110010110	↓ ↑ ↑ ↓ ↓ ↑ ↓ ↑ ↑ ↓	71.8	3.0	0.1	0.7
S.0000111001	↓ ↓ ↓ ↓ ↑ ↑ ↑ ↓ ↓ ↑	25.7	6.5	0.0	0.7
S.0010010011	↓ ↓ ↑ ↓ ↓ ↑ ↓ ↓ ↑ ↑	25.6	6.5	0.0	0.7
S.0111001011	↓ ↑ ↑ ↑ ↓ ↓ ↑ ↓ ↑ ↑	32.3	3.0	0.1	0.7
S.0110111100	↓ ↑ ↑ ↓ ↑ ↑ ↑ ↑ ↓ ↓	32.3	3.0	0.1	0.7
S.0001100011	↓ ↓ ↓ ↑ ↑ ↓ ↓ ↓ ↑ ↑	25.5	6.5	0.0	0.7
S.0111001001	↓ ↑ ↑ ↑ ↓ ↓ ↑ ↓ ↓ ↑	0.0	1.0	0.1	0.7
S.0110011100	↓ ↑ ↑ ↓ ↓ ↑ ↑ ↑ ↓ ↓	0.0	1.0	0.1	0.7
S.0010010101	↓ ↓ ↑ ↓ ↓ ↑ ↓ ↑ ↓ ↑	24.2	6.5	0.0	0.7
S.0001011001	↓ ↓ ↓ ↑ ↓ ↑ ↑ ↓ ↓ ↑	23.9	6.5	0.0	0.7
S.0110011001	↓ ↑ ↑ ↓ ↓ ↑ ↑ ↓ ↓ ↑	104.3	3.0	0.0	0.7
S.0001111101	↓ ↓ ↓ ↑ ↑ ↑ ↑ ↑ ↓ ↑	0.0	1.0	0.1	0.7
S.0011010111	↓ ↓ ↑ ↑ ↓ ↑ ↓ ↑ ↑ ↑	0.0	1.0	0.1	0.7
S.0001101010	↓ ↓ ↓ ↑ ↑ ↓ ↑ ↓ ↑ ↓	24.0	6.5	0.0	0.7
S.0010111110	↓ ↓ ↑ ↓ ↑ ↑ ↑ ↑ ↑ ↓	0.0	1.0	0.1	0.7

S.0011101011	↓ ↓ ↑ ↑ ↑ ↓ ↑ ↓ ↑ ↑	0.0	1.0	0.1	0.7
S.0000110011	↓ ↓ ↓ ↓ ↑ ↑ ↓ ↓ ↑ ↑	52.4	9.0	0.0	0.7
S.0011011101	↓ ↓ ↑ ↑ ↓ ↑ ↑ ↑ ↓ ↑	0.0	1.0	0.0	0.7
S.0011101110	↓ ↓ ↑ ↑ ↑ ↓ ↑ ↑ ↑ ↓	0.0	1.0	0.0	0.7
S.0011010101	↓ ↓ ↑ ↑ ↓ ↑ ↓ ↑ ↓ ↑	112.4	2.6	0.0	0.7
S.0111100001	↓ ↑ ↑ ↑ ↑ ↓ ↓ ↓ ↓ ↑	98.4	2.7	0.0	0.7
S.0001011101	↓ ↓ ↓ ↑ ↓ ↑ ↑ ↑ ↓ ↑	114.6	2.6	0.0	0.7
S.0010101110	↓ ↓ ↑ ↓ ↑ ↓ ↑ ↑ ↑ ↓	50.6	3.0	0.0	0.7
S.0011101010	↓ ↓ ↑ ↑ ↑ ↓ ↑ ↓ ↑ ↓	48.4	3.0	0.0	0.7
S.0100011110	↓ ↑ ↓ ↓ ↓ ↑ ↑ ↑ ↑ ↓	98.5	2.7	0.0	0.7
S.0110101000	↓ ↑ ↑ ↓ ↑ ↓ ↑ ↓ ↓ ↓	61.6	7.0	0.0	0.7
S.0110001010	↓ ↑ ↑ ↓ ↓ ↓ ↑ ↓ ↑ ↓	61.7	7.0	0.0	0.7
S.0101101011	↓ ↑ ↓ ↑ ↑ ↓ ↑ ↓ ↑ ↑	0.0	1.0	0.1	0.7
S.0101001010	↓ ↑ ↓ ↑ ↓ ↓ ↑ ↓ ↑ ↓	33.9	5.0	0.2	0.7
S.0110110110	↓ ↑ ↑ ↓ ↑ ↑ ↓ ↑ ↑ ↓	0.0	1.0	0.1	0.7
S.0111101001	↓ ↑ ↑ ↑ ↑ ↓ ↑ ↓ ↓ ↑	0.0	1.0	0.0	0.7
S.0110100100	↓ ↑ ↑ ↓ ↑ ↓ ↓ ↑ ↓ ↓	33.9	5.0	0.2	0.7
S.0110011110	↓ ↑ ↑ ↓ ↓ ↑ ↑ ↑ ↑ ↓	0.0	1.0	0.0	0.7
S.0010011101	↓ ↓ ↑ ↓ ↓ ↑ ↑ ↑ ↓ ↑	93.8	2.3	0.0	0.7
S.0011100110	↓ ↓ ↑ ↑ ↑ ↓ ↓ ↑ ↑ ↓	100.8	2.3	0.0	0.7
S.0011011001	↓ ↓ ↑ ↑ ↓ ↑ ↑ ↓ ↓ ↑	103.5	2.3	0.0	0.7
S.0001101110	↓ ↓ ↓ ↑ ↑ ↓ ↑ ↑ ↑ ↓	102.2	2.3	0.0	0.7
S.0100111001	↓ ↑ ↓ ↓ ↑ ↑ ↑ ↓ ↓ ↑	55.8	3.0	0.1	0.7

S.0110010011	↓ ↑ ↑ ↓ ↓ ↑ ↓ ↓ ↑ ↑	55.8	3.0	0.1	0.7
S.0111011001	↓ ↑ ↑ ↑ ↓ ↑ ↑ ↓ ↓ ↑	0.0	1.0	0.1	0.7
S.0110011101	↓ ↑ ↑ ↓ ↓ ↑ ↑ ↑ ↓ ↑	0.0	1.0	0.1	0.7
S.0110111001	↓ ↑ ↑ ↓ ↑ ↑ ↑ ↓ ↓ ↑	0.0	1.0	0.1	0.7
S.0000011101	↓ ↓ ↓ ↓ ↓ ↑ ↑ ↑ ↓ ↑	60.9	7.0	0.0	0.8
S.0000101110	↓ ↓ ↓ ↓ ↑ ↓ ↑ ↑ ↑ ↓	60.8	7.0	0.0	0.8
S.0011010001	↓ ↓ ↑ ↑ ↓ ↑ ↓ ↓ ↓ ↑	60.8	7.0	0.0	0.8
S.0010100110	↓ ↓ ↑ ↓ ↑ ↓ ↓ ↑ ↑ ↓	38.0	6.3	0.0	0.8
S.0011100010	↓ ↓ ↑ ↑ ↑ ↓ ↓ ↓ ↑ ↓	60.7	7.0	0.0	0.8
S.0111000001	↓ ↑ ↑ ↑ ↓ ↓ ↓ ↓ ↓ ↑	55.2	6.6	0.0	0.8
S.0100011100	↓ ↑ ↓ ↓ ↓ ↑ ↑ ↑ ↓ ↓	55.1	6.6	0.0	0.8
S.0010100101	↓ ↓ ↑ ↓ ↑ ↓ ↓ ↑ ↓ ↑	54.7	9.0	0.0	0.8
S.0001011010	↓ ↓ ↓ ↑ ↓ ↑ ↑ ↓ ↑ ↓	54.8	9.0	0.0	0.8
S.0000110111	↓ ↓ ↓ ↓ ↑ ↑ ↓ ↑ ↑ ↑	28.1	5.0	0.1	0.8
S.0000111011	↓ ↓ ↓ ↓ ↑ ↑ ↑ ↓ ↑ ↑	28.0	5.0	0.1	0.8
S.0010110011	↓ ↓ ↑ ↓ ↑ ↑ ↓ ↓ ↑ ↑	28.0	5.0	0.1	0.8
S.0001110011	↓ ↓ ↓ ↑ ↑ ↑ ↓ ↓ ↑ ↑	28.0	5.0	0.1	0.8
S.0101111010	↓ ↑ ↓ ↑ ↑ ↑ ↑ ↓ ↑ ↓	0.0	1.0	0.1	0.8
S.0110100111	↓ ↑ ↑ ↓ ↑ ↓ ↓ ↑ ↑ ↑	0.0	1.0	0.1	0.8
S.0111100011	↓ ↑ ↑ ↑ ↑ ↓ ↓ ↓ ↑ ↑	26.6	3.0	0.1	0.8
S.0000111111	↓ ↓ ↓ ↓ ↑ ↑ ↑ ↑ ↑ ↑	0.0	1.0	0.1	0.8
S.0010110101	↓ ↓ ↑ ↓ ↑ ↑ ↓ ↑ ↓ ↑	27.0	5.0	0.1	0.8
S.0001011011	↓ ↓ ↓ ↑ ↓ ↑ ↑ ↓ ↑ ↑	27.0	5.0	0.1	0.8

S.0100111110	↓ ↑ ↓ ↓ ↑ ↑ ↑ ↑ ↑ ↓	26.7	3.0	0.1	0.8
S.0010100111	↓ ↓ ↑ ↓ ↑ ↓ ↓ ↑ ↑ ↑	27.0	5.0	0.1	0.8
S.0011110011	↓ ↓ ↑ ↑ ↑ ↑ ↓ ↓ ↑ ↑	0.0	1.0	0.1	0.8
S.0001111010	↓ ↓ ↓ ↑ ↑ ↑ ↑ ↓ ↑ ↓	27.0	5.0	0.1	0.8
S.0111101010	↓ ↑ ↑ ↑ ↑ ↓ ↑ ↓ ↑ ↓	27.6	3.0	0.1	0.8
S.0110101010	↓ ↑ ↑ ↓ ↑ ↓ ↑ ↓ ↑ ↓	0.0	1.0	0.1	0.8
S.0101011010	↓ ↑ ↓ ↑ ↓ ↑ ↑ ↓ ↑ ↓	24.4	5.0	0.1	0.8
S.0111000011	↓ ↑ ↑ ↑ ↓ ↓ ↓ ↓ ↑ ↑	0.0	1.0	0.1	0.8
S.0110100101	↓ ↑ ↑ ↓ ↑ ↓ ↓ ↑ ↓ ↑	24.4	5.0	0.1	0.8
S.0100111100	↓ ↑ ↓ ↓ ↑ ↑ ↑ ↑ ↓ ↓	0.0	1.0	0.1	0.8
S.0111100010	↓ ↑ ↑ ↑ ↑ ↓ ↓ ↓ ↑ ↓	0.0	1.0	0.1	0.9
S.0100101110	↓ ↑ ↓ ↓ ↑ ↓ ↑ ↑ ↑ ↓	0.0	1.0	0.1	0.9
S.0100101010	↓ ↑ ↓ ↓ ↑ ↓ ↑ ↓ ↑ ↓	40.7	7.0	0.1	0.9
S.0110100010	↓ ↑ ↑ ↓ ↑ ↓ ↓ ↓ ↑ ↓	40.7	7.0	0.1	0.9
S.0111001010	↓ ↑ ↑ ↑ ↓ ↓ ↑ ↓ ↑ ↓	0.0	1.0	0.1	0.9
S.0000111100	↓ ↓ ↓ ↓ ↑ ↑ ↑ ↑ ↓ ↓	42.2	7.0	0.1	0.9
S.0100101100	↓ ↑ ↓ ↓ ↑ ↓ ↑ ↑ ↓ ↓	43.5	7.0	0.1	0.9
S.0111000010	↓ ↑ ↑ ↑ ↓ ↓ ↓ ↓ ↑ ↓	43.6	7.0	0.1	0.9
S.0011000011	↓ ↓ ↑ ↑ ↓ ↓ ↓ ↓ ↑ ↑	42.2	7.0	0.1	0.9
S.0110100011	↓ ↑ ↑ ↓ ↑ ↓ ↓ ↓ ↑ ↑	64.6	2.4	0.0	0.9
S.0110100110	↓ ↑ ↑ ↓ ↑ ↓ ↓ ↑ ↑ ↓	55.0	2.5	0.0	0.9
S.0000111101	↓ ↓ ↓ ↓ ↑ ↑ ↑ ↑ ↓ ↑	51.1	2.5	0.0	0.9
S.0101101010	↓ ↑ ↓ ↑ ↑ ↓ ↑ ↓ ↑ ↓	42.8	2.7	0.0	0.9

S.0011100011	↓ ↓ ↑ ↑ ↑ ↓ ↓ ↓ ↑ ↑	56.3	2.4	0.0	0.9
S.0011010011	↓ ↓ ↑ ↑ ↓ ↑ ↓ ↓ ↑ ↑	58.0	2.4	0.0	0.9
S.0000111110	↓ ↓ ↓ ↓ ↑ ↑ ↑ ↑ ↑ ↓	56.0	2.3	0.0	1.0

The spin ordering of Mn atoms in the cluster are arranged according to their energy as shown in the table above. The first 10 cluster with different spin ordering are selected and again optimized by running several iteration in order to find the lower energy clusters compare to the ferromagnetic one. These optimized clusters are again investigated by computing MAE, M.M, H-L gap and E-E_{FM} which are shown in the table below.

Table 3.24: Data for optimized lowest energy molecules for the $As_{21}Ni_2Mn_{10}$ system

Systems	**MAE (K)**	**M.M μ_B**	**H-L gap (eV)**	**E_{AFM}-E_{FM} (eV)**
S.000010001 ↓↓↓↓↓↑↓↓↓↑	35.58	13	0.27	-0.12
S.0000000100 ↓↓↓↓↓↓↓↑↓↓	26.63	15	0.2	-0.02
S.0001000000 ↓↓↓↑↓↓↓↓↓↓	27.08	15	0.2	0.01
S.0111110100 ↓↑↑↑↑↑↓↑↓↓	23.06	3	0.22	0.07
S.0000100000 ↓↓↓↓↑↓↓↓↓↓	26.86	15	0.19	0.09
S.0000010000 ↓↓↓↓↓↑↓↓↓↓	25.55	15	0.13	0.10
S.0000000010 ↓↓↓↓↓↓↓↓↑↓	25.60	15	0.14	0.10
S.0010001000 ↓↓↑↓↓↓↑↓↓↓	25.80	13	0.11	0.13
S.0001000100 ↓↓↓↑↓↓↓↑↓↓	26.62	13	0.11	0.13
S.0000010001 ↓↓↓↓↓↑↓↓↓↑	29.35	13	0.18	0.14
S.0000001000 ↓↓↓↓↓↓↑↓↓↓	25.81	15	0.12	0.16
S.0010000000 ↓↓↑↓↓↓↓↓↓↓	25.82	15	0.12	0.16
S.0000100001 ↓↓↓↓↑↓↓↓↓↑	41.69	13	0.15	0.18
S.0000010010 ↓↓↓↓↓↑↓↓↑↓	41.40	13	0.15	0.19

In the above table it is evident that the first two clusters have lower energy compare to the ferromagnetic case. The cluster with spin ordering S.000010001 has the lowest energy and it can be

considered as the most favorable cluster of the $As@Ni_2Mn_{10}@As_{20}$ system which has magnetic anisotropy energy of 35.58 K. In the S.000010001 spin ordering, eight of the Mn atoms have spin down (0) and the other two Mn atoms have up spin (1).

CHAPTER 4: CONCLUSIONS

We have investigated the Mn doped $As@Ni_{12-x}Mn_x@As_{20}$ cages for x=1-10. The $As@Ni_{12}@As_{20}$ cage is symmetric and as a result does not have any magnetic anisotropy. In this cage each Ni atom is coordinated with five As atoms. The Ni atoms form an icosahedral inner cage and thus each Ni atom is also coordinated to five other Ni atoms. The doping is substitutional in nature, that is, Ni atoms are replaced by the Mn atoms. As a result, the Mn atoms in these clusters also have similar coordination with As and Ni/other Mn atoms. The substitutional doping of As atoms by multiple Mn atoms can result in various different isomers. We considered all possible substitutional ordering/permutations, that is, for a given x in $As@Ni_{12-x}Mn_x@As_{20}$ all possible isomers arising due to different configurations of substitutional doping were considered. The resultant geometry of every such an isomer was optimized simultaneously with spin optimization to find most stable isomers with ferromagnetic spin ordering. These results indicated that the spin charges are mainly located on the Mn atoms. Due to this reason, the search of possible ferrimagnetic spin ordering involved spin orientations of only Mn atoms. We find that the doping by Mn increases the atomization energy of the whole cluster. The atomization energy of the parent $As@Ni_{12}@As_{20}$ cage is 4.8 eV which increases to 5.86 eV for the $As@Ni_2Mn_{10}@As_{20}$ cluster. The As-Mn bonds are shorter than the As-Ni bonds and the overall cluster size is reduced. The lowest energy isomers have a relatively large HOMO-LUMO gap compared to pure metal clusters due to the coordination with the As atoms. We stress that the HOMO-LUMO gap is typically underestimated in DFT and therefore the gaps are likely to be even larger. The larger gaps also indicate higher chemical stability of the clusters. In general our study which included a large number of isomers indicated that the $Ni_{12-x}Mn_x$ alloy clusters within the As_{20} cage exhibit a rich phase space with a large number of possible spin states. This is particularly true for clusters with larger number of Mn atoms. The clusters with ferrimagnetic spin ordering are found to be more stable compared to those with ferromagnetic ordering. It can be mentioned here that in the pure Mn clusters also anti-ferromagnetic or ferrimagentic spin ordering is preferred. The

spin charges on the Mn atoms range from 2 – 3 μB in the alloy clusters, which are lower than the spin charge in pure Mn clusters. The net spin moment of the alloy clusters is lower than the spin of single molecule magnets with similar number of Mn ions. For example, the $As_{21}Mn_{10}Ni_2$ cluster has a spin moment of 15 μB which is lower than the Mn_{10} SMM which has S=13 in the ground state. The magnetic anisotropy energy in this cluster is 35K as opposed to the calculated value of 9.5K of Mn_{10} SMM. However, these comparisons are not straightforward since the configuration of the cluster and the SMM are significantly different. The encapsulation within the As_{20} cage helps in stabilizing the alloy cluster and making it chemically more stable, the metallic bonds within the Mn_xNi_{12-x} cluster reduce the spin moment on each Mn atom. The magnetic anisotropy energy of the $As_{21}Ni_2Mn_{10}$ system is larger than the Mn_{10} SMM, but it is still much smaller that the room temperature to be viable for storage devices. Moreover, these clusters have a large number of low-lying spin states. On the other hand the encapsulation is a good way to make the cluster chemically more stable and larger encapsulated clusters or multi atom doped clusters may have better technological potential.

REFERENCES

1. Joshua Ahab Maurer. (2003). I. Structure-Function Analysis of the Mechanosensitive Channel of Large Conductance. II. Design of Novel Magnetic Materials using Crystal Engineering. Retrieved from Caltech Thesis.
2. Verdaguer. M. How molecules become magnetic and the resulting wonderland [pdf document] Retrieved from Lecture Notes online website: http://obelix.physik.uni-bielefeld.de/~schnack/molmag/material/Verdaguer-Text-How-Magnetism.pdf.
3. M. R. Pederson, S. N. Khanna, (1999). Magnetic Anisotropy barrier for spin tunneling in $Mn_{12}O_{12}$ molecules. Physical Review B, 60(13).
4. Beach, G. Hysteresis in Ferromagnetic Materials [pdf document] .Retrieved from Lecture Notes online website: http://ocw.mit.edu/courses/materials-science-and-engineering/3-024-electronic-optical-and-magnetic-properties-of-materials-spring-2013/lecture-notes/MIT3_024S13_2012lec25.pdf .
5. Juan Carlos Cuevas, Introduction to Density Functional Theory. Retrieved from https://www.uam.es/personal_pdi/ciencias/jcuevas/Talks/JC-Cuevas-DFT.pdf .
6. Thomas-Fermi Model. Retrieved from Wiki: https://en.wikipedia.org/wiki/Thomas%E2%80%93Fermi_model.
7. Jack Simons, Electronic structure theory- Density functional theory [Video file]. Retrieved from https://www.youtube.com/watch?v=3Kv-m4XeX-c .
8. Magnetic Anisotropy Energy. Retrieved from Wiki: https://en.wikipedia.org/wiki/Magnetic_anisotropy.
9. Donatella Cassettari, Lectures 11-13 spin-orbit interaction.pdf [PowerPoint slides]. Retrieved from http://www.st-andrews.ac.uk/~dc43/PH4021/Lectures%2011-13%20SPIN-ORBIT%20INTERACTION.pdf.
10. Jens Kortus, Mark R. Pederson, Tunna Baruah, N. Bernstein, C.S Hellberg. (2003). Density functional studies of single molecule magnets. Polyhedron, 22
11. Jordi Ribas-Arino, Tunna Baruah, Mark R. Pederson. (2005). Density-functional study of two Fe_4-based single-molecule magnets. Journal of Chemical Physics. 123,044303-1.
12. M.R.Pederson, D.V. Porezag, J. Kortus, S.N. Khanna. (2000). Theoretical calculations of magnetic order and anisotropy energy in molecular magnets. Journal of Applied Physics, 87,9
13. Jens Kortus, Tunna Baruah, N.Bernstein, Mark Pederson. (2002). Magnetic ordering, electronic structure and magnetic anisotropy energy in the high-spin Mn_{10} single molecule magnet. Physical Review,66,092403.
14. Melanie J. Moses, James C. Fettinger, Bryan W. Eichhorn. (2003). Interpenetrating As_{20} fullerene and Ni_{12} icosahedra in the onion skin $[As@Ni12@As20]^{3-}$ Ion. Science, 300
15. Tunna Baruah, Rajendra R. Zope, Steven L. Richardson, Mark R. Pederson. (2004). Electronic structure, vibrational stability, and predicted infrared-Raman spectra of the As20, $As@Ni_{12}$ and $As@Ni_{12}@As_{20}$ clusters. (2004). 121, 22.

VITA

Nabil Md Rakinul was born in Australia. He completed his Bachelor of Science and Masters of Science in Physics from University of Dhaka which is the top ranked university in Bangladesh. He joined at the University of Texas at El Paso in January 2014 as a graduate student. He got the opportunity to work as a Teaching Assistant and Research Assistant in the Physics Department at the University of Texas at El Paso.

Permanent address: Vill: Kharia, Thana: Shibpur, District: Narshingdi
Narshingdi, Bangladesh.

This thesis/dissertation was typed by Nabil Md Rakinul Hoque.